

UC Berkeley
SEMM Reports Series

Title

Solidification of Portland Cement

Permalink

<https://escholarship.org/uc/item/37f6n4tw>

Author

Williamson, Robert

Publication Date

1970-12-01

REPORT NO.
UC SESM 70-23

STRUCTURES AND MATERIALS RESEARCH
DEPARTMENT OF CIVIL ENGINEERING

SOLIDIFICATION OF PORTLAND CEMENT

by

ROBERT BRADY WILLIAMSON

This research was sponsored by
the Office of Naval Research under
Contract N 00014-69-A-0200-1007,
Project NR 032 522.
This is TECHNICAL REPORT NO. 1

DECEMBER 1970

STRUCTURAL ENGINEERING LABORATORY
UNIVERSITY OF CALIFORNIA
BERKELEY CALIFORNIA

Structures and Materials Research
Department of Civil Engineering

Report No. UCSESM 70-23

SOLIDIFICATION OF PORTLAND CEMENT

by

Robert Brady Williamson

This research was sponsored by the Office of Naval Research
under Contract N 00014-69-A-0200-1007, Project NR 032 522.
This is TECHNICAL REPORT NO. 1.

Reproduction is permitted
for any purpose of the
United States Government

Structural Engineering Laboratory
University of California
Berkeley, California

December 1970

Unclassified

Security Classification

DOCUMENT CONTROL DATA - R & D

(Security classification of title, body of abstract and indexing annotation must be entered when the overall report is classified)

1. ORIGINATING ACTIVITY (Corporate author) Department of Civil Engineering University of California, Berkeley Berkeley, California 94720	2a. REPORT SECURITY CLASSIFICATION Unclassified
	2b. GROUP None

3. REPORT TITLE
SOLIDIFICATION OF PORTLAND CEMENT

4. DESCRIPTIVE NOTES (Type of report and inclusive dates)
Interim technical report

5. AUTHOR(S) (First name, middle initial, last name)
Robert Brady Williamson

6. REPORT DATE December 1970	7a. TOTAL NO. OF PAGES 109	7b. NO. OF REFS 49
---------------------------------	-------------------------------	-----------------------

8a. CONTRACT OR GRANT NO. N00014-69-A-0200-1007 b. PROJECT NO. NR 032 522 c. d.	9a. ORIGINATOR'S REPORT NUMBER(S) Technical Report No. 1
	9b. OTHER REPORT NO(S) (Any other numbers that may be assigned this report) UCSESM 70-23

10. DISTRIBUTION STATEMENT
Reproduction in whole or in part is permitted for any purpose of the United States Government.

11. SUPPLEMENTARY NOTES	12. SPONSORING MILITARY ACTIVITY Office of Naval Research
-------------------------	--

13. ABSTRACT

Solidification of materials is introduced, and the constitution and hydration of portland cement is reviewed. Microstructural zones are introduced in the cement system: A "columnar" zone of hydration products on solid surfaces and "equiaxed" products which form within the originally water-filled space.

The microstructure of hydrated β -dicalcium silicate is shown in scanning electron micrographs of fracture surfaces of neat pastes at 60, 100, 171, and 384 days age. Similar micrographs for tricalcium silicate pastes and commercial portland cement pastes are shown and discussed. The hardening of portland cement is discussed as a solidification process. The potential flaws and stress concentrators within the cement paste are identified and their effect on mechanical properties is discussed.

14.	KEY WORDS	LINK A		LINK B		LINK C	
		ROLE	WT	ROLE	WT	ROLE	WT
	Portland Cement						
	Hydration						
	Solidification						
	Scanning Electron Microscope						
	Fracture						

ABSTRACT

The general field of solidification is introduced, and the constitution and hydration of portland cement is reviewed. The relative volumes of original cement and mixing water and the volumes of the final hydration products are discussed in detail. The study of cement paste by optical microscopy is reviewed and several microstructural zones are identified on the basis of the previous optical studies. A "columnar" zone of outer hydration products is indicated to form around each cement grain and grow into the originally water-filled space. The analogy of this columnar zone with that found in metal castings is presented and discussed. The portlandite crystals (i.e., calcium hydroxide) which form throughout the originally water-filled space are compared to the equiaxed crystals that form in the liquid of a solidifying metal casting.

The microstructure of hydrated β -dicalcium silicate is shown in scanning electron micrographs of fracture surfaces of neat pastes at 60, 100, 171 and 384 days age. At age of 60 days the fracture occurred generally through the water-filled space which initially separates the grains. The 60 day old specimen shows a well developed columnar zone on each grain. As the age increases, the columnar zones come in contact and appear to intergrow; this causes the fracture to traverse the hydrated grains. The latter are essentially pseudomorphs of the original β -dicalcium silicate grains.

Fracture surfaces of tricalcium silicate paste are shown at ages ranging from 200 hours to 4 years. The presence of large areas of portlandite distinguish tricalcium silicate pastes from β -dicalcium silicate pastes. The engulfed grains are shown and their probable degree of hydration is discussed. The hydration within the cement grain is

investigated by observing fracture surfaces of partially hydrated passages within unground clinker. The hydration of commercial portland cement appears to be similar to the individual phases alone.

The relationship of mechanical properties to microstructure of brittle materials in general is discussed and a distinction between stress concentrators and Griffith flaws is presented. These concepts are applied to portland cement paste and the potential flaws in the system are listed. One set of possible flaws are the boundaries between:

- (1) the unhydrated core and the surrounding hydration product on each grain,
- (2) the inner hydration products and the outer product columnar zone around each grain,
- (3) the outer product columnar zones of two different grains,
- (4) portlandite and outer product columnar zone of cement grains,
- (5) portlandite crystals (i.e., a grain boundary),
- (6) the hydration products of the minor compounds and other features.

Other potential flaws in cement paste are the cleavage planes of portlandite crystals and cracks caused by shrinkage or other effects. The possible stress concentrators are

- (1) the portions of the originally water-filled space which remain as pores in the final microstructure,
- (2) the entrapped and/or intentionally entrained air voids visible in most cement pastes, and
- (3) the pseudomorphs of the original cement grains.

The relative sizes of these flaws and stress concentrators change with time during the hydration process and the need for future research in understanding these processes is discussed.

TABLE OF CONTENTS

	<u>Page</u>
1. Introduction	
1.0 General.	1
1.1 Forward to the Report.	1
1.2 The Solidification of Materials.	3
1.3 Materials Science--Relationship between Structure and Properties	5
2. Constitution and Hydration of Portland Cement	
2.1 Constitution of Portland Cement.	7
2.2 The Nature of Clinker.	9
2.3 Hydration of Portland Cement	14
2.4 Calcium Silicates - Most Important for Strength	20
3. Microstructure of Hydrated Cement Paste	
3.0 History.	24
3.1 Identification of Microstructure Zones	25
3.2 Microstructure of β -Dicalcium Silicate Pastes.	32
3.3 Microstructure of Tricalcium Silicate Pastes	56
3.4 Microstructure of Hydrated Portland Cement	71
3.5 The Hardening of Cement Paste--A Solidification Process.	85
4. Relationship of Mechanical Properties to Microstructure	
4.1 Stress Concentration in Multiphase Brittle Microstructures.	93
4.2 Flaws and Stress Concentrators in Cement Paste	97

LIST OF FIGURES

<u>Figure</u>	<u>Page</u>
2.1 Part of $\text{CaO-Al}_2\text{O}_3\text{-SiO}_2$ phase diagram	10
2.2 Electron microanalyzer micrographs of cement clinker	12
2.3 Graphical representation relative volumes of hydration products	16
2.4 Strength vs time for portland cement components.	22
3.1 Schematic representation of microstructure zones	28
3.2 Metal ingots with "columnar" and "equiaxed zones".	30
3.3 Fracture surface of $\beta\text{-C}_2\text{S}$ paste, age 60 days	34
3.4 Fracture surface of $\beta\text{-C}_2\text{S}$ paste, age 100 days.	36
3.5 Another area on 100 day old $\beta\text{-C}_2\text{S}$ paste.	38
3.6 Fracture surface of $\beta\text{-C}_2\text{S}$ paste, age 171 days.	40
3.7 Fracture surface of $\beta\text{-C}_2\text{S}$ paste, age 384 days.	42
3.8 Another area on 384 day old $\beta\text{-C}_2\text{S}$ paste.	44
3.9 Details of boundary of filled cavity in Fig. 3.7	46
3.10 Details of portlandite growth within paste	48
3.11 Another area on specimen showing an unfilled pore.	50
3.12 A 389 day old $\beta\text{-C}_2\text{S}$ paste, vacuum dried before fracture.	52
3.13 Close-ups of an air bubble visible in Fig. 3.12.	54
3.14 Fracture surface of C_3S paste hydrated over two years.	58
3.15 Another area on fracture surface shown in Fig. 3.14 showing range of portlandite morphology.	60
3.16 Fracture surface of C_3S paste hydrated 200 hrs showing unhydrated grains engulfed in portlandite.	62
3.17 Fracture surface of C_3S paste cured under water four years.	64

<u>Figure</u>	<u>Page</u>
3.18 Another area on C_3S paste of Fig. 3.17	66
3.19 Another area on fracture surface shown in Figs. 3.14 and 3.15 illustrating differences in porosity.	68
3.20 Fracture through a passage of a partially hydrated portland cement clinker.	72
3.21 The same passage shown in Fig. 3.20 shown here from another angle	74
3.22 Another area on the clinker shown in Fig. 3.20	76
3.23 Morphology of outer hydration products	78
3.24 Different morphology of outer hydration products	80
3.25 Fracture surface of a poorly hydrated paste.	82
3.26 Equilibrium phase diagram for aluminum-copper alloys . . .	86
3.27 Solidification of portland cement-schematically.	90
4.1 The effect of stress concentration on strength	96
4.2 Schematic illustration of the solidification process showing the gain of strength	98

ACKNOWLEDGMENTS

I should like to express my gratitude to the students, colleagues, and other friends with whom I have studied the solidification of ice, metals, polymers, cement, and other materials during the past few years. Much of the point of view and many of the ideas have come in discussions with them. I would like to express my deepest appreciation to the late Alexander Kline, whose keen interest and encouragement was particularly valuable. I wish to convey special thanks to all my University of California colleagues, particularly Professors David Pirtz, Milos Polivka, P. K. Mehta, and Thomas Everhart, who have given me such strong support and encouragement since I arrived on the campus. Finally, I would like to thank Lou Copeland of the Portland Cement Association and Brian and Kay Mather of the Army Corps Engineers for their firm guidance in my early exposure to portland cement. It is impossible to name everyone to whom I would like to convey thanks, and I stop this acknowledgment here because of lack of space and trust that those not mentioned will accept my implied thanks.

1. INTRODUCTION

1.0 General

Our direct knowledge of the nature and behavior of matter is almost always derived from the observation of samples that are very large compared to the size of their smallest units, and thus when new more powerful techniques of observation are developed they may be used to gain insight about materials which have been in use for a long time. The new techniques might be capable of supplying certain important details. It should be recognized that the observations that we make and the terms used to describe them relate to the average behavior of a very large number of atoms, whose individual behavior may depart drastically from the average. Even the use of powerful microscopes does not end this situation in general, but in certain situations these or other new techniques make it possible to observe some of the exceptions to the average case which were not observable previously. These exceptions can be the important link in understanding some aspects of the behavior. While many of the properties of materials are controlled by the statistical average, there are some important properties, such as fracture strength, which are very sensitive to the exceptions.

1.1 Forward to the Report

This is the first technical report of a research project on "The Relationship between Microstructure and Mechanical Properties of Cementitious Materials" which is being performed in the Division of Structural Engineering and Structural Mechanics, Department of Civil Engineering, University of California at Berkeley.

The purpose of the research is as follows:

1. To conduct detailed studies of the microstructure of hydrated portland cement and its principal constituents.
2. To study changes in microstructure which can be induced by controlled changes in the hydrating environment.
3. To measure the effect of such microstructure which can be induced by controlled changes in the hydrating environment.
4. To search for mechanisms which will optimally control the morphology of hydrated cement for greatest improvement of macroscopic behavior.

This report is organized into four chapters with the first being the Introduction, of which this is a part. In the remaining two sections of this chapter the general field of solidification will be introduced as well as the materials science approach to the structure-property relationship. In the second chapter the constitution and hydration of portland cement will be presented in sufficient detail to allow the widest possible audience for the findings presented in the report. The third chapter contains the results of the microscopic study of hydrated portland cement and its principle constituents. Such a presentation can only consist of a fraction of the actual micrographs obtained during the study, but as broad a coverage is presented as possible. The general philosophy has been to present a picture atlas similar to the Bilderatlas of Zementklinkers (1) of the German Cement Laboratory in Dusseldorf and the Transmission Micrographs of Grudermo (2). The discussion of what the micrographs mean is based on the author's ideas and contributions of others as

noted, but it is hoped that they will stimulate general discussion. The fourth and final chapter presents a further discussion of the relationship between engineering properties and the microstructure of cement paste. An appendix is added which contains specific information about how each specimen was prepared and some general discussion of using the scanning electron microscope for the study of cementitious materials.

1.2 The Solidification of Materials

Solidification can be defined as a process by which a solid grows at the expense of a liquid with which it is in contact, and within this definition the hardening of cement paste will be shown to be a solidification process. The principles developed to understand the solidification of metallic systems have been reviewed by Chalmers (3), and there are many of them which are directly applicable to the cement system.

First of all, the solidification of any material is an atomic or molecular process where the nature of the solids, liquids, and interfaces between them can play a deciding role in the total process. There are important questions of the kinetics of the reactions and how these affect the nucleation and growth of crystals and other solids. The concepts of nucleation and crystal multiplication under dynamic stimulus are probably of great importance in the cement system; although there is little direct evidence at this time.

A second area is in the microscopic flow of heat within a solidifying system. The metallic systems have the release of latent heat at growing crystal surfaces, and in some cases it flows into the liquid

ahead of the crystal and in others it flows into the crystal. The differences between the two heat flow cases can make profound changes in the microstructure of the cast metal and thus its engineering properties. The microscopic distribution, production, and flow of heat in a hardening cement paste is a complex problem which has not been analyzed in the detail of the metallic systems, but it will be necessary before the origin of the observed microstructural features can be understood and controlled. A closely coupled phenomenon to heat flow is the redistribution of solute during solidification. This also occurs on the microscopic scale, and it can make important changes in the microstructure.

The morphology of the solid products and their distribution within the microstructure are completely controlled by the principles of kinetics, solute redistribution, and heat flow, and the morphology and interrelation of the solid products in turn control some of the engineering properties of the material. The overall objective of the study of the solidification of cement or any other material is the economic improvement of the engineering properties. In many ways the easiest technique of improving engineering properties is to change the existent microstructure by new treatment during fabrication.

An important result of studying solidification which has been noted by metallurgists is that one can often understand the process by carefully observing the resultant microstructure and thus build a mental picture or set of mechanisms that can be used to solve actual problems. Many improvements in industrial techniques were made because the microstructure was visible through available microscopes.

The use of the scanning microscope and its improved future models may usher in an era where substantial technical progress may be made by an improved ability to see what one is dealing with on a microscopic level.

1.3 Materials Science--Relationship between Structure and Properties

Portland cement is one of the most widely utilized materials for engineering structures, and yet the relationship between strength and microstructure has not been presented in context with other engineering materials. The fracture strength of brittle materials and the yield point of ductile materials can often be improved by controlling the microstructure through relatively simple processes. Physical metallurgy and ceramics can be the basic foundation for the understanding of any materials, and there is unique perspective that can be gained from this approach.

There are a number of principles that have been useful in understanding the behavior of metallic, ceramic, and polymeric materials. Many of these principles are the direct application of physics or chemistry to engineering materials, but a few are unique to the materials field. One of these unique principles is the classification of properties as sensitive or insensitive to the microstructure of the materials. Chalmers (4) divides the properties of metallic materials along these lines and shows that properties such as density, elastic modulus, and thermal expansion coefficient are insensitive to the microstructure of a metallic alloy. To illustrate this point, Chalmers shows that the change of microstructure associated with a slight (5-10%) change of alloying elements does not appreciably change

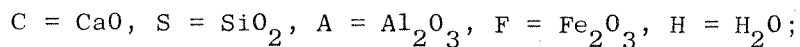
the elastic modulus from the value of the pure base metal. On the other hand, the yield strength of the same metals is raised several orders of magnitude by the changes in microstructure. The most important example is steel; the yield strength of iron can be raised two orders of magnitude by the additions of small amounts of carbon and other alloying elements and by controlling the resultant microstructure. The yield point of metals is very microstructure sensitive, and the strengthening of metallic alloys by microstructure control is the basis of many high performance materials.

The fracture of all materials is another one of the phenomena that are very sensitive to the microstructure. Both ductile and brittle fracture are dependent on the presence of microscopic cracks, voids, inclusions, and other microstructural features. Some of the possible implications of the solidified microstructure of cement pastes will be discussed in Chapter 4 of this report.

2. CONSTITUTION AND HYDRATION OF PORTLAND CEMENT

2.1 Constitution of Portland Cement

The reaction of portland cement and water is the basic chemical reaction associated with the hardening of cement paste. The subsequent carbonation of the hydration products is not necessary for them to gain strength, and this often is associated with the deterioration of cement. Anhydrous portland cement contains four principal compounds: tricalcium silicate, β -dicalcium silicate, tricalcium aluminate, and a solid solution series which until recently was generally believed to have the fixed composition of tetracalcium alumino ferrite. The composition of cement compounds are often represented as the sum of oxides, the formulae of which are abbreviated:



thus, for example, tricalcium silicate, Ca_3SiO_5 is represented by $3\text{CaO}\cdot\text{SiO}_2$ and shortened to just C_3S . This system is used in cement chemistry interchangeably with ordinary chemical notation. The typical composition of the four standard types of portland cement used in the United States are given in Table 2.1 with the abbreviated forms shown in addition to the chemical names. Small amounts of MgO , CaO and alkali sulphates also occur in many cements. The types of cements shown in Table 2.1 are used for special purposes which will be described below.

Table 2.1 Proportions of Major Compounds in Four Basic Types of Portland Cement Made in the U.S.A.

	I General Use	II Moderate Heat of Hardening	III High Early Strength	IV Low Heat of Hardening
TRICALCIUM SILICATE C_3S	53	47	58	26
β -DICALCIUM SILICATE $\beta-C_2S$	24	32	16	54
TRICALCIUM ALUMINATE C_3A	8	3	8	2
CALCIUM ALUMINATE FERRITE SOLID SOLUTION Between C_2F and C_6A_2F	8	12	8	12
Total	93	94	90	94

These are average percentages obtained by X-ray diffraction analysis of several cements. The remaining 6-7 percent consists of 2-3% $CaSO_4$, 0.2-0.8% Free CaO , and trace amounts of moisture, insoluble residue and alkali oxides combined in various ways. (5)

The formation of portland cement occurs by a high temperature reaction where a molten flux is formed by partially melting certain materials, and the compounds described above are the equilibrium chemical constituents at the elevated temperature. The temperature is then rapidly decreased to prevent the newly-formed cement compounds from transforming to phases which are the equilibrium forms at room temperature. This metastable nature of portland cement is important in visualizing its subsequent reaction with water.

Portland cement is usually manufactured in a rotary kiln which is continuously charged with a mixture of limestone and clay or similar

sources of SiO_2 , CaO , Al_2O_3 and Fe_2O_3 . The general zone of compositions is shown on the SiO_2 - CaO - Al_2O_3 ternary phase diagram in Figure 2.1. As the charge material is moved down the kiln by rotation, it encounters an increasing temperature until partial melting occurs. This melting of 20 to 30 percent of the charge occurs in the hottest zone of the cement kiln (at a temperature between 1300 and 1500°C), and the reaction occurs rapidly. The material coheres into small, rounded lumps which are known as cement clinker, and which are ground after cooling to a fine powder. When water is added to the anhydrous powder made by grinding the clinker, it acts as an hydraulic cement, i.e., it forms an insoluble, rigid solid even when kept under water.

2.2 The Nature of Clinker

The chemical reactions and physical changes which occur in the cement kiln can be considered a solidification process. Many of the principles developed for metallic systems can be used to describe those occurring in the cement kiln, but that is not the object here. The objective here is to illustrate the microstructure of anhydrous cement clinker so that the subsequent hydration can be interpreted.

A polished section of a typical, quickly-cooled clinker is shown by back scattered electrons in Figure 2.2(a). The two predominant constituents are rather angular tricalcium silicate crystals and more rounded β -dicalcium silicate crystals. Both types of calcium silicates are embedded in a matrix of interstitial material which includes tricalcium aluminate, ferrite solid solution and minor phases. This is evident in Figures 2.2(b), (c), and (d) where the distribution of

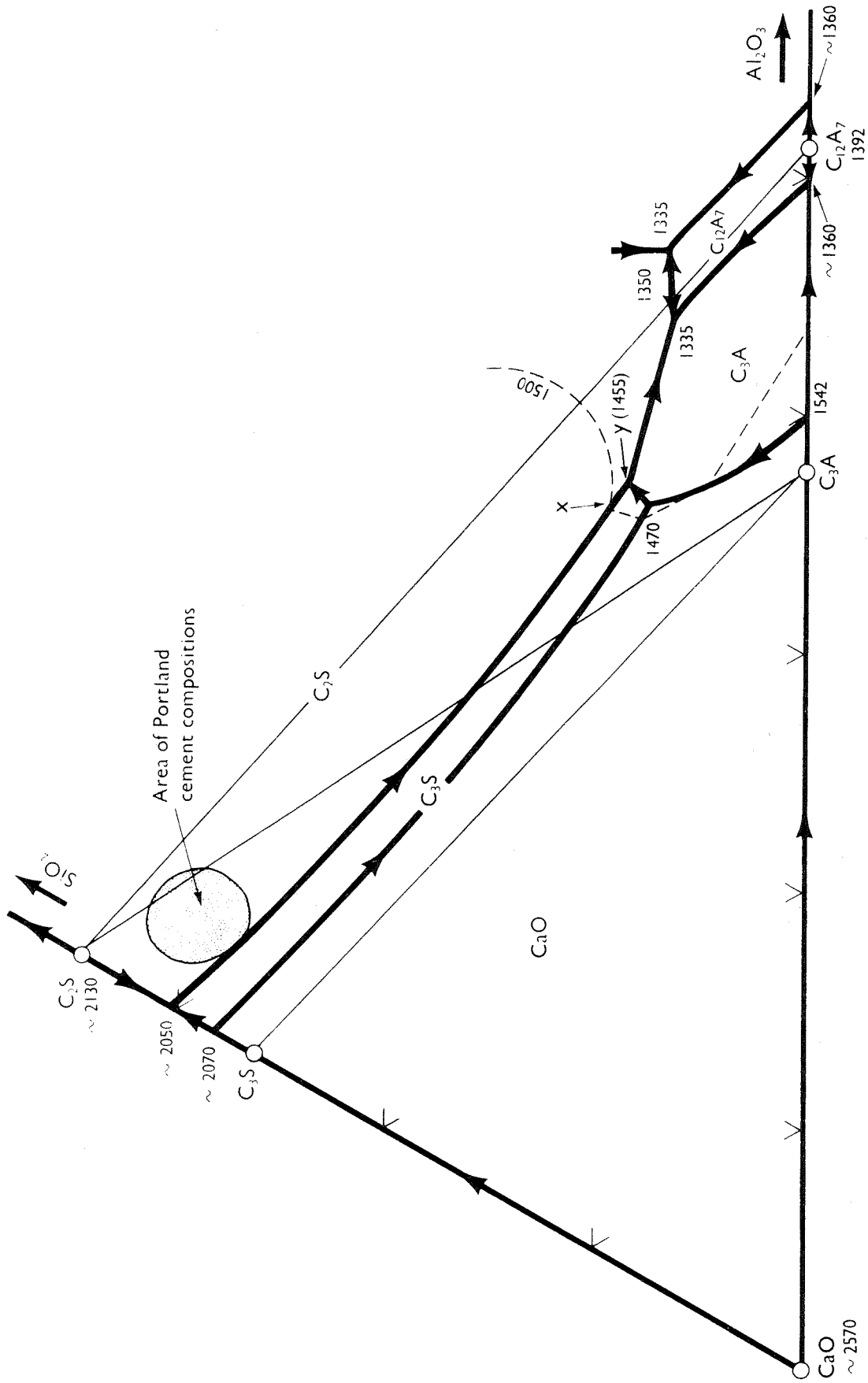


Figure 2.1 Part of the CaO-Al₂O₃-SiO₂ phase diagram, illustrating the solidification of portland cement clinker.

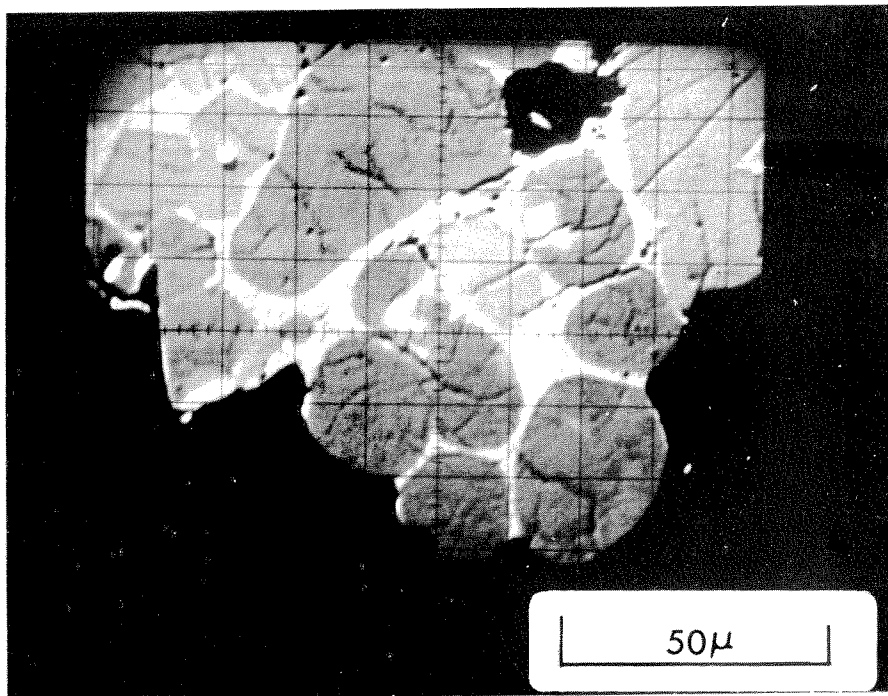
calcium, silica and aluminum are shown for the same area. There have been many studies of the microstructure of clinkers (1,6,7), and it is generally like that in Figure 2.2.

The theoretical basis for understanding the origins of the clinker composition and morphology is provided in Figure 2.1 where the lime corner of the $\text{CaO-Al}_2\text{O}_3\text{-SiO}_2$ phase diagram is reproduced. The heavy lines define primary phase fields where a particular solid phase will crystallize from the melt under equilibrium conditions. Taylor (8) describes how the process occurs in the cement kiln:

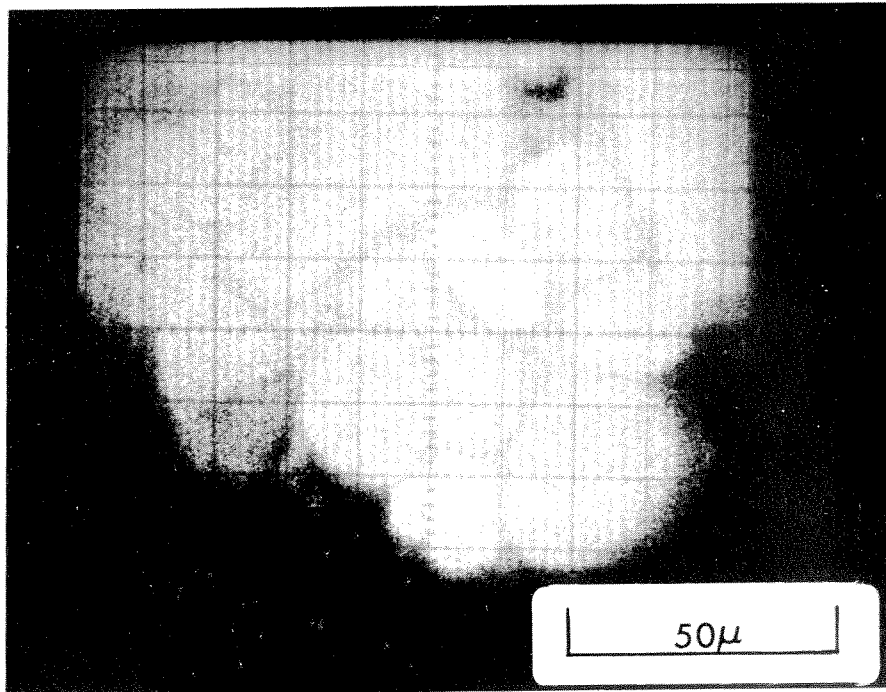
"Modern portland cement compositions lie in the area shown in Figure 2.1. Let us assume that the clinkering temperature (i.e., the highest temperature reached in the kiln) is 1500°C and that equilibrium is reached at this temperature. The phases present will be C_3S , C_2S , and liquid of a composition represented by point X, the intersection of the $\text{C}_3\text{S-C}_2\text{S}$ boundary curve with the 1500°C isotherm. On cooling, if equilibrium is constantly maintained, the liquid composition will move along this boundary curve until point Y is reached, when C_3A will also be formed. The product may therefore be expected to consist of relatively large crystals of C_3S and C_2S which have been formed at the clinkering temperature, embedded in a matrix consisting chiefly of C_3A ." (This agrees with the microscopic observations already described.)

"The position is not radically altered if the presence of other components such as Fe_2O_3 and MgO is allowed for, though it is naturally more complex. It can be predicted that the Fe_2O_3 will occur as ferrite solid solution, which will generally be the last phase to crystallize and will therefore form part of the matrix."

Much of the research reported below has been performed with pure phases rather than portland cement clinker. The possible implications of the clinker microstructure will be discussed below, but there may be possibilities in varying the clinker microstructure to enhance the hydration process.

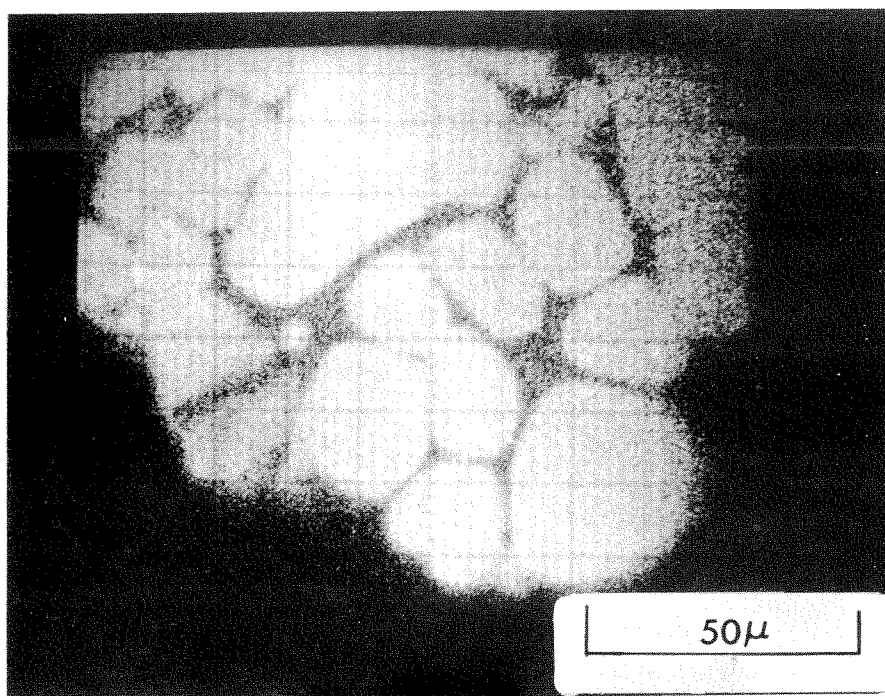


(a)

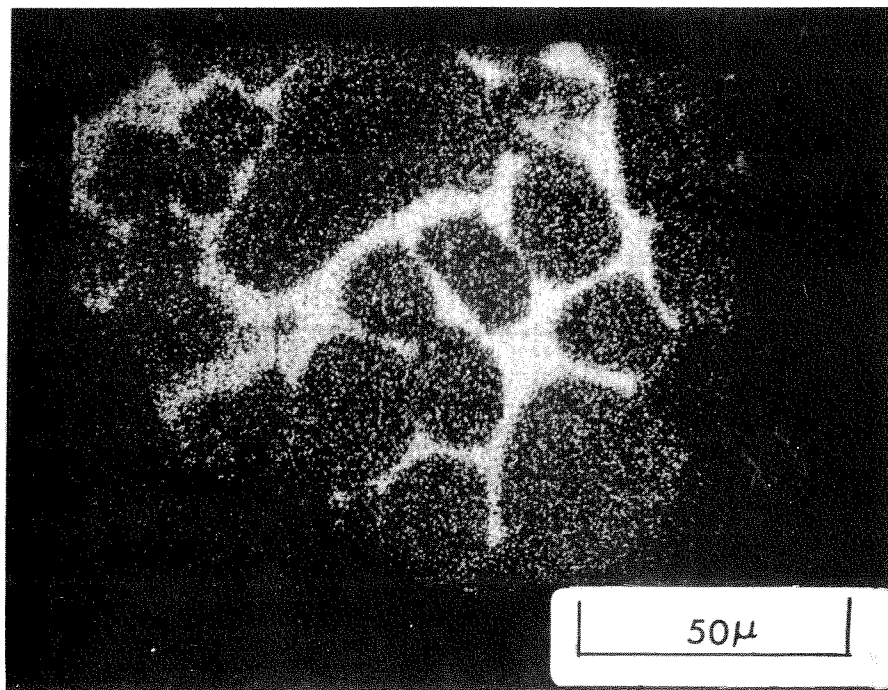


(b)

Figure 2.2 Electron microanalyzer micrographs of polished surface of a typical portland cement clinker, showing angular grains of C_3S and rounded grains of $\beta-C_2S$ in a matrix consisting of the aluminum and iron rich liquid which solidified last. (a) Back scattered electron image, C_3S appears lighter than βC_2S . (b) Distribution of calcium shown by CaK_{α} x-rays.



(c)



(d)

Figure 2.2 (Continued from opposite page)...(c) Distribution of SiO_2 as shown by SiK_α x-rays; notice there is less silica in the intergranular liquid. (d) Distribution of aluminum as shown by AlK_α x-rays; the iron shows an identical pattern of being primarily in the intergranular liquid. [Experimental details are given in the Appendix.]

2.3 Hydration of Portland Cement

Each of the phases of portland cement react with water to give solid products that form the structure of portland cement paste. These reactions are shown in Table 2.2. Note that both tricalcium silicate and β -dicalcium silicate yield the same reaction products: a calcium silicate hydrate (C-S-H) and calcium hydroxide. The C-S-H material has drawn particular attention over the past twenty years, and Taylor (9) has recently reviewed the state of knowledge concerning it. It has been called tobermorite gel in the past, but Taylor (9) suggests that it is more appropriate to refer to it as calcium silicate hydrate. In this paper it will be referred to as calcium silicate hydrate, but there is no intention of differentiating

Table 2.2 Principle Reactions of Portland Cement with Water

$2(3\text{CaO}\cdot\text{SiO}_2)$ (TRICALCIUM SILICATE)	$+ 5.5\text{H}_2\text{O}$	$= 3\text{CaO}\cdot 2\text{SiO}_2\cdot 2.5\text{H}_2\text{O}$ (CALCIUM SILICATE HYDRATE)	$+ 3\text{Ca}(\text{OH})_2$ (PORTLANDITE)
$2(2\text{CaO}\cdot\text{SiO}_2)$ (DICALCIUM SILICATE)	$+ 3.5\text{H}_2\text{O}$	$= 3\text{CaO}\cdot 2\text{SiO}_2\cdot 2.5\text{H}_2\text{O}$ (CALCIUM SILICATE HYDRATE)	$+ \text{Ca}(\text{OH})_2$ (PORTLANDITE)
$4\text{CaO}\cdot\text{Al}_2\text{O}_3\cdot\text{Fe}_2\text{O}_3$ (TETRALCIUM ALUMINOFERRITE)	$+ 10\text{H}_2\text{O}$	$+ 2\text{Ca}(\text{OH})_2$	$= 6\text{CaO}\cdot\text{Al}_2\text{O}_3\cdot\text{Fe}_2\text{O}_3\cdot 12\text{H}_2\text{O}$ (CALCIUM ALUMINOFERRITE HYDRATE)
$3\text{CaO}\cdot\text{Al}_2\text{O}_3$ (TRICALCIUM ALUMINATE)	$+ 12\text{H}_2\text{O}$	$+ \text{Ca}(\text{OH})_2$	$= 4\text{CaO}\cdot\text{Al}_2\text{O}_3\cdot 13\text{H}_2\text{O}$ (TETRALCIUM ALUMINATE HYDRATE)
$3\text{CaO}\cdot\text{Al}_2\text{O}_3$	$+ 10\text{H}_2\text{O}$	$+ \text{CaSO}_4\cdot 2\text{H}_2\text{O}$ (GYPSUM)	$= 3\text{CaO}\cdot\text{Al}_2\text{O}_3\cdot\text{CaSO}_4\cdot 12\text{H}_2\text{O}$ (CALCIUM MONOSULFO- ALUMINATE)

between it and tobermorite gel. The calcium hydroxide is also known by its mineralogical name portlandite, and this will be used in general.

The reactions of tricalcium aluminate and the iron bearing solid solution (labeled C_4AF) are shown in Table 2.2, but for the most part these reactions will not be discussed in this paper. Two reactions are shown in Table 2.2 for tricalcium aluminate, one with and one without gypsum, $CaSO_4 \cdot 2H_2O$. The gypsum is added to most portland cement as it is ground, a process called intergrinding, in order to prevent a premature setting of the paste; this process has been reviewed by Hansen (10).

In its simplest terms, the hydration of cement is a reaction in which a solid of low solubility reacts with water to form solid products of even lower solubility. The chemical reactions shown in Table 2.2 can be thought of in this simplified framework. A graphical representation shown in Figure 2.3 can be used to describe the sequence of events as the cement minerals react with water. This reaction produces the continuous solid matrix in the space that was originally occupied by discrete particles dispersed in the water. In Figure 2.3 the relative volume of water and cement are represented by a bar graph labeled "Fresh Paste" for the case of 0.5 water-to-cement ratio. The specific gravity of the cement has been taken at 3.15, and thus there is 1.55 cubic centimeters of water for one cubic centimeter of cement. The hydration reaction is then represented at 33%, 67%, and 100% completion on the basis that one half unit of cement yields one unit volume of hydration products (11). The nomenclature of inner and outer

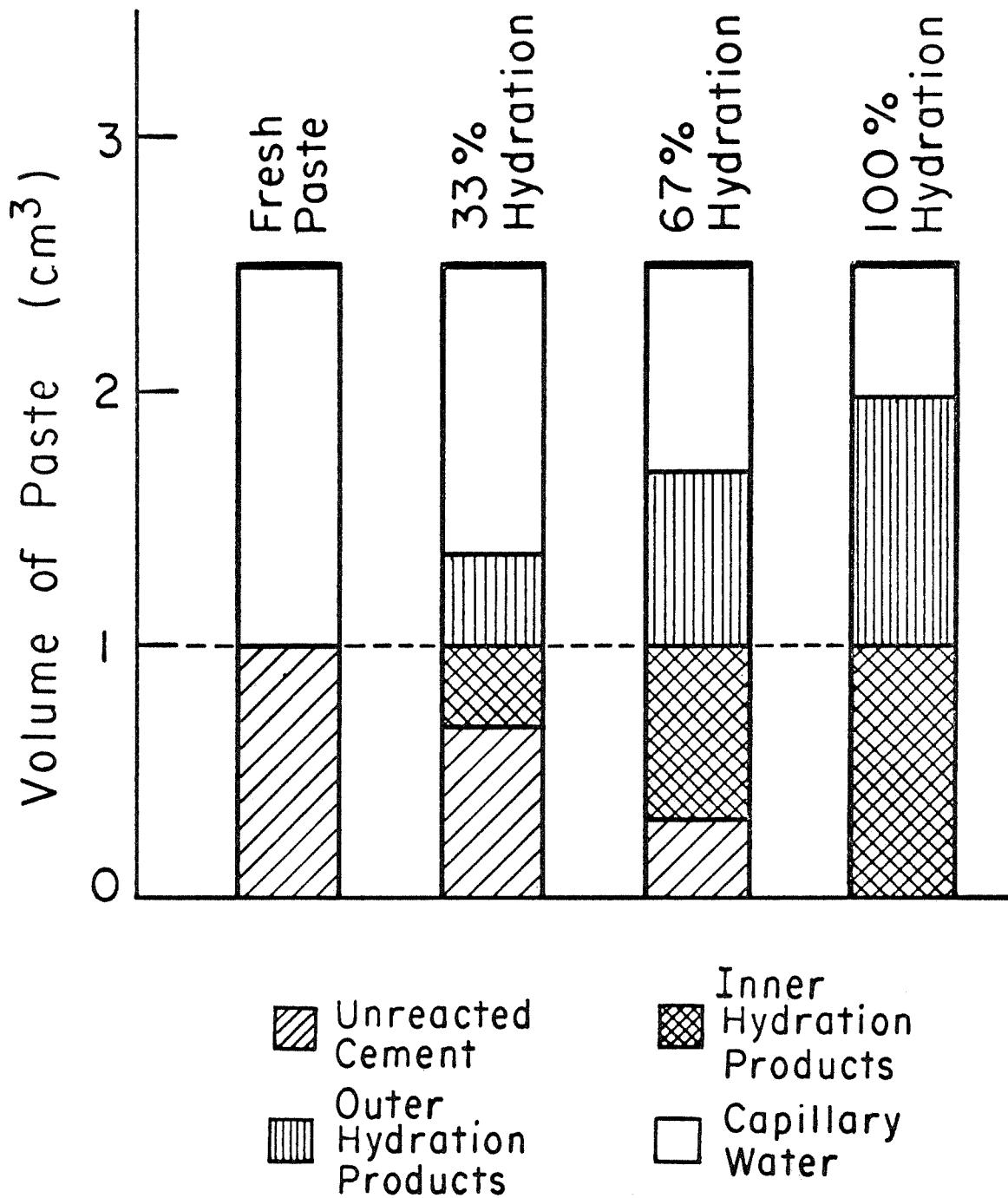


Figure 2.3 Graphical representation of the relative volumes of hydration products of portland cement at three stages of hydration; 33%, 67%, and 100% completion. The initial water-to-cement ratio is 0.5, and one unit volume of cement is shown to produce two unit volumes of hydration products (this is an empirical relationship discussed in the text).

hydration products has been introduced into Fig. 2.3 in order to discriminate between the products laid down within the boundaries of the original cement grains and the products laid down in the originally water-filled space. This nomenclature is due to Taplin (12), although others had come close to it previously (13).

It is important to note that the basis of one half unit volume of anhydrous cement yielding one unit volume of the hydration products is an empirical result which is true in general for portland cement at normal water-to-cement ratios (11). For the purpose of discussion, however, another relationship will be investigated: The volume of anhydrous material plus stoichiometric water is equal to the volume of the reaction products. This special relationship can be applied to the reaction of the tricalcium and β -dicalcium silicate phases with water in order to illustrate the possible spatial relations imposed by the chemical reactions shown in Table 2.2. The formula weights for the reaction of tricalcium silicate with water are written as follows:

$$2(3\text{CaO}\cdot\text{SiO}_2) + 5.5\text{H}_2\text{O} = 3\text{CaO}\cdot 2\text{SiO}_2\cdot 2.5\text{H}_2\text{O} + 3\text{Ca}(\text{OH})_2$$

g molar wt.	456	99	333	222
Density (gm/cc)	3.15	1	2.3	2.34
Molar volume (cc)	145	99	144	99
Total volume (cc)	244 Initially		243 Finally	

At a density of 3.15 grams per cubic centimeter the 456 grams of tricalcium silicate would occupy a volume of 145 cubic centimeters. The volumes of the hydration products are difficult to determine directly,

but if the calcium hydroxide in cement has its normal density of 2.34 then it occupies 99 cubic centimeters. The calcium silicate hydrate must then have a density of 2.3 gm/cc for the initial and final volumes to be approximately the same. Although this value of density is lower than the value of 2.85 gm/cc estimated by Brunauer and Greenberg (14), it is very close to the density recently obtained by Feldman (15). The measurement of densities of 2.3 gm/cc and higher supports the supposition that the final volume of the hydration products of tricalcium silicate is equal to, or less than, the original volumes of the anhydrous tricalcium silicate plus the stoichiometric water. In direct contrast to this, if the empirical relationship of one half unit volume of anhydrous material yielding one unit volume of the hydration products is applied to this case, the final volume would be 290 cubic centimeters which would require approximately 1.75 gm/cc for the density of the calcium silicate hydrate. This value is exactly what Powers suggested for "nominal gel," (defined as the actual gel plus the calcium hydroxide associated with it,) which he estimated to have a porosity of 26 percent (16).

The reaction of β -dicalcium silicate with water is different than the tricalcium silicate, although the products appear to be the same. If the analysis is presented in a similar fashion, the formula weights for the reaction of β -dicalcium silicate with water are written as follows:

$$2(2\text{CaO}\cdot\text{SiO}_2) + 3.5\text{H}_2\text{O} = 3\text{CaO}\cdot 2\text{SiO}_2\cdot 2.5\text{H}_2\text{O} + \text{Ca}(\text{OH})_2$$

g molar wt.	344	63	333	74
Density (gm/cc)	3.27	1	2.4	2.34
Molar volume	105	63	139	31.6
Total volume	168 Initially		171 Finally	

The calcium silicate hydrate would have to have a density of 2.4 gm/cc to make the initial and final volumes approximately equal, but it would only have 1.87 gm/cc if the empirical result were applied instead. As with the case of the calcium silicate hydrate from tricalcium silicate, the former density is close that obtained by Feldman (15), and the latter close to that suggested by Powers (16). Feldman has made his measurements using helium as a medium which would penetrate most of the pores in the gel Powers describes; so it is quite likely that both of the possible conditions apply to the hydrating system. The choice of one viewpoint over the other really depends on what frame of reference is important for understanding a particular phenomena.

In order to understand the solidification process occurring in a cement paste, the conflicting implications of these two points of view must be resolved. Hansen (17) has used the constant volume viewpoint to conclude that the calcium silicate hydrate remains within the original grain boundaries while the calcium hydroxide diffuses promptly into the liquid during the hydration of tricalcium silicate. He notes this is less true for β -dicalcium silicate where some of the calcium silicate hydrate would have to form outside the original

grains. Brunauer and Greenberg (14) have used the other argument to suggest that much more gel forms outside the original grain boundaries, although their argument is stronger for β -dicalcium silicate than for tricalcium silicate. The possible resolution of these viewpoints will be discussed below.

2.4 Calcium Silicates - Most Important for Strength

The relative importance of the reactions shown in Table 2.2 can be best measured as they affect the strength of portland cement paste. The first definitive study of the strengths of pastes made from individual samples of the pure compounds was made by Bogue and Lerch (18). The experimental procedure followed in that study was described by the authors as follows:

"The compounds and mixtures of compounds were each mixed rapidly with water. An amount of water equal to 50 percent of the weight of the cementing material (except as otherwise noted) was measured out, and as much of this was mixed with the material as was required to give a plastic paste. The paste was then placed to a depth of about $1\frac{1}{2}$ inches in shell vials, $4 \times 15/16$ inch, and the balance of the 50 percent of water, if any remained, was placed on top of the pastes in the vials. This total water was considered from preliminary data to be sufficient to hydrate completely the compounds present. The calcium aluminates, however, required somewhat more than that amount of water to give a plastic paste. In those cases the required water was used, but none was placed on top of the specimens. The charged vials were stoppered and sealed with paraffin so that the reactions with water could proceed unaffected by external influence, such as evaporation of water at the surface, carbonation by reaction with the carbon dioxide of the air, or extraction by storage water. All specimens were stored at room temperature until tested.

"Tests of compressive strength of the neat materials were carried out as follows:

"The glass around the specimens was broken away, the cylinders were placed in a clamp, and the ends were ground down to give a cylinder one inch long. These were then tested for compressive strength in duplicate at the ages of 1, 3, 7, 28 days, 3, 6, 12 months, and 2 years. Where the values obtained on duplicate

specimens differed by more than 10 percent, a third specimen was broken. The results given in the table have been calculated to pounds per square inch."

The maximum compressive stress recorded in these experiments is given in Table 2.3 and plotted twice in Figure 2.4, once against a linear time scale in (a) and once against a logarithmic time scale in (b). The logarithmic time scale essentially expands the early ages and the differences between the strength gain of tricalcium silicate and the β -dicalcium silicate pastes are highlighted. The development of compressive strength with time shown in Figure 2.4 illustrates that the tricalcium silicate hardened most rapidly and formed the strongest

Table 2.3 Compressive Strength of Cement Compounds
(Calculated from cylinders 15/16 x 1 inch)

Com- pound	Gyp-	Mix-	Total	Compressive Strengths (Average of Two Specimens Only)							
	sum Added	ing Water	Water Used	1 day	3 days	7 days	28 days	3 mo.	6 mo.	1 yr.	2 yr.
	%	%	%	Pounds per square inch							
C ₃ S	0	35	50	1450	2800	5960	7100	7100	9690	10,300	11,300
	5	35	50	1770	2780	5830	6760	6330	8700	9,800	11,300
β C ₂ S	0	30	50	0	60	140	910	5160	7560	10,250	14,350
	5	30	50	0	90	220	1200	3900	7700	9,800	12,600
C ₃ A	0	60	60	30	170	250	600	670	890	1,090	800
	15	60	60	600	900	1000	1580	1280	1770	1,320	1,320
C ₂ F	0	30	50	0	0	0	0	0	0	0	0
	5	30	50	0	0	0	0	0	0	0	0
C ₄ AF	0	50	50	0	300	290	360	380	580	650	720
	15	50	50	20	390	440	720	1110	1330	1,420	1,500

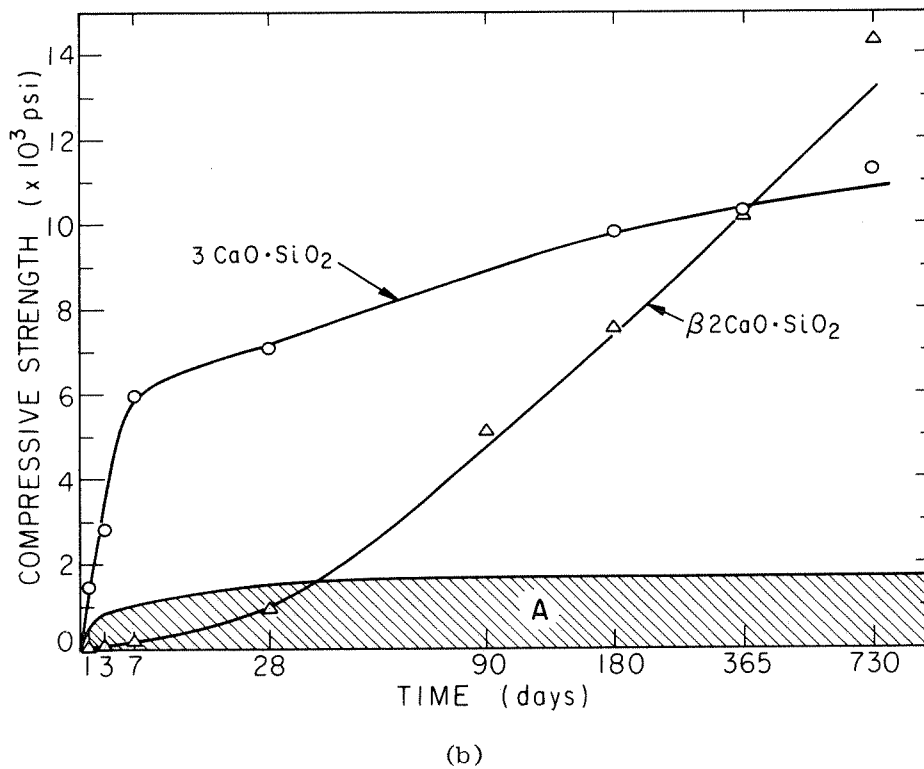
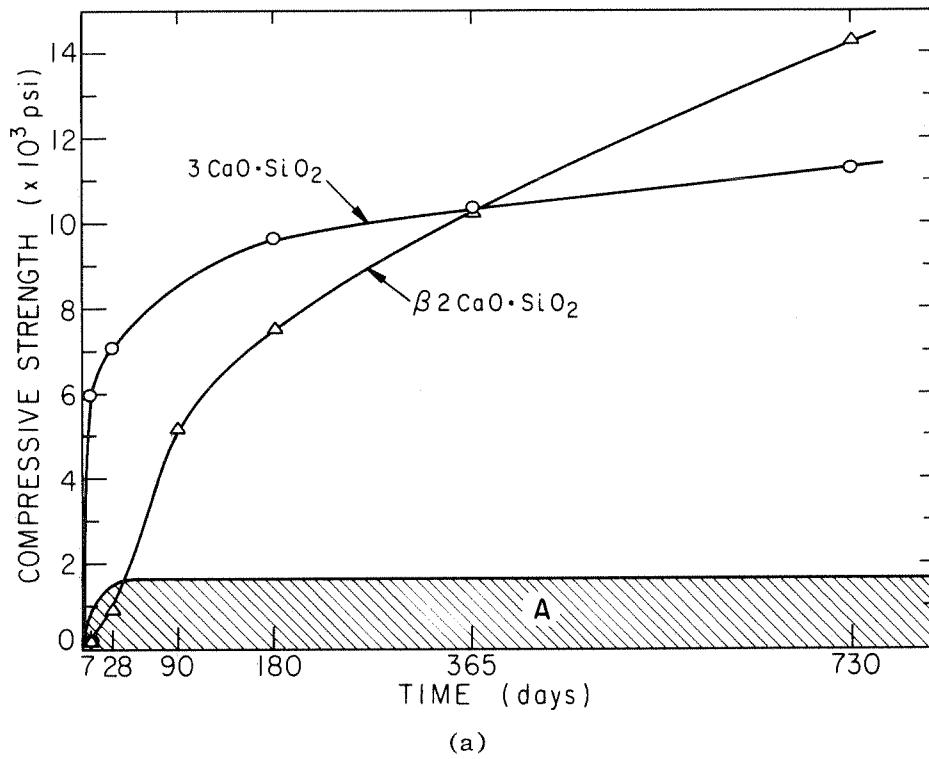


Figure 2.4 The compressive strength found by Bogue and Lerch (18) for hydrated samples of the pure cement phases C_3S and $\beta\text{-}\text{C}_2\text{S}$ are plotted as a function of age. The compressive strengths of C_3A and C_4AF , hydrated alone and with gypsum, fall within the cross-hatched region labeled A and have not been plotted explicitly. (a) The time scale is linear. (b) The time scale is logarithmic, which has the effect of expanding the early ages, and this shows the differences between strength gain C_3S and $\beta\text{-}\text{C}_2\text{S}$ pastes.

material during the first year. Pastes of β -dicalcium silicate are shown in Figure 2.4 to harden more slowly than those of tricalcium silicate, but attain strengths approximately equal to those by tricalcium silicate within a year. The subsequent gain in strength from one year to two years will be discussed later.

Another important feature shown in Figure 2.4 is that neat pastes made from the tricalcium aluminate and the ferrite phase develop only slight strengths, and their presence in portland cement contribute little to the strength of the hardened product. The latter statement implies that there is little synergistic effect of the aluminate and ferrite on the hardening of portland cement contain all four compounds. This point will be discussed later but perhaps it is enough to say that the strengths obtained with the calcium silicates are approximately those obtained from a normal portland cement paste.

3. MICROSTRUCTURE OF HYDRATED CEMENT PASTE

3.0 History

The most advanced microscopic techniques have always been applied to study the hydration of cement as they became available, and much of our knowledge of the microstructure of these systems dates back to classic work in the nineteenth century. LeChatelier (19) studied the hydration of portland cement very carefully and completely for that time, and he came to understand it very well. Any student of this system would do well to read this work, since it is instructive to see how much was known before the invention of many experimental techniques. LeChatelier studied the in situ hydration by optical microscopy and based many of his deductions on these observations. Following LeChatelier's work, similar studies were conducted by many investigators, including Stern (20,21), Ambronn (22), and Klein and Phillips (23). These studies were limited to high water-to-solids ratios and the resolution of the microscopes was poor by today's standards.

More recent studies of the hydration of cement in situ (24,25,26) have reduced the water-to-solids ratio to those encountered in practice, and quantitative information has been gained about growth of the hydration products, particularly portlandite. The in situ observation allows direct measurement of the growth rates of portlandite, but the calcium silicate hydrates remain below the resolution of the optical microscopes. The resolution is generally limited in these studies by the thickness of the sample and the differences in index of refraction between the materials being observed.

The use of petrographic thin sections has allowed more detailed study of the microstructure of cement pastes than the in situ studies, but they are necessarily limited to samples where hydration has been arrested in order to prepare the thin section. Colony (27) used petrographic techniques to study the hydration of neat cement pastes mixed at practical water-to-solids ratios. Further developments in optics and petrographic specimen preparation have led to greater insight in the subsequent studies (28,29,30). The observations of Brown and Carlson (29) were presented in the context of a solidification process and will be used in the following section to identify the microstructural zones in cement paste. The more recent study of Terrier and Moreau (30) has brought the technique of optical microscopy to the point where many aspects of the microstructure can be clearly depicted. Their work is a strong base on which to interpret the scanning electron micrographs presented below.

3.1 Identification of Microstructure Zones

In their classic paper "Petrographic Studies of Hydrated Cements," Brown and Carlson (29) described the events that occur within the originally water-filled space:

On mixing portland cement with water in the proportions commonly employed, it was observed that gel and calcium hydroxide began to form almost immediately. The hydroxide crystallized at numerous centers within the mass, the crystals gradually growing in size as hydration progressed. The gel developed around every cement particle and did not form in isolated units as did the hydroxide. After a few days of hydration, all of the intergranular spaces, excepting the air bubbles, appeared to be filled with either gel or calcium hydroxide.

This description was based on observations of polished thin sections of neat pastes using a light microscope, and it contains the essential features of the solidification of portland cement paste. The sequence of events and the location of deposition of products described by Brown and Carlson are organized in Table 3.1 for discussion of the solidification process. The "almost" immediate crystallization of portlandite throughout the originally water-filled space is the first feature of the reaction of cement with water. The exact timing of the early hydration was not possible in the thin sectional techniques used by Brown and Carlson, but it can be understood that "almost" immediately means between 8 and 24 hours after mixing with water. They noted that the portlandite was nucleated at "numerous"

Table 3.1 The Solidification of Cement Based on the Observations of Brown and Carlson (29)

TIME	LOCATION
1. "almost immediately"	portlandite at "numerous centers" within mass
2. not noted when first observed	"gel developed around every cement particle"
3. "as hydration progressed"	portlandite" gradually grow in size"
4. "after a few days hydration"	"all intergranular spaces appear filled with either gel or portlandite"
5. throughout hydration	"gel did not form in isolated unite" (in contrast to portlandite)

centers. This is a second important feature described by Brown and Carlson, and they also found that the number of portlandite nucleation sites could be increased by intergrinding a high-lime portland cement with 20 percent of volcanic tuff. Volcanic tuff is defined as a fragmental rock consisting of the smaller kinds of volcanic detritus, usually more or less stratified.

A third feature in Table 3.1 is that the "gel" formed around every grain. Brown and Carlson also noted that the "gel" did not form in isolated units, but this observation must be interpreted with the knowledge that the resolution was limited to 5-10 μ for the poorly defined hydrate material. This point will be discussed below since new scanning electron microscope evidence suggests that calcium silicate hydrate does form isolated units. It is sufficient to say that the framework provided by Brown and Carlson is complete and if new experimental tools help with the details it only means a minor change in the microstructure they describe.

The isolated portlandite crystals and the material which Brown and Carlson called "gel" are the most prominent outer hydration products. In very high water-to-cement ratios Brown and Carlson found that the "gel" was capable of filling all of the space not filled by the portlandite crystals, but necessarily it showed much greater porosity. In all cases they observed that the "gel" formed only around the cement grains, and although the terminology changes with other investigators (30) there is a zone of products around each grain. For the purpose of the following discussion, the outer hydration products growing at right angle to a cement grain or any other surface will

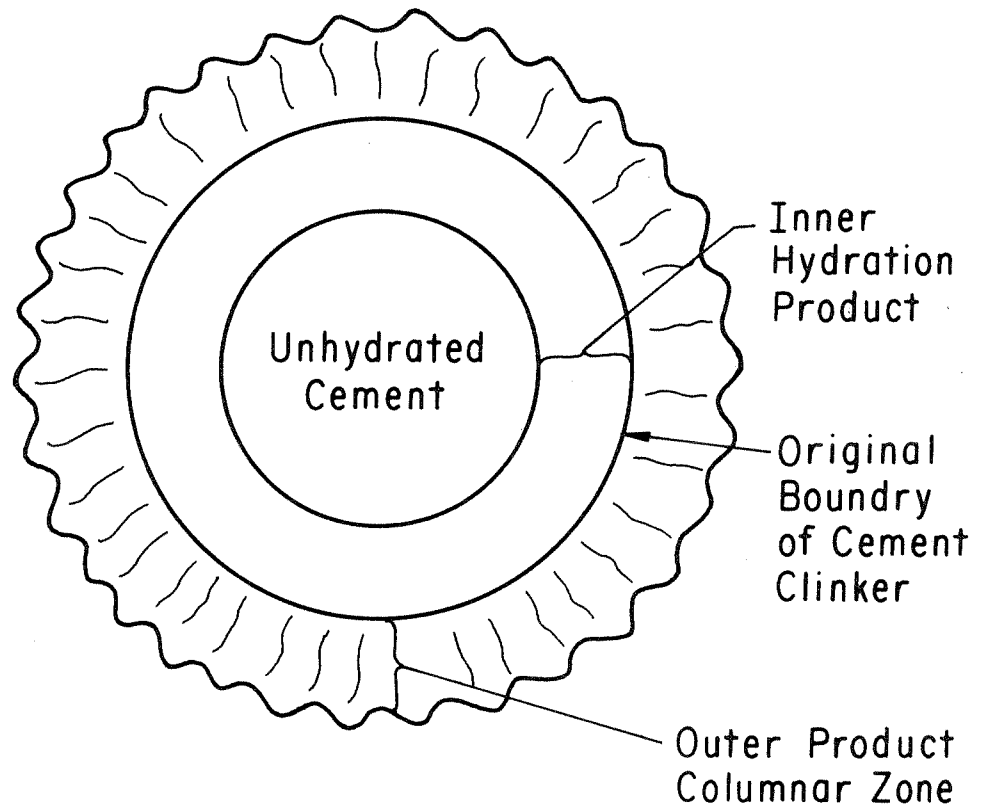


Figure 3.1 The hydration products formed inside and outside the cement grain are schematically represented. The multiphase nature of the cement grain is neglected and is assumed to be a single phase that shows two types of hydration products.

be said to be the "Columnar Zone" as shown schematically in Figure 3.1. This columnar zone is named for a similar structure that grows perpendicular to the walls of metal castings (3). A polished and etched section through a small aluminum ingot is shown in Figure 3.2(a) where the columnar zone has grown right to the center of the mold.

Another ingot is shown in Figure 3.2(b) in which the columnar zone in the lower half of the casting has been restricted to less than one quarter of the diameter by the growth of "equiaxed" grains which have filled the central portion of the casting. The grain refiners mentioned above are used to eliminate the columnar zone in metal casting by promoting the growth of thousands of equiaxed grains which choke off the growth from the walls of the mold.

In choosing the term "columnar zone" there is no intent to restrict the possible origins of the morphology observed there. The column aspect of this zone is due to the growth perpendicular to the surfaces, and there is no single phase or chemical feature assumed for this zone.

The growth of the inner hydration product shown in Figure 3.1 under some conditions can lead to the formation of a pseudomorph of the original cement grain. There have been both optical (30,31) and electron microscope (32) observations of pseudomorphs in cement pastes, but their identification has not been possible in all cement pastes. This has led to some controversy as a general effect (14). This will be discussed at some length below.

The formation of a pseudomorph in the space originally occupied by a cement grain does not necessarily mean a simple or easily

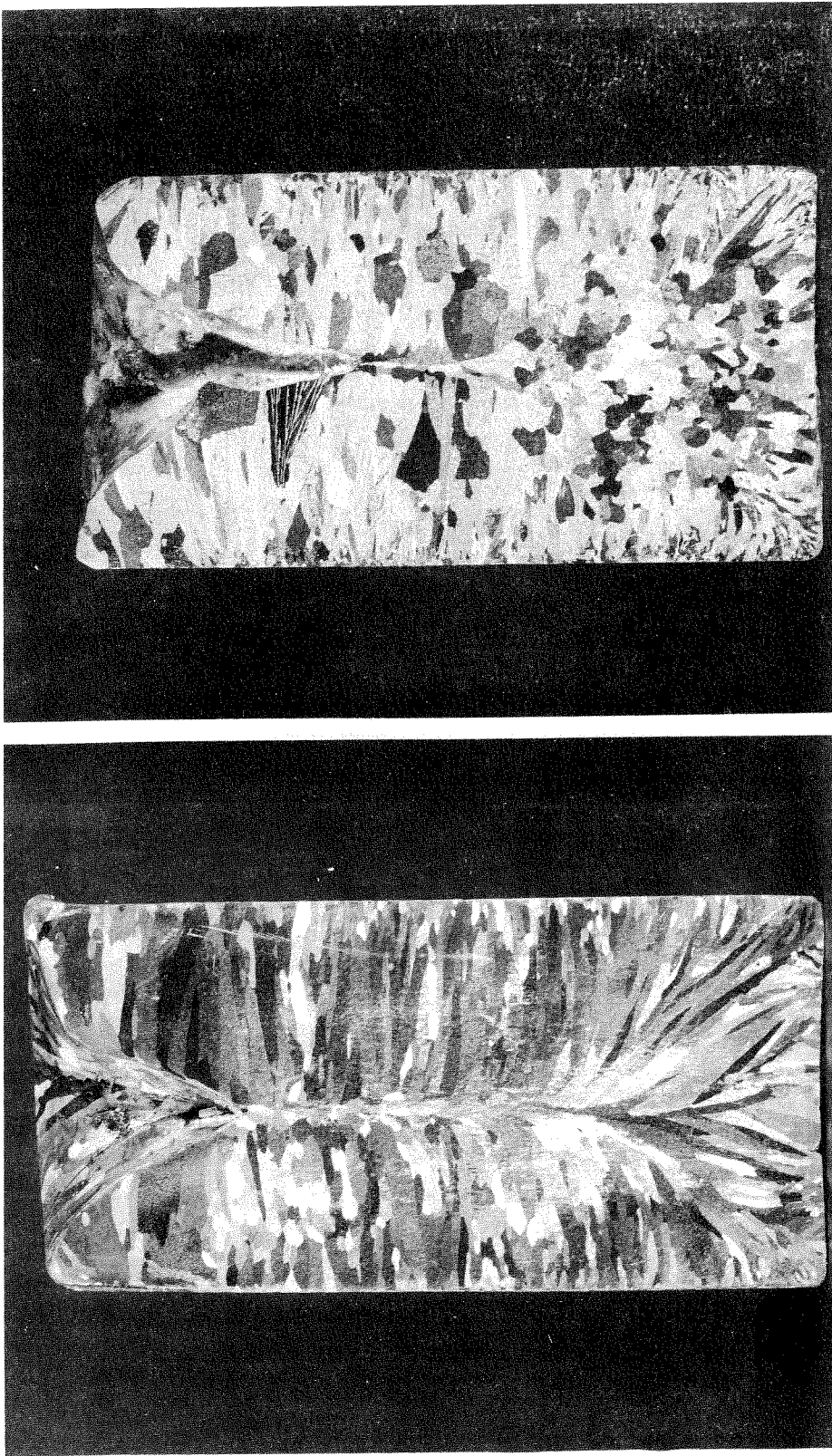


Figure 3.2 Solidified structure on a polished and etched section at the mid-plane of small aluminum ingots showing columnar zones growing at right angles to the mold walls; molds approximately two inches in diameter. (a) A pure aluminum ingot showing a columnar zone that has grown right to the center. (b) An aluminum -2.5% copper alloy ingot where the columnar zone in the lower half has been restricted to less than one quarter of the diameter by the growth of equiaxed grains. The columnar zone in the upper portion of the ingot grew right to the center since the equiaxed grains settled to the bottom. Chalmers reviews the structure of cast metals in Chapter 8 of Ref. 3. The ingots shown here appear in that discussion.

characterized process occurs. Powers described the general phenomenon in a most matter-of-fact way (13):

"Although tricalcium silicate dissolves congruently, the composition of the hydration product laid down inside the original crystal boundary may not be the same as that of the product outside. In the first place, if the inside product forms in a supersaturated solution, its stoichiometry might not be the same as that of the outside product. In the second place, if the calcium ions can diffuse through the gel faster than silicate ions, which seems very likely to be the case, calcium hydroxide should reach the outside faster than calcium silicate. Indeed, it seems likely that all the calcium hydroxide derived from the calcium silicate is deposited outside the original crystal boundaries."

The chemistry of this reaction has been presented in many different ways (33), but it is difficult to interpret the possible mechanisms without direct microscopic observation of the process. The following presentation of the microstructure of cement pastes will illustrate how both the inner and outer products intergrow so that a complete analysis of their formation is difficult to formulate.

One of the primary advantages of the scanning electron microscope is that the spatial distribution of hydration products can be shown with approximately the same detail that metallurgists can observe cast structure of metals. If the lessons of optical microscopy are utilized in analyzing the scanning electron micrographs, then the cement and concrete specialist should have a new research tool to help in solving service failure problems as well as gaining new insight into the mechanisms of cement hydration.

3.2 Microstructure of β -Dicalcium Silicate Pastes

Pure β -dicalcium silicate* paste was cast in miniature metal molds with a 0.5 water-to-solids ratio, and fracture surfaces were observed by scanning microscopy at 60, 100, 171 and 384 days age. The 60-day specimen is shown in a sequence of micrographs in Figures 3.3(a,b,c,d). The fracture has occurred generally through the water-filled space which initially separates the grains. These micrographs show hydration products growing on each grain in a columnar zone.

A region of the fracture surface of 100 day old β -dicalcium silicate paste is shown in a series of micrographs in Figures 3.4(a,b,c,d). These appear similar to the 60 day old specimen shown in the previous figures with slightly more growth of hydration products in the columnar zone around each grain. It is interesting to compare Figure 3.4(d) with Figure 3.3(d); it appears in Figure 3.4(d) that the unhydrated core in the center of the grain has been uncovered by the fracture process in much the same way that the unhydrated core may have been removed from the grain shown in Figure 3.3(d). Another region of the fracture surface of the 100 day old β -dicalcium silicate paste is shown in Figure 3.5(a,b,c,d) since it illustrates microstructural features not found in the 60-day specimen. There appear to be areas in the central portion of Figure 3.5(b) where the hydration products growing from each grain have interlocked to form a solid material. Portions of a portlandite crystal may be behind the smooth areas in Figures 3.5(b) and 3.5(c), but the fracture path does not

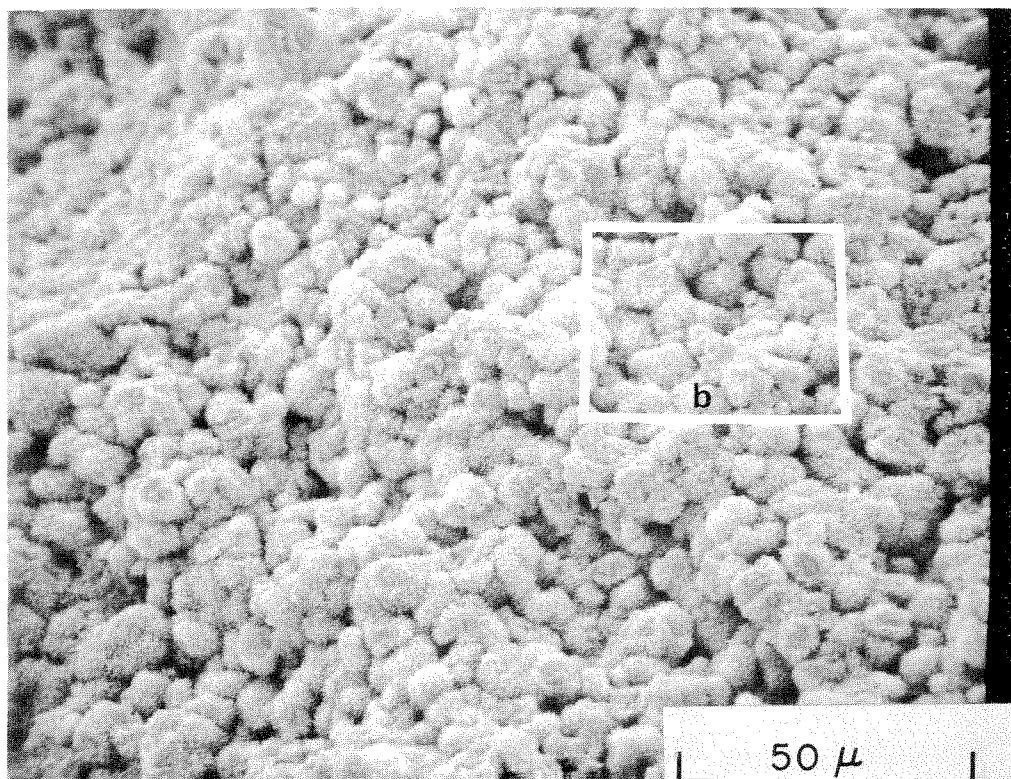
* Please see Appendix for experimental details and analysis of materials.

appear to have traversed any portlandite crystals by cleavage.

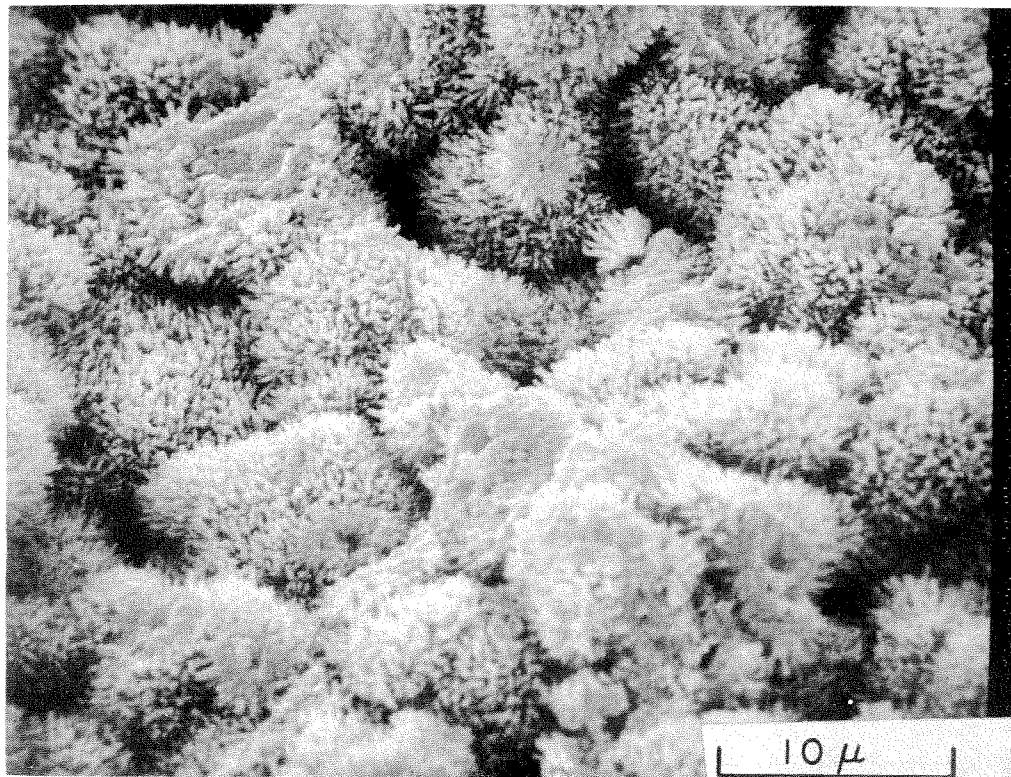
Micrographs of the fracture surface of the 171 day old paste are shown in Figures 3.6(a,b,c,d). There appears to be more solid material between the grains in these micrographs than those from earlier ages. On the other hand, the characteristic columnar zone is still visible in the pores between the grains as shown in Figures 3.6(c) and 3.6(d).

The fracture surface of the 384 day old specimen contains two large cavities over 200μ in diameter which had been apparently filled by portlandite. One of these filled cavities is shown in Figures 3.7(a) and (b), and the other cavity is shown in Figures 3.8(a) and (b). The entire volume of each cavity is occupied by a single crystal of portlandite which shows evidence of growth into the paste in several places shown in Figures 3.7(c), 3.7(d), and 3.8(d). The single crystal nature of these areas is evident from the parallel cleavage traces, and it is identified as portlandite by its size and fracture pattern. These large areas of fractured portlandite are the first observed in this series of β -dicalcium silicate pastes, and their implication to the strength of the paste will be discussed below.

The growth of the portlandite into the paste is shown in more detail in Figures 3.9(a,b,c,d), and it is apparent that the portlandite within the paste has the same orientation as that in the cavity. The portlandite above the cavity shown in Figure 3.7(a) grew at least 200μ into the paste. The interface between the cavity and the paste is shown in Figure 3.9(b) and micrographs showing the details of the portlandite-intergrown paste above the cavity are shown

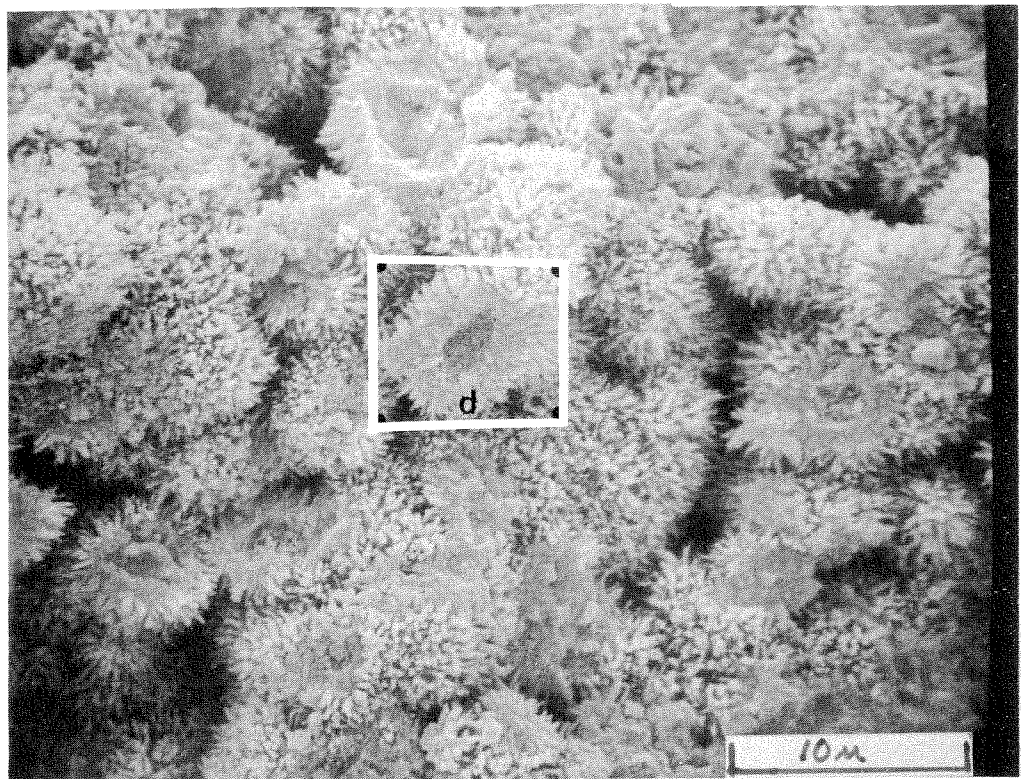


(a)

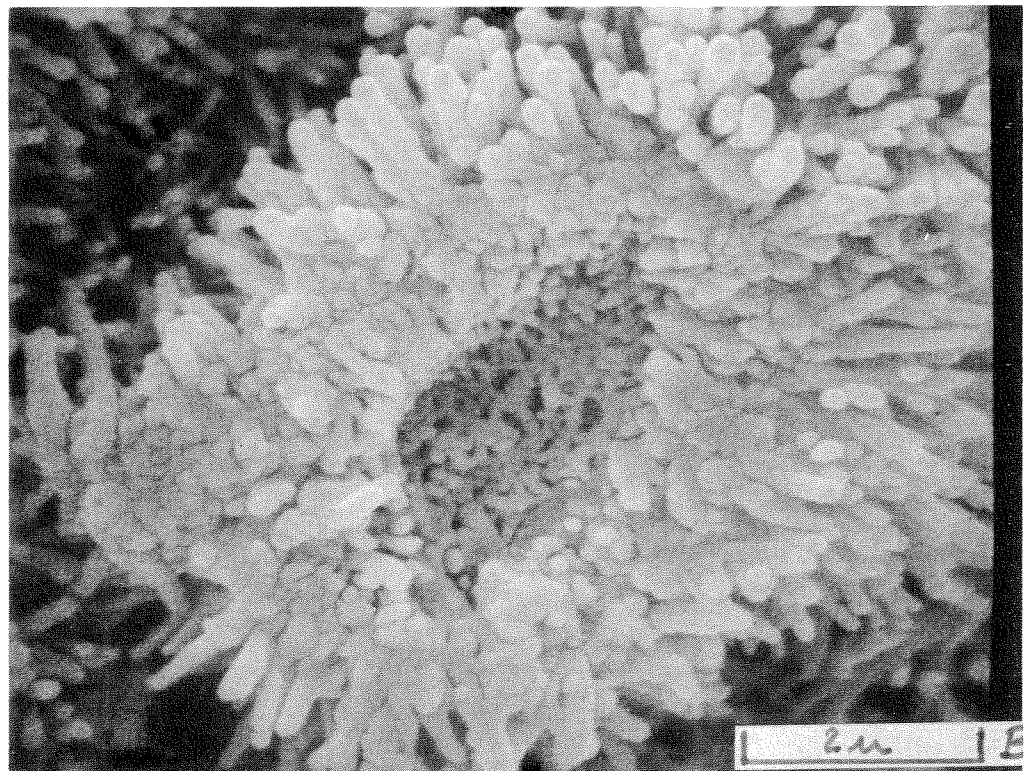


(b)

Figure 3.3 Fracture surface of β -dicalcium silicate paste hydrated 60 days. Details of specimen preparation given in Appendix. (a) Low magnification scanning electron micrograph showing that the fracture occurred primarily through water-filled space leaving the individual grains exposed. (b) Close-up of an area marked in (a).

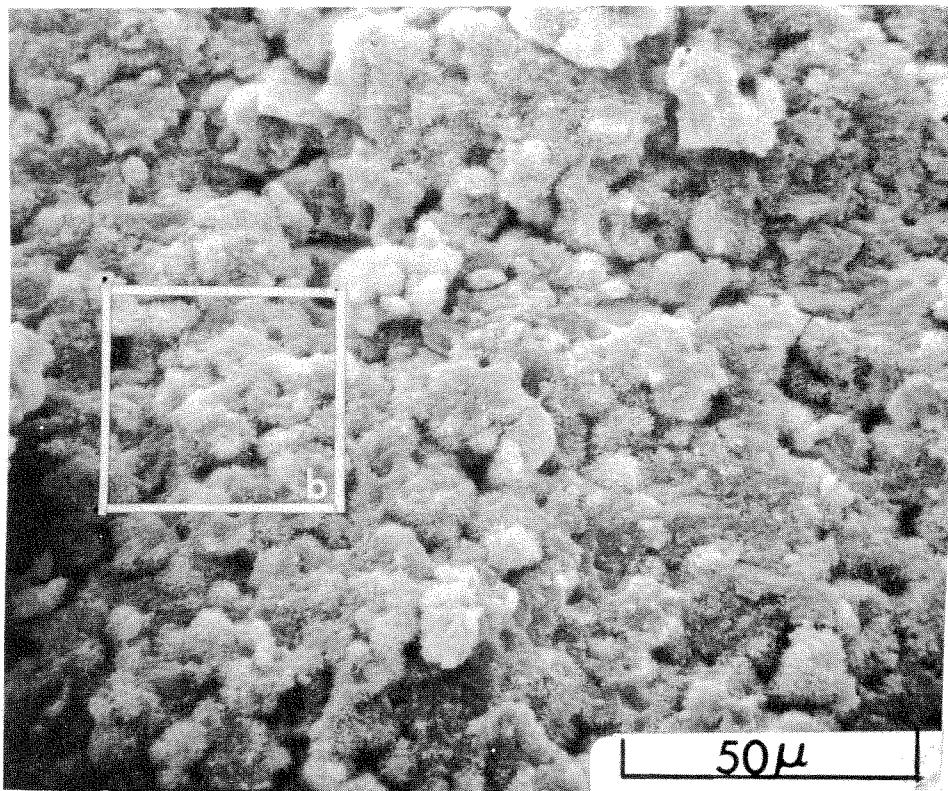


(c)

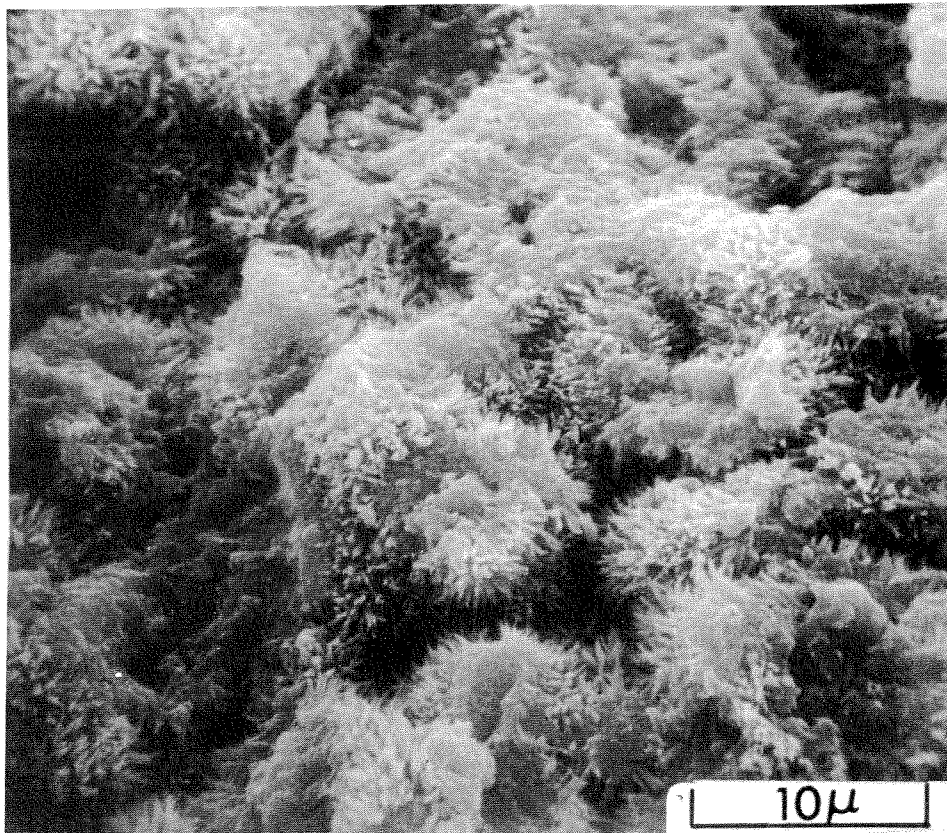


(d)

Figure 3.3 (Continued from opposite page)... (c) Another region on the same fracture surface showing places where unhydrated cores apparently pulled out of the surrounding hydration products. (d) Close-up of an area marked in (c).

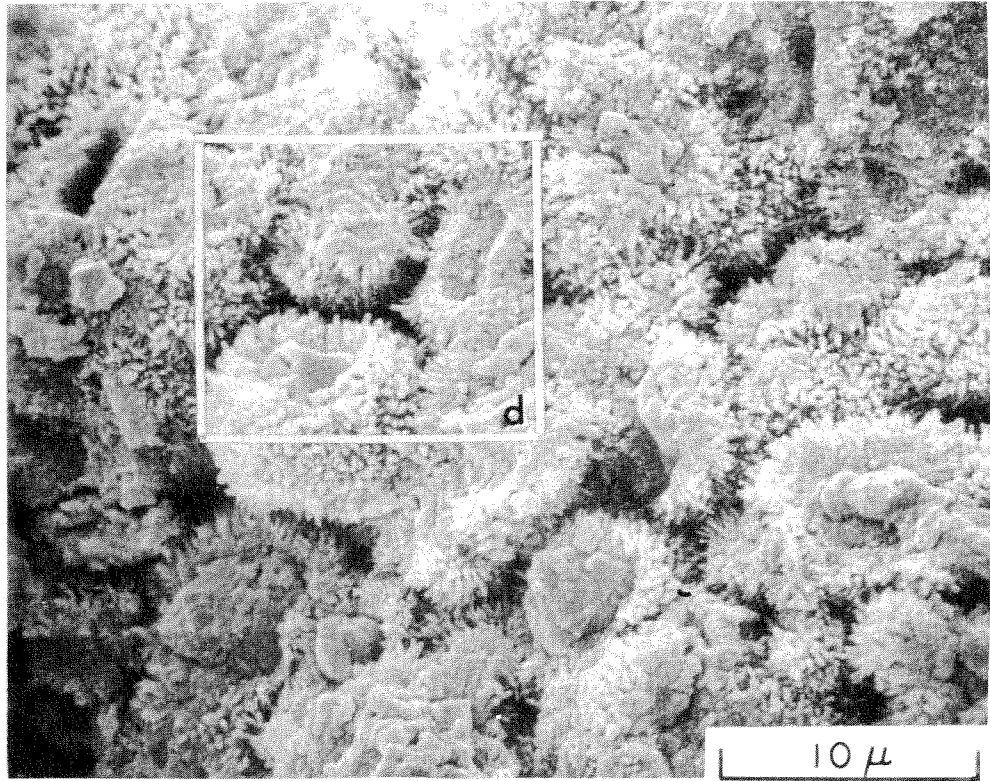


(a)

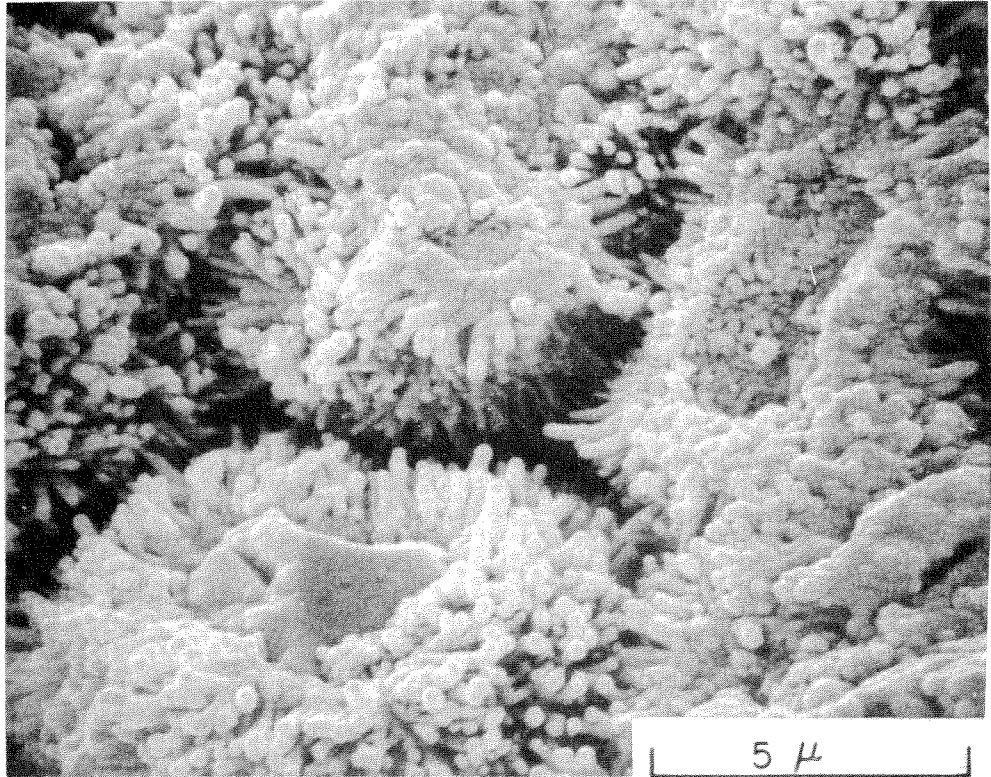


(b)

Figure 3.4 Fracture surface of β -dicalcium silicate paste hydrated 100 days. (a) Low magnification scanning electron micrograph showing the granular texture of the 60-day specimen is still apparent. (b) Close-up of an area marked in (a).

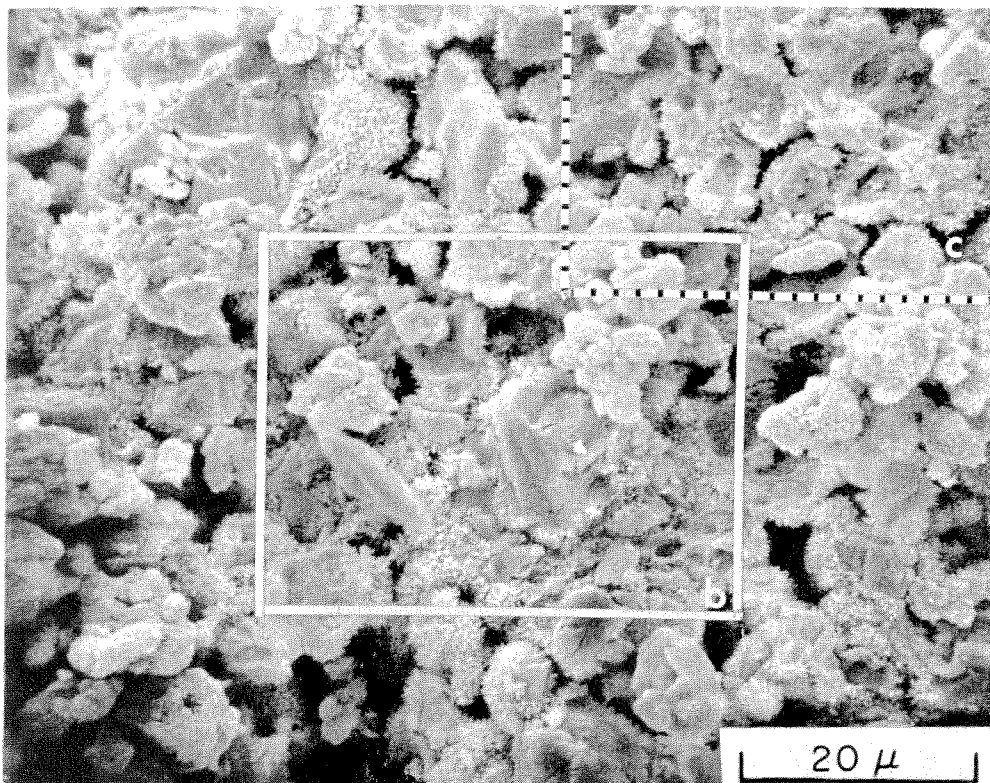


(c)

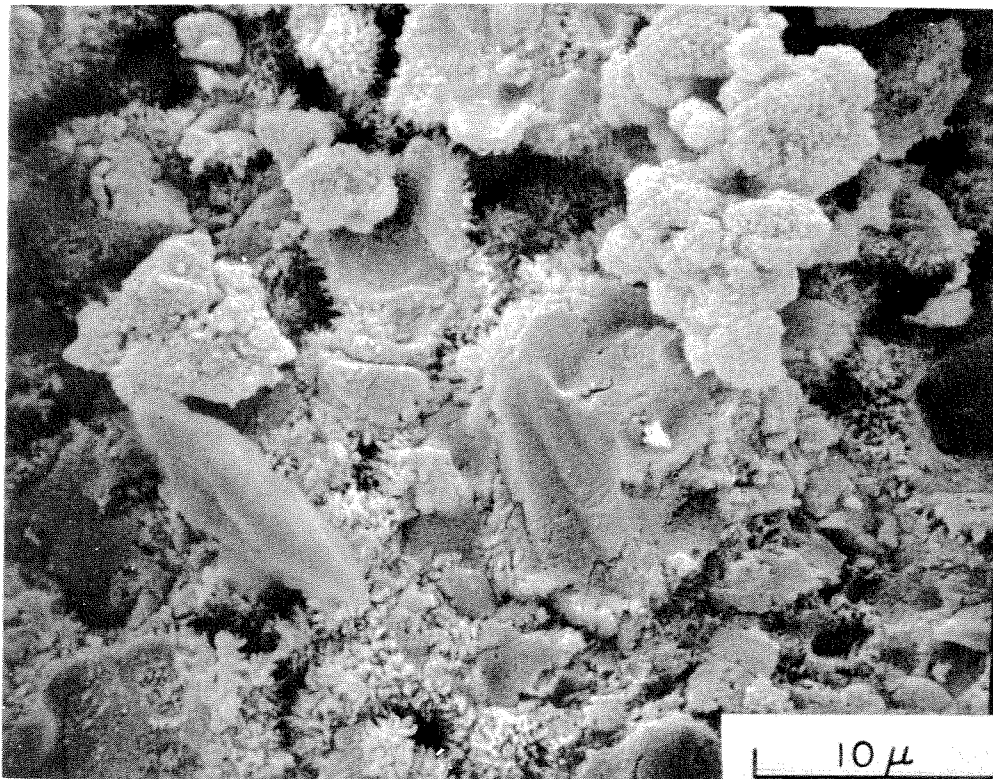


(d)

Figure 3.4 (Continued from opposite page)...(c) Another region on the same fracture surface showing places where unhydrated cores have been uncovered. (d) Close-up of an area marked in (c).

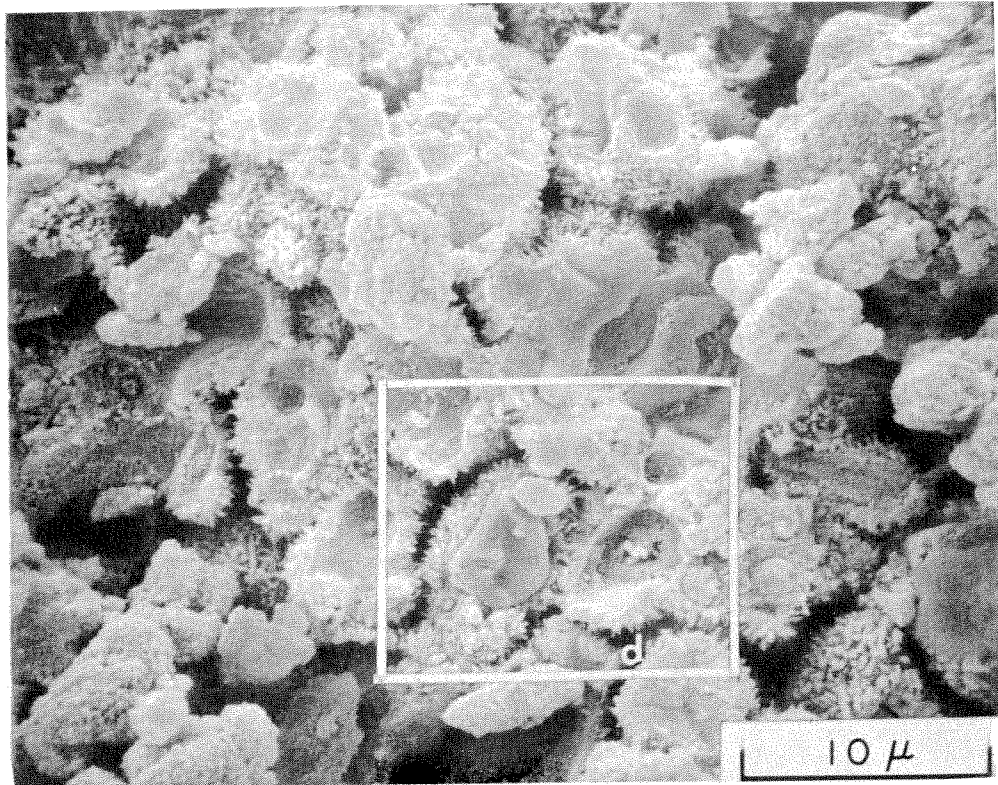


(a)

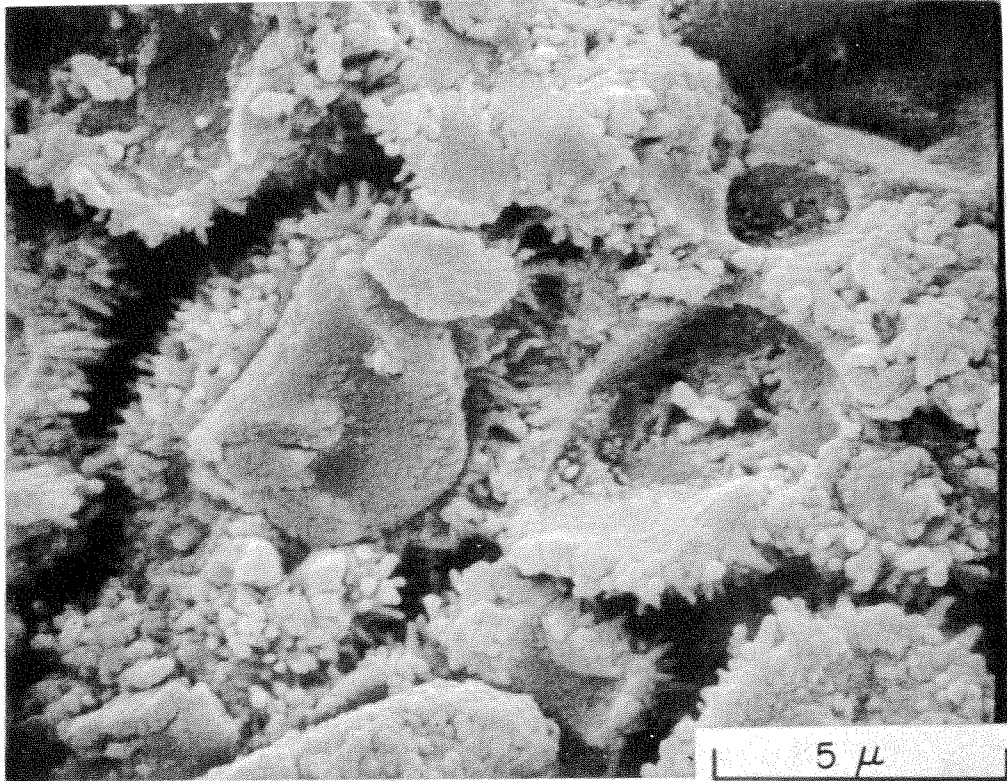


(b)

Figure 3.5 Another area of the 100-day old β -dicalcium silicate paste showing how the hydration products growing from each grain have interlocked to form a solid material. (a) Portlandite crystals may be under several of the denser regions such as the one enlarged in (b).

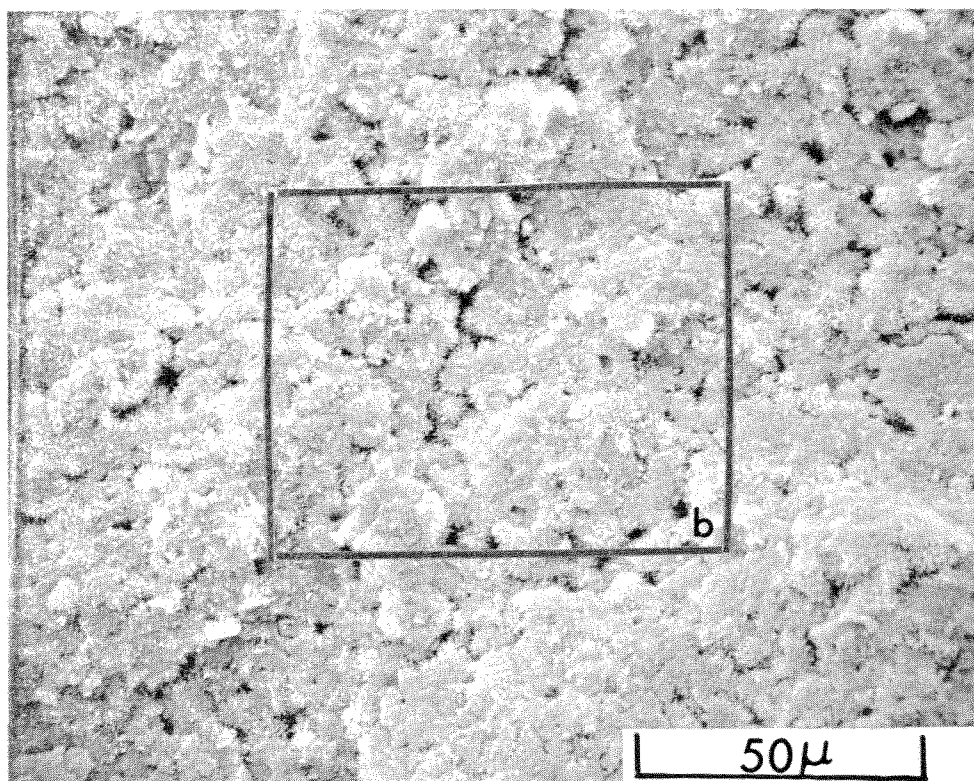


(c)

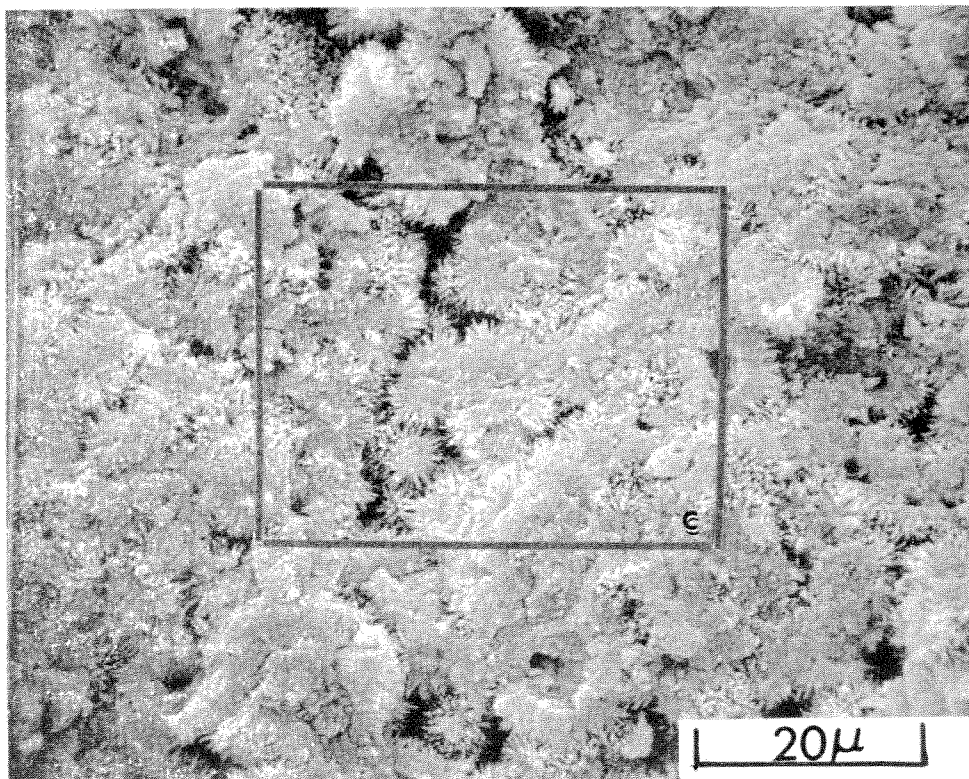


(d)

Figure 3.5 (Continued from opposite page)...(c) Another close-up of an area marked in (a) where the interlocking is particularly clear. (d) A close-up of an area marked in (c) where both a core (possibly unhydrated) and a pocket formed by the removal of a core are shown.

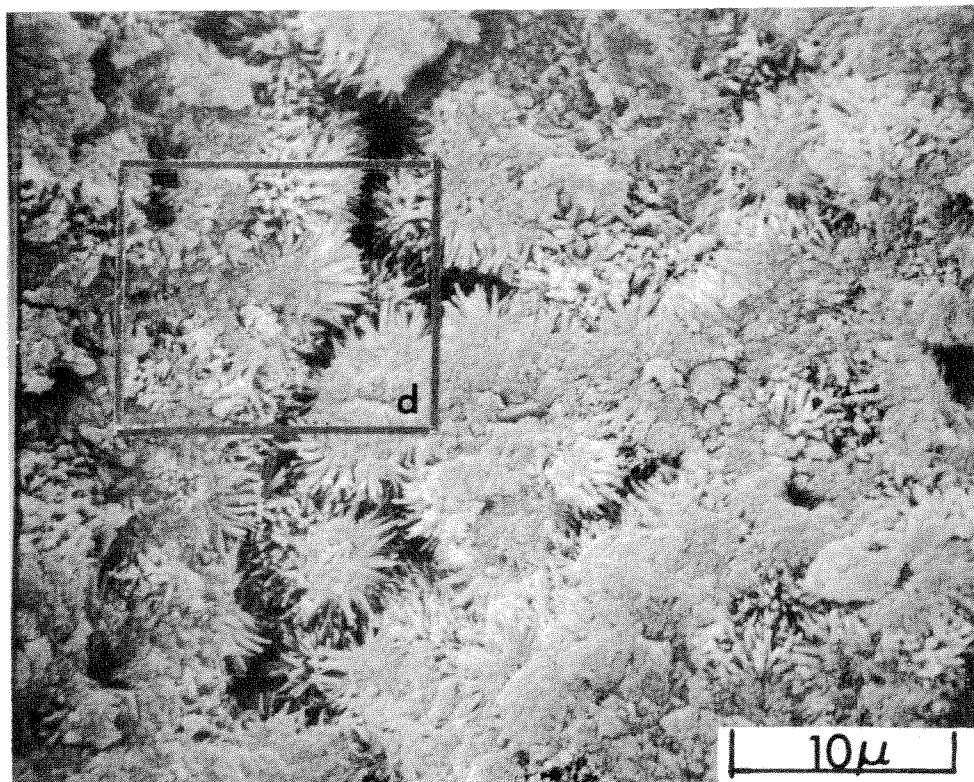


(a)

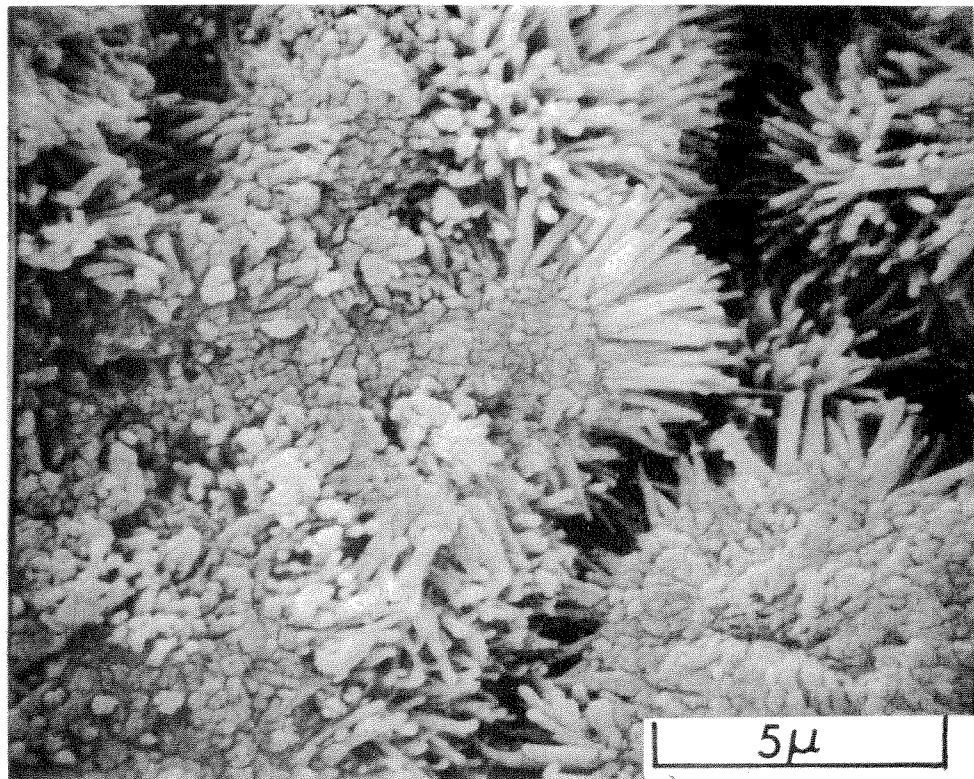


(b)

Figure 3.6 Fracture surface of β -dicalcium silicate paste hydrated 171 days. (a) Low magnification scanning electron micrograph showing large areas where the individual grains have been "cemented" together by their columnar zones intergrowing. (b) A close-up of an area marked in (a).

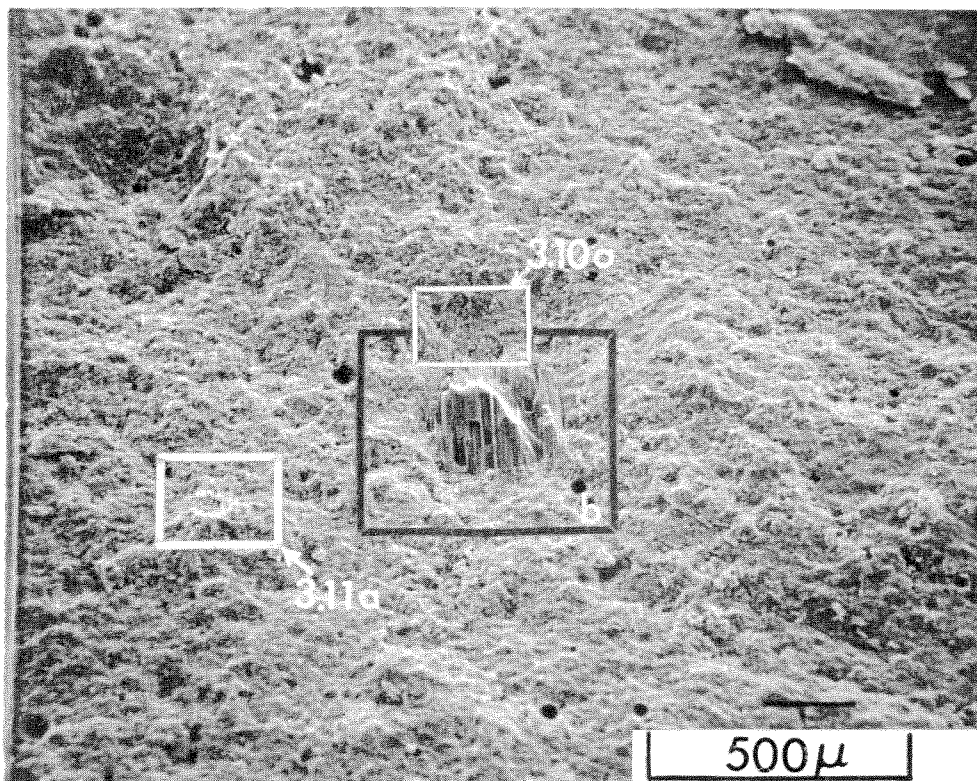


(c)

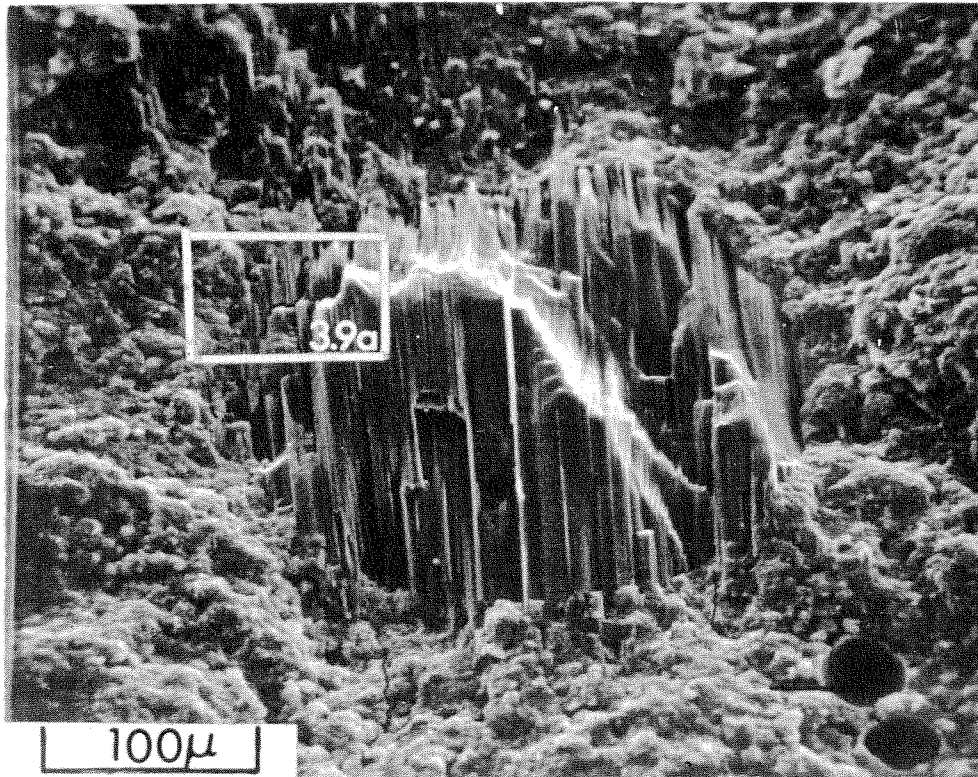


(d)

Figure 3.6 (Continued from opposite page)... (c) A close-up of an area marked in (b). (d) A close-up of an area marked in (c), the granular texture visible in this micrograph may be an artifact of specimen preparation.

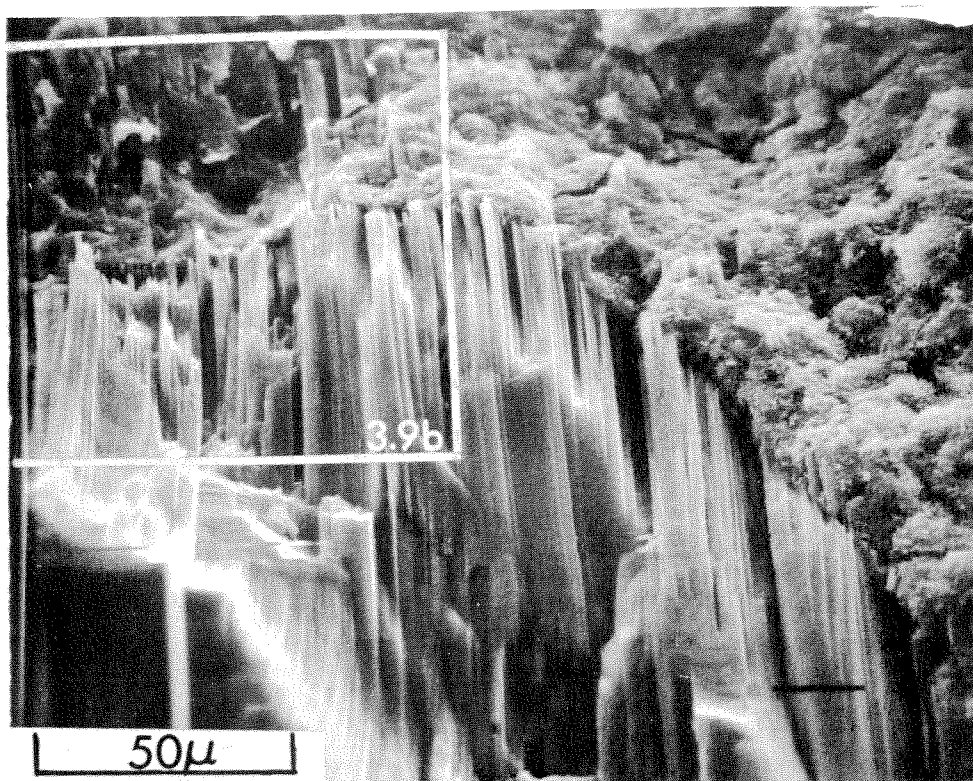


(a)

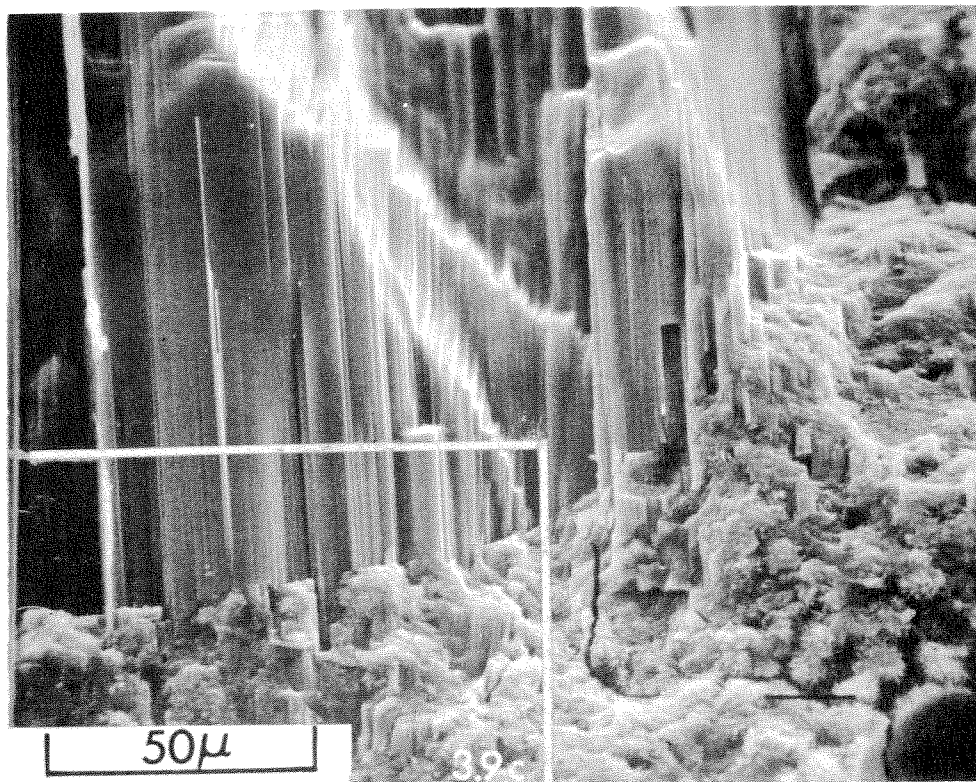


(b)

Figure 3.7 Fracture surface of β -dicalcium silicate paste hydrated 384 days. (a) Very low magnification scanning electron micrograph showing at the center a large cavity apparently filled by a portlandite crystal. (b) Close-up (although still at low magnification) of the filled cavity as marked in (a). Note that later figures will show details of several areas on this fracture surface.

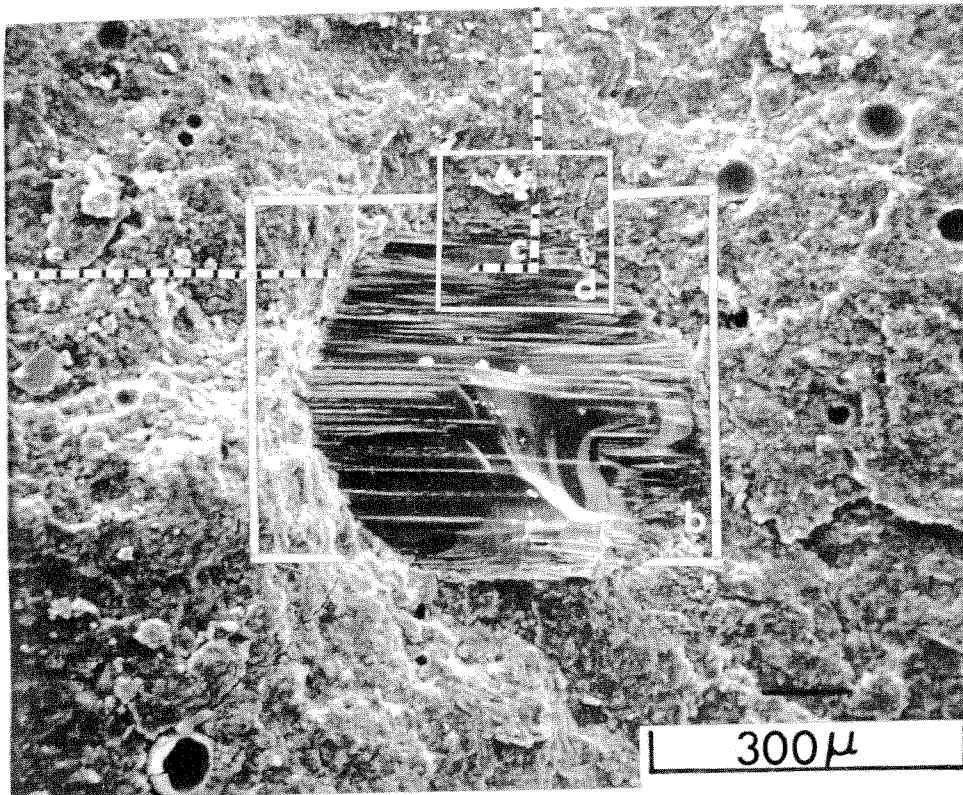


(c)

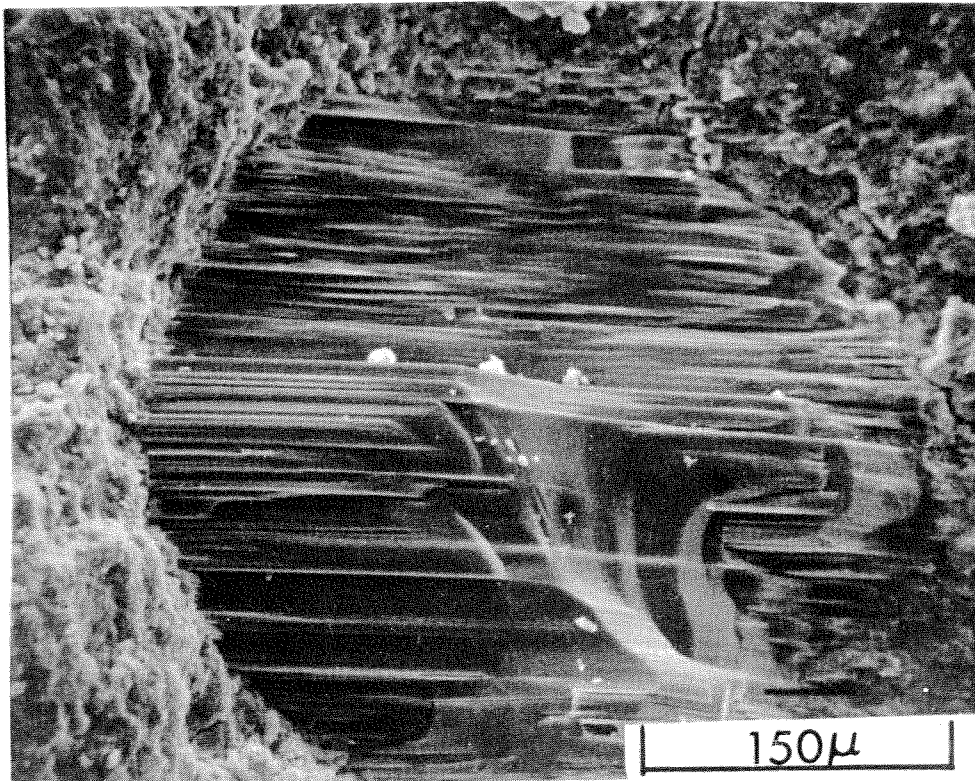


(d)

Figure 3.7 (Continued from opposite page)...(c) A close-up of an area marked in (b). (d) Another area marked in (b). Note that these "close-ups" are at approximately the same magnification of the lowest magnification of the fracture surfaces shown in Figures 3.3 through 3.6.

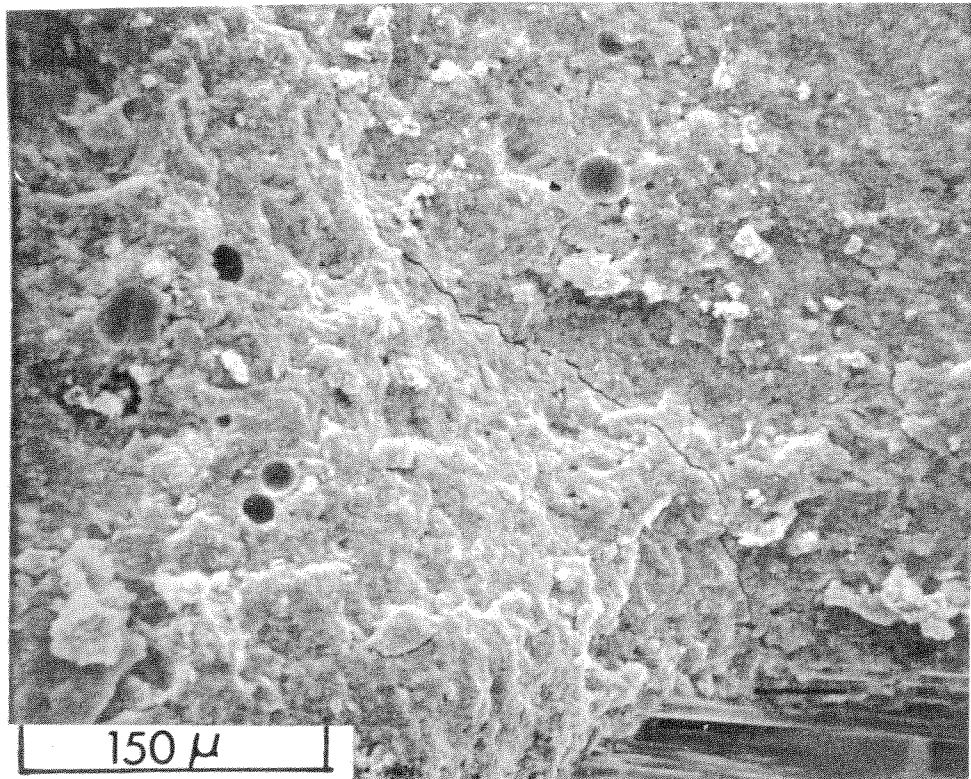


(a)

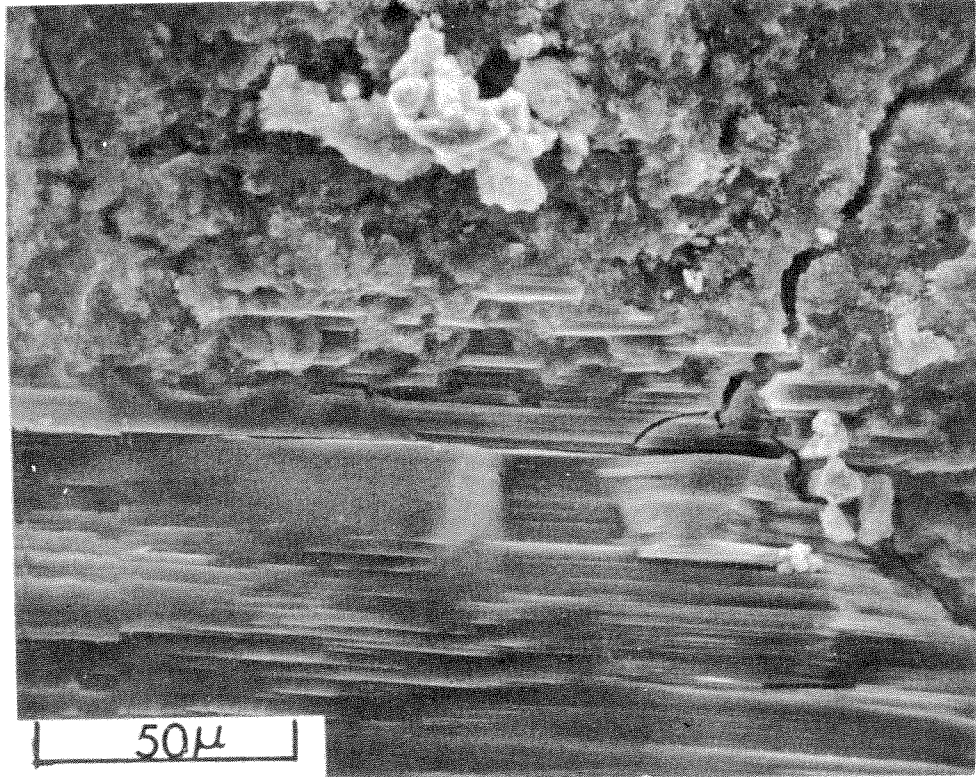


(b)

Figure 3.8 Another area of the 384-day old β -dicalcium silicate paste showing a large cavity filled apparently with portlandite. (a) Very low magnification scanning electron micrograph showing that this is a different area from that shown in Figure 3.7(a). (b) A close-up of the cavity as marked in (a).

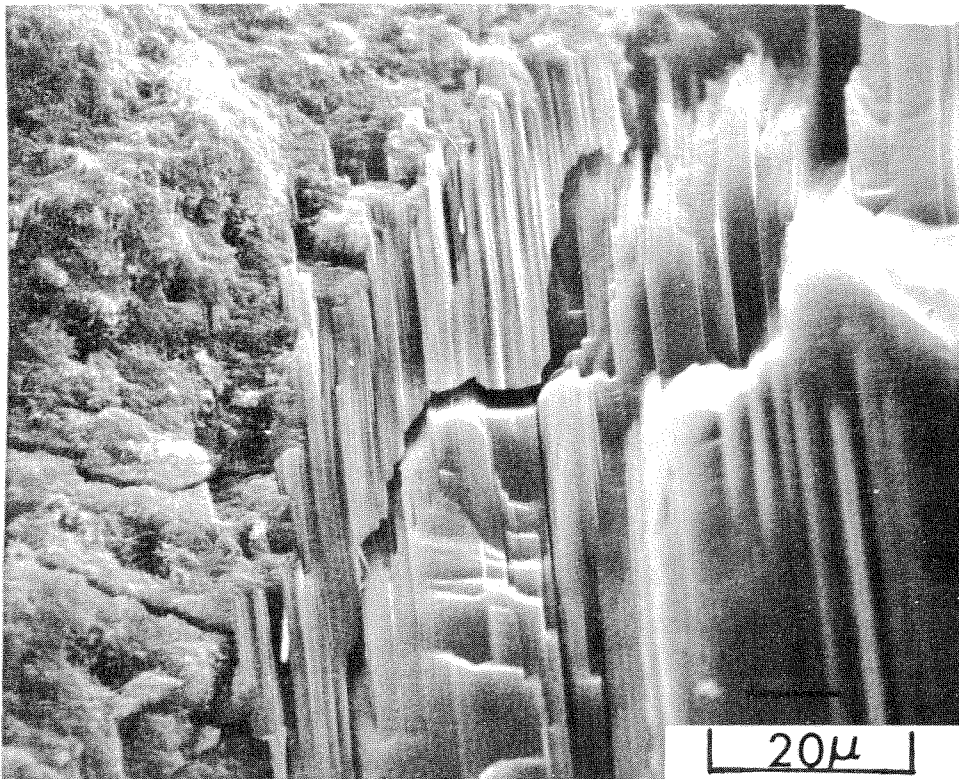


(c)

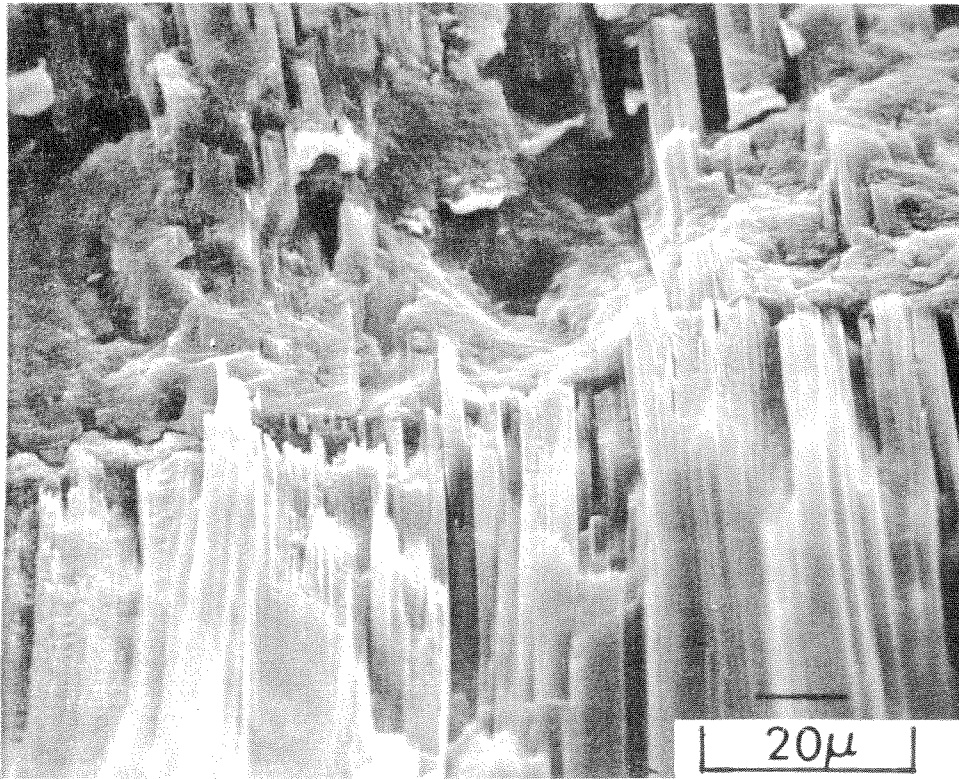


(d)

Figure 3.8 (Continued from opposite page)...(c) An area just above the cavity as marked in (a). (d) Close-up of the boundary between filled cavity and the paste.

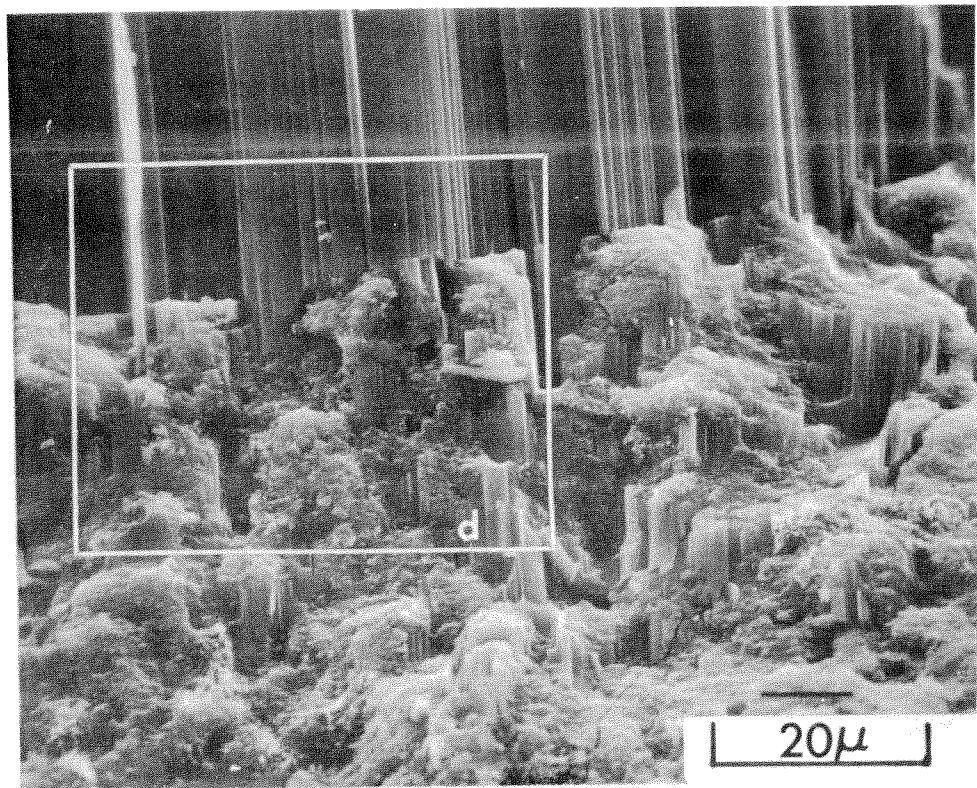


(a)

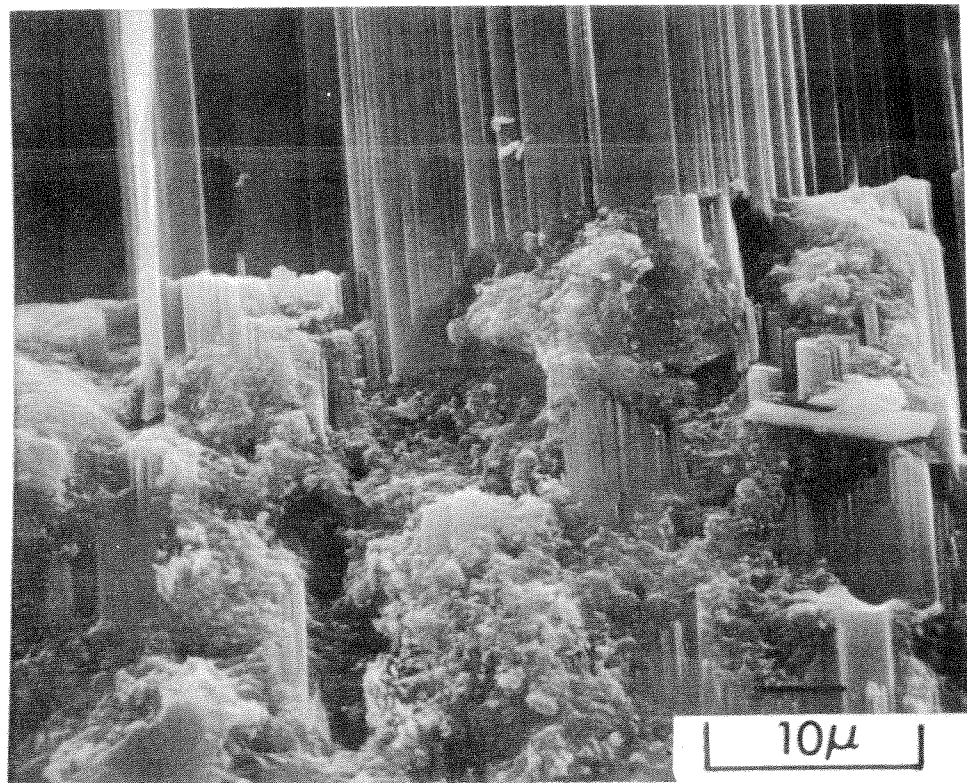


(b)

Figure 3.9 Higher magnification micrographs showing the details of the boundary of the filled cavity shown in Figure 3.7. (a) This picture shows an area where the crystal filling the cavity has fractured leaving some attached to the paste, but there is little growth into paste. (b) This picture shows where the crystal filling the cavity has grown right into the paste and more micrographs in Figure 3.10 will show the extent of this growth.

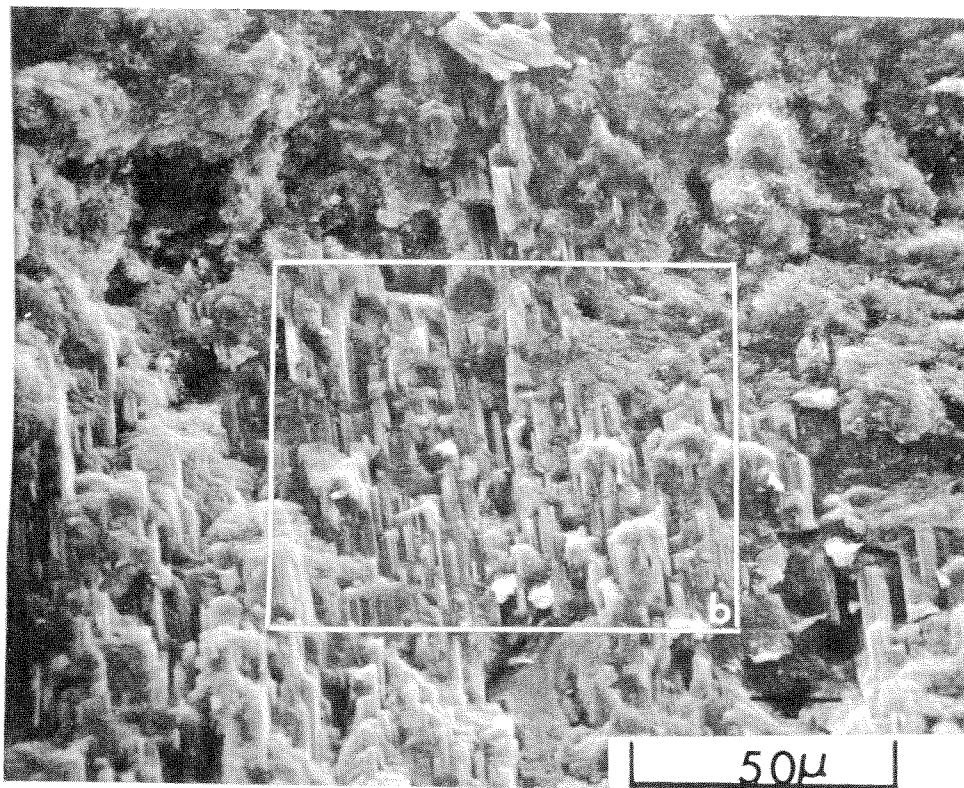


(c)

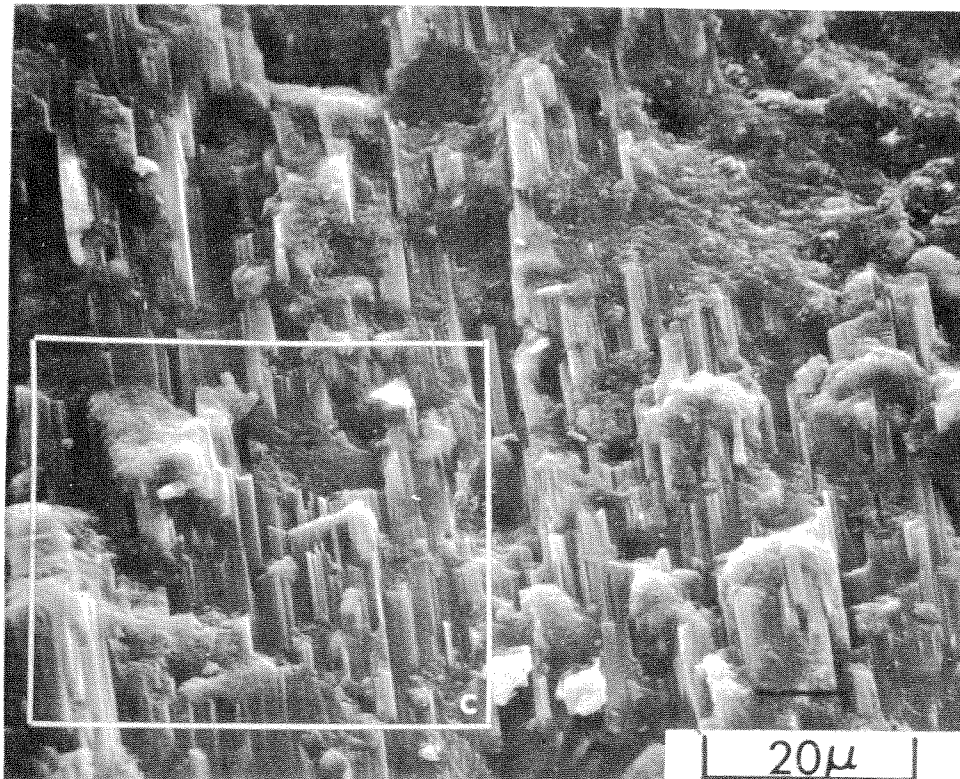


(d)

Figure 3.9 (Continued from opposite page)...(c) The opposite side of the cavity from that shown in (b) also show extensive intergrowth of cavity filling crystal, presumably portlandite. (d) Close-up of an area marked in (c).

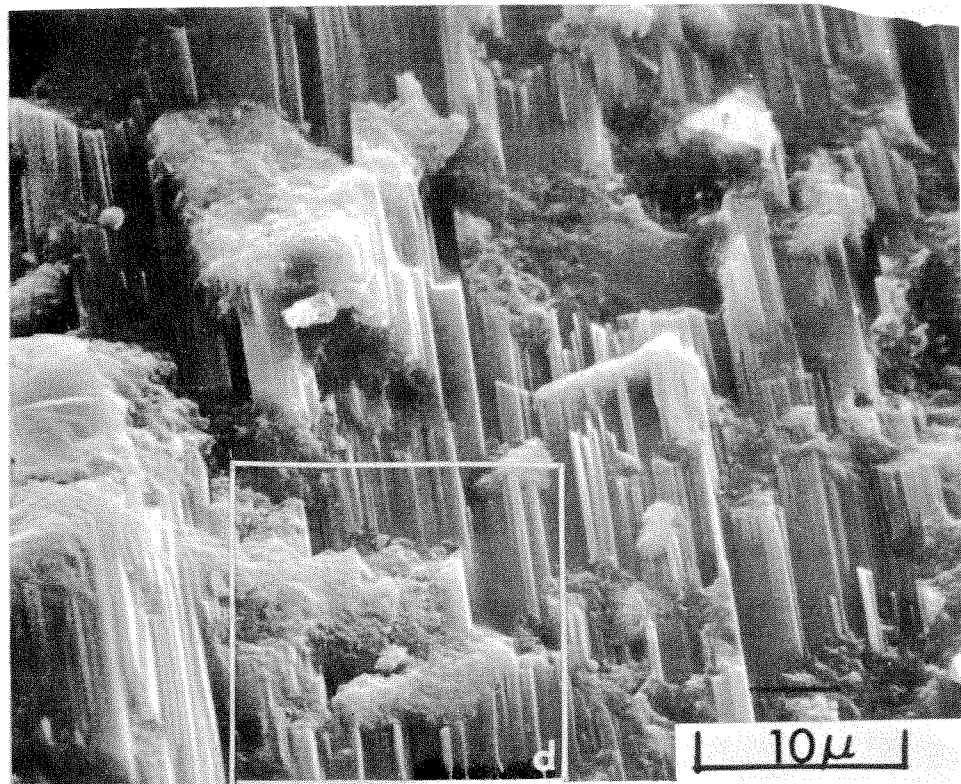


(a)

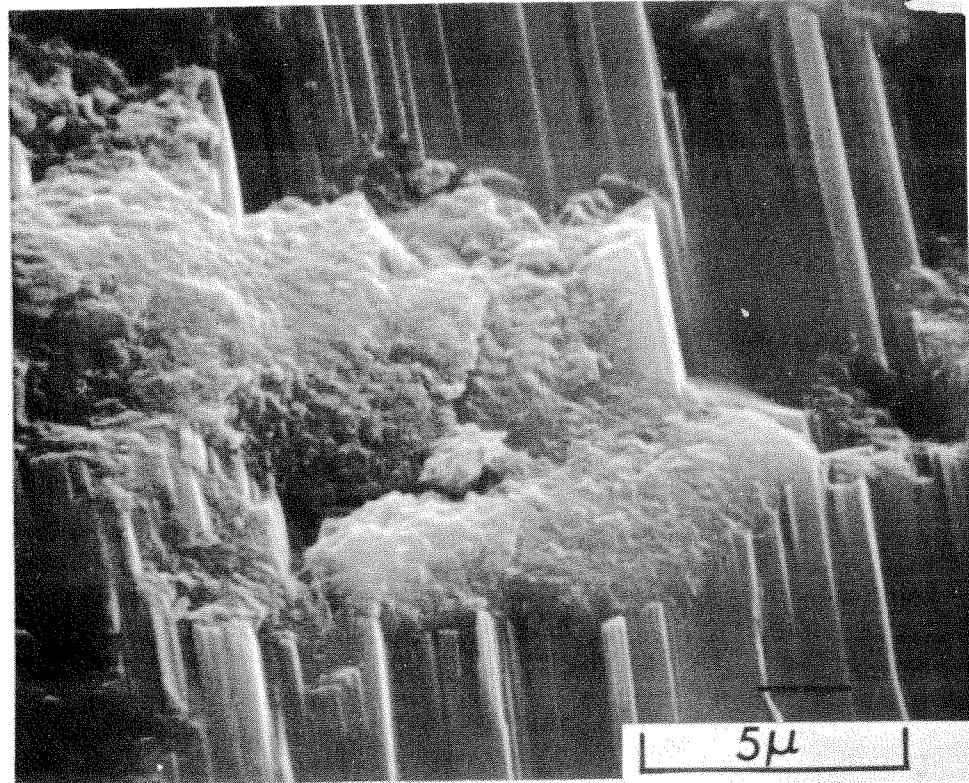


(b)

Figure 3.10 Micrographs showing how the single crystal of portlandite from the cavity shown in Figure 3.7 has grown within the water-filled space between the β -dicalcium silicate grains. (a) The location of this area is indicated in Figure 3.7(a). (b) Close-up of an area marked in (a).

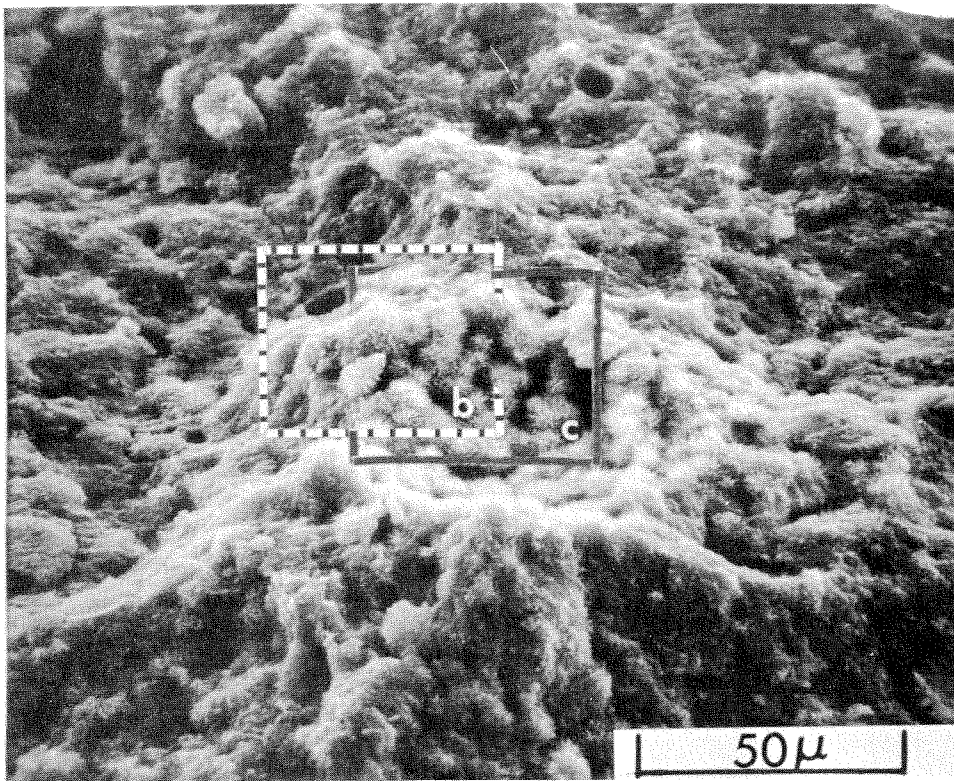


(c)

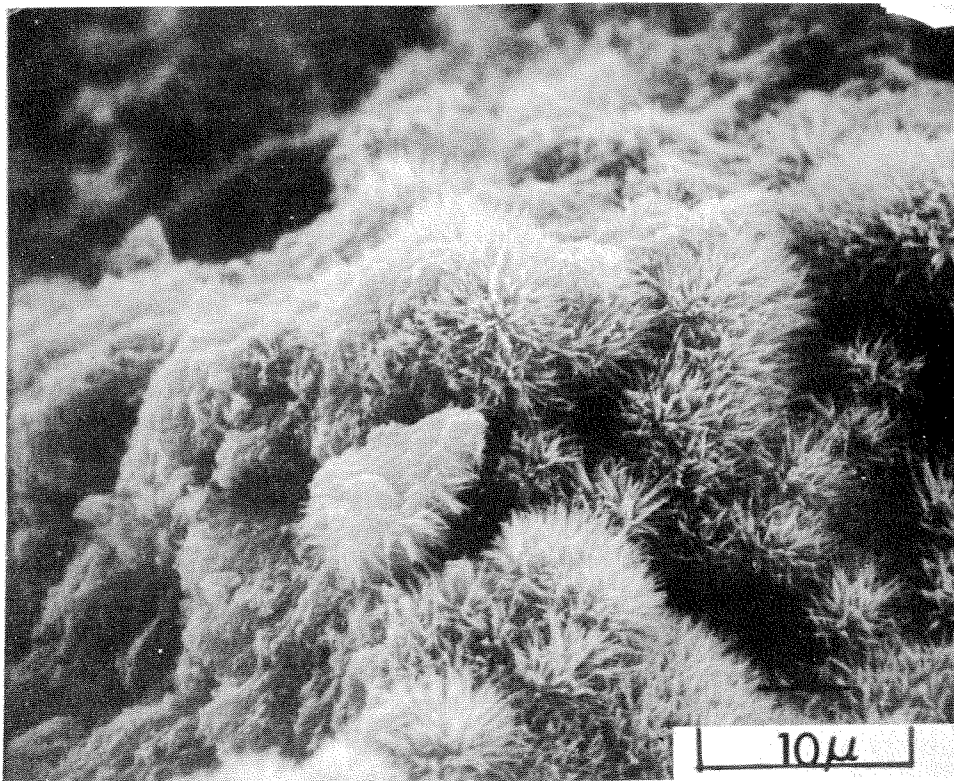


(d)

Figure 3.10 (Continued from opposite page)... (c) A close-up of an area marked in (b) which is typical of the region. (d) A close-up of an area marked in (c) which shows a lack of a well developed columnar zone around the engulfed grains; this seems to indicate that this portlandite grew at an early age.

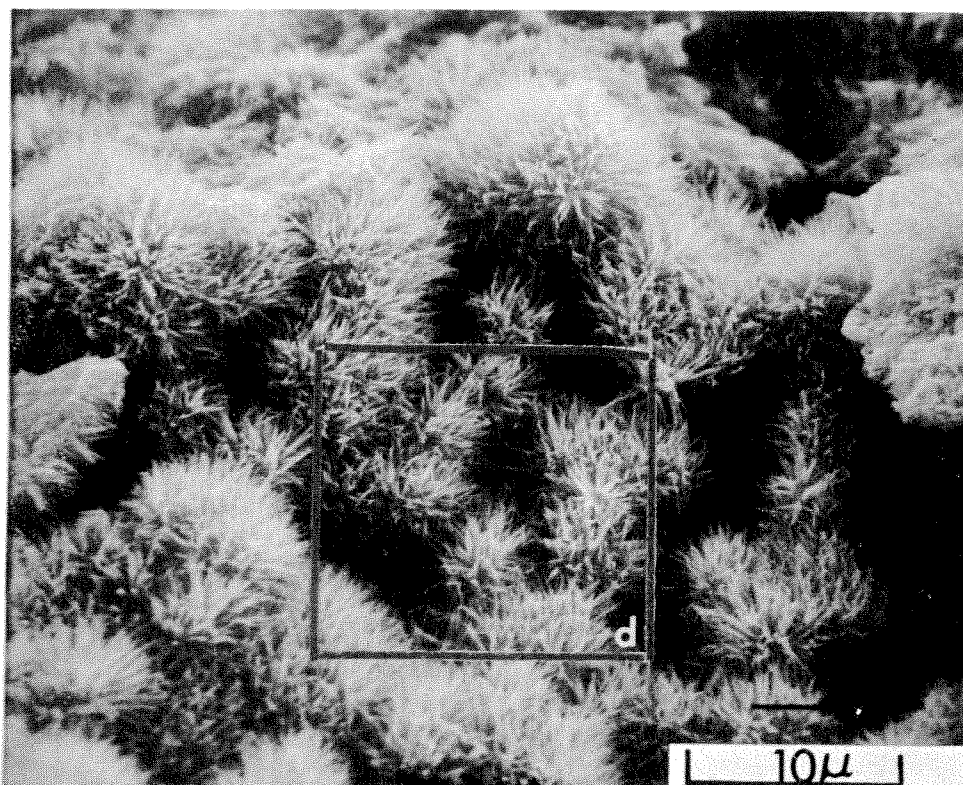


(a)

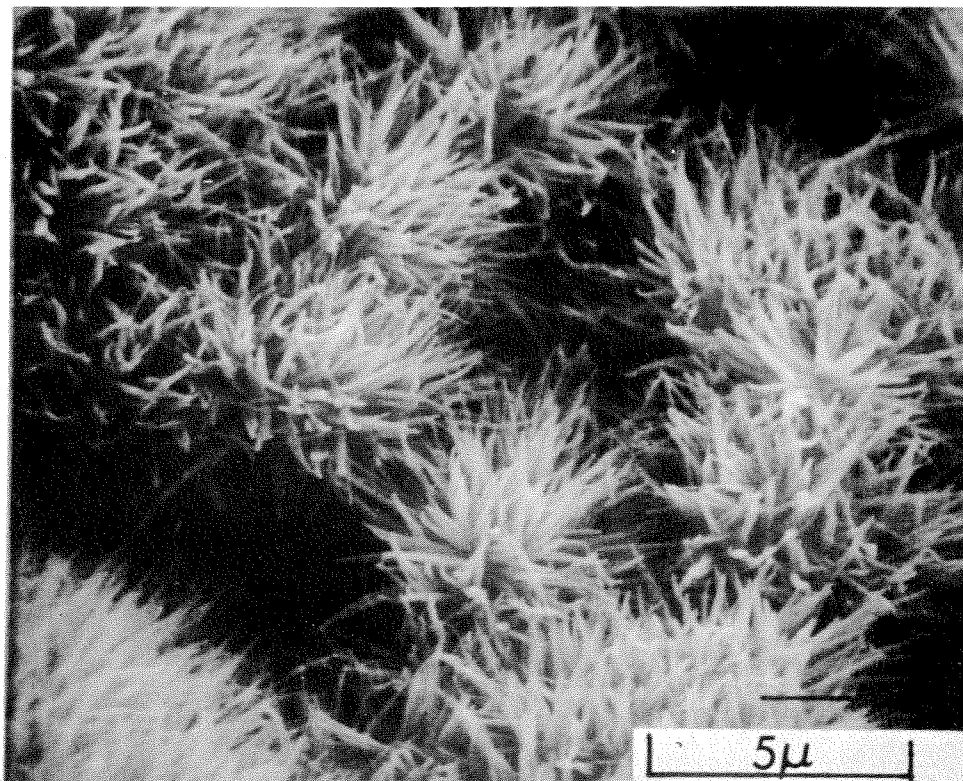


(b)

Figure 3.11 An isolated area of the fracture surface of the 384-day old β -dicalcium silicate paste showing extensive columnar zones that have not fused together (probably because there was excess water-filled space or a pore). (a) The location of this area is indicated in Figure 3.7(a). (b) A close-up of an area marked in (a) at the edge of the open space or pore.



(c)



(d)

Figure 3.11 (Continued from opposite page)...(c) An area adjacent to that in (b) showing more of the columnar structure. (d) A close-up of an area marked in (c).

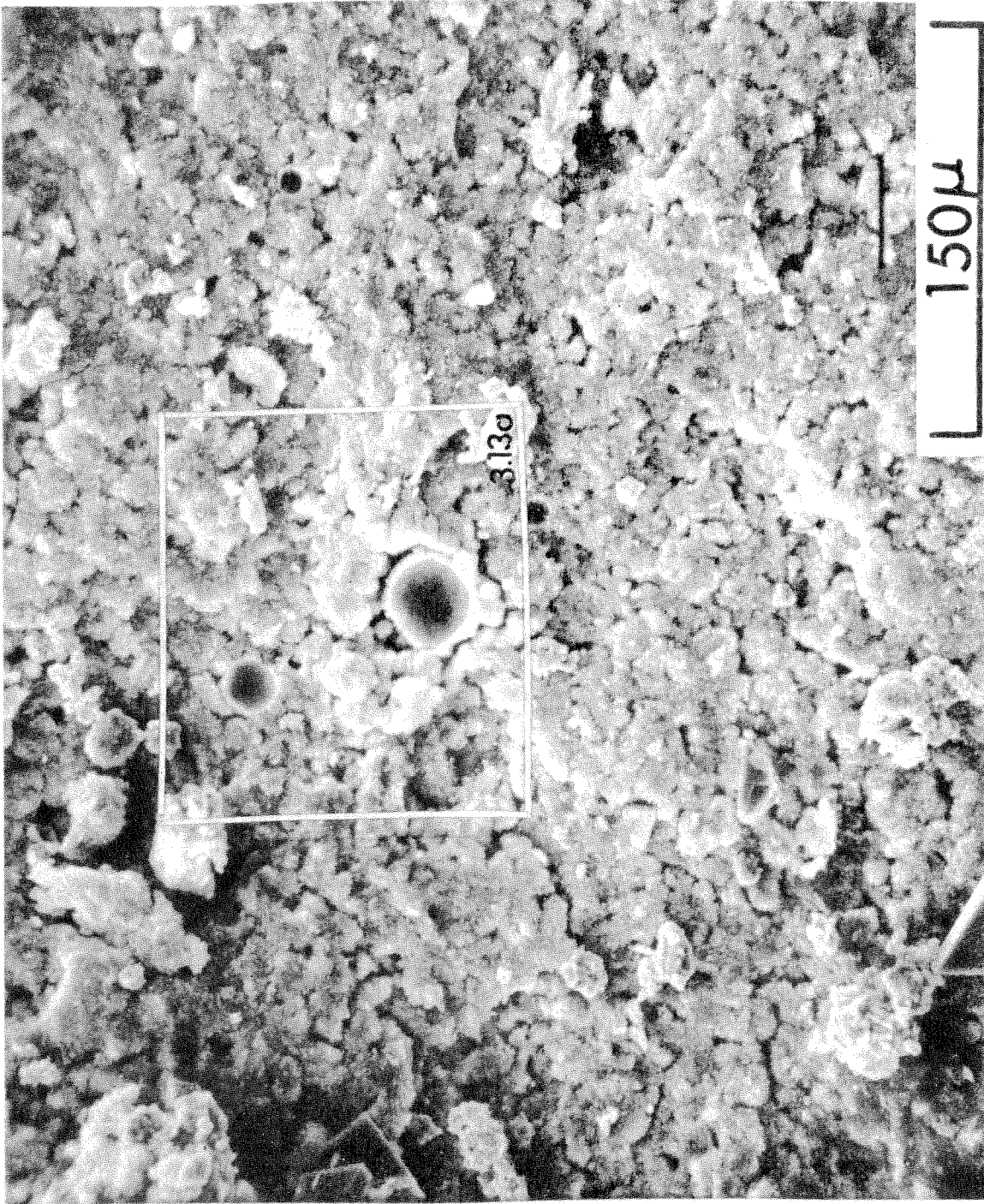
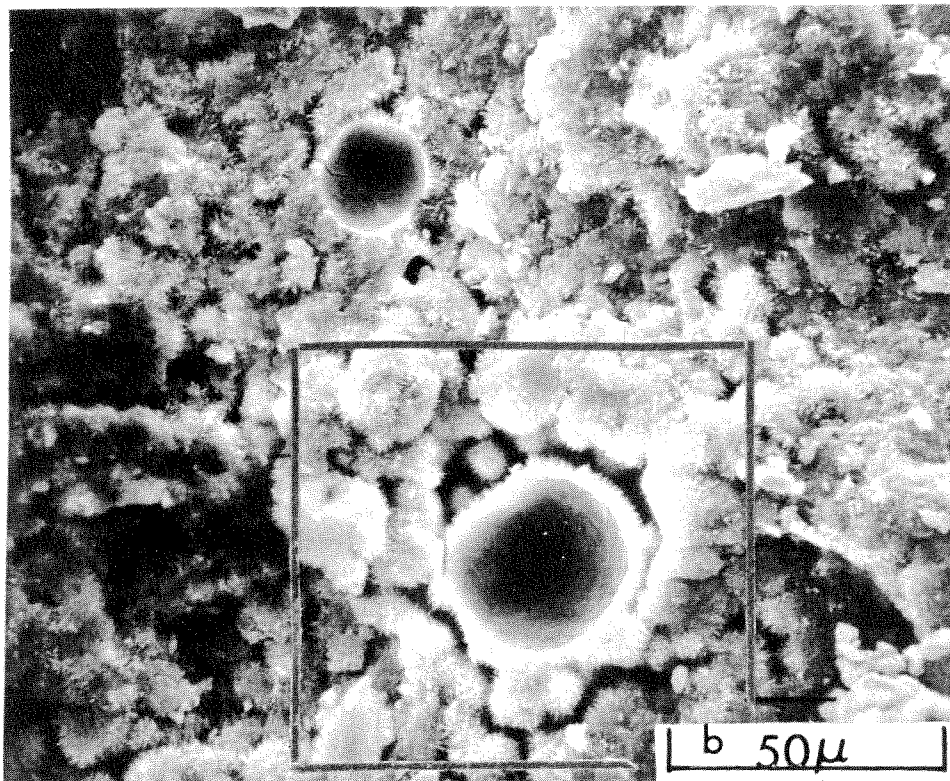


Figure 3.12 Fracture surface of β -dicalcium silicate paste hydrated 389 days and subjected to two days of drying in vacuum (approximately 0.5 microns) before fracture. This specimen was much weaker than the specimen shown in Figures 3.7 through 3.11 and there appear to be many drying shrinkage cracks between the cement grains.

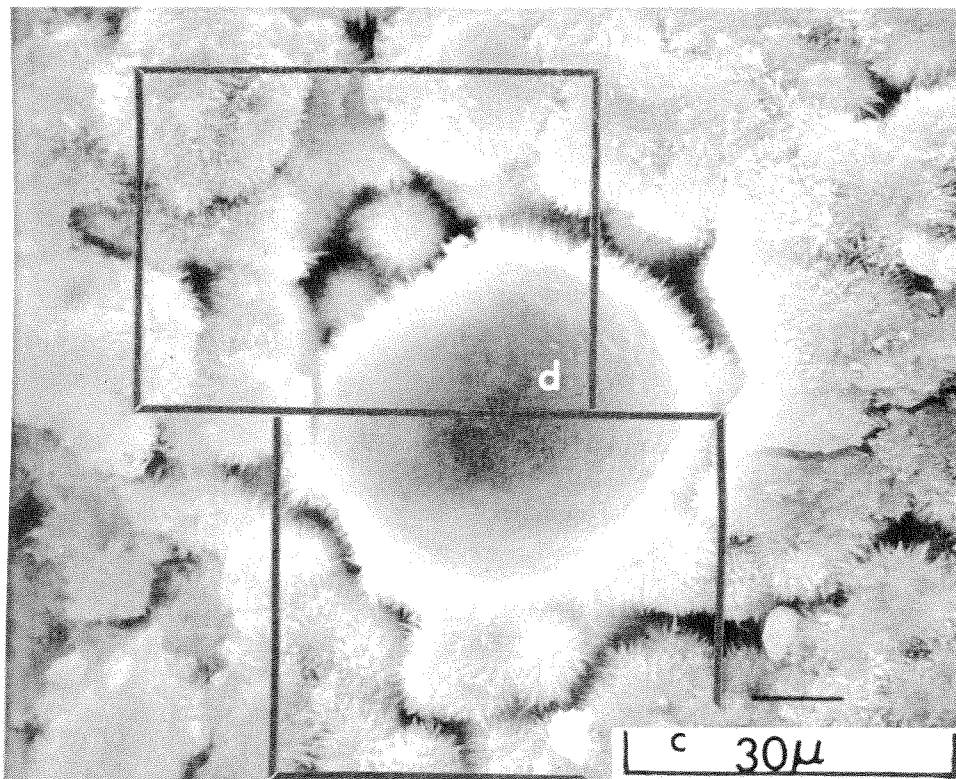
in Figures 3.10(a,b,c,d). The lack of a well developed columnar zone around the engulfed grains would appear to indicate that this portlandite grew at an early age. Further discussion of this point will be left until the microstructure of tricalcium silicate pastes has been presented.

Away from the areas showing intergrown portlandite the individual grains of β -dicalcium silicate appear to have been fused together by the hydration products in a manner similar to that shown in Figure 3.6(b) for the 171 day old specimen. In isolated places, however, a more open microstructure is observed which is like the 60 day old specimen; one such area is shown in Figures 3.11(a,b,c,d). The columnar products shown in Figures 3.11(b,c,d) have much the same appearance as those shown in Figures 3.3 and 3.4 except that they are longer and tend to have pointed tips rather than the blunt ends in the earlier age specimens. Further discussion of these differences, however, will be deferred until the other systems have been presented since the differences in morphology may be due to different drying conditions rather than growth conditions.

Another specimen of the β -dicalcium silicate paste was removed from the curing tank at an age of 389 days and subjected to two days of drying in the vacuum evaporator before fracturing. It is noted in the Appendix that those shown in Figures 3.3 through 3.11 were fractured in a wet condition within one minute of their removal from the curing water. All of the latter specimens had good strength with a general trend of increasing strength consistent with Figure 2.4. The 389 day old dried specimen had very little strength and many shrinkage

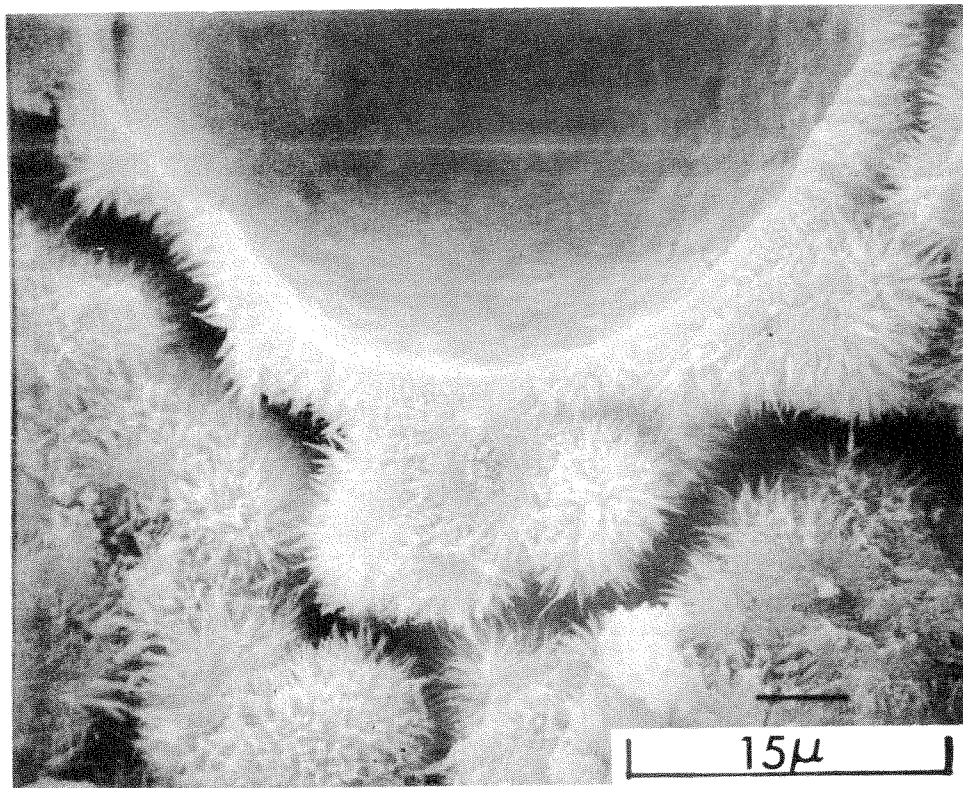


(a)

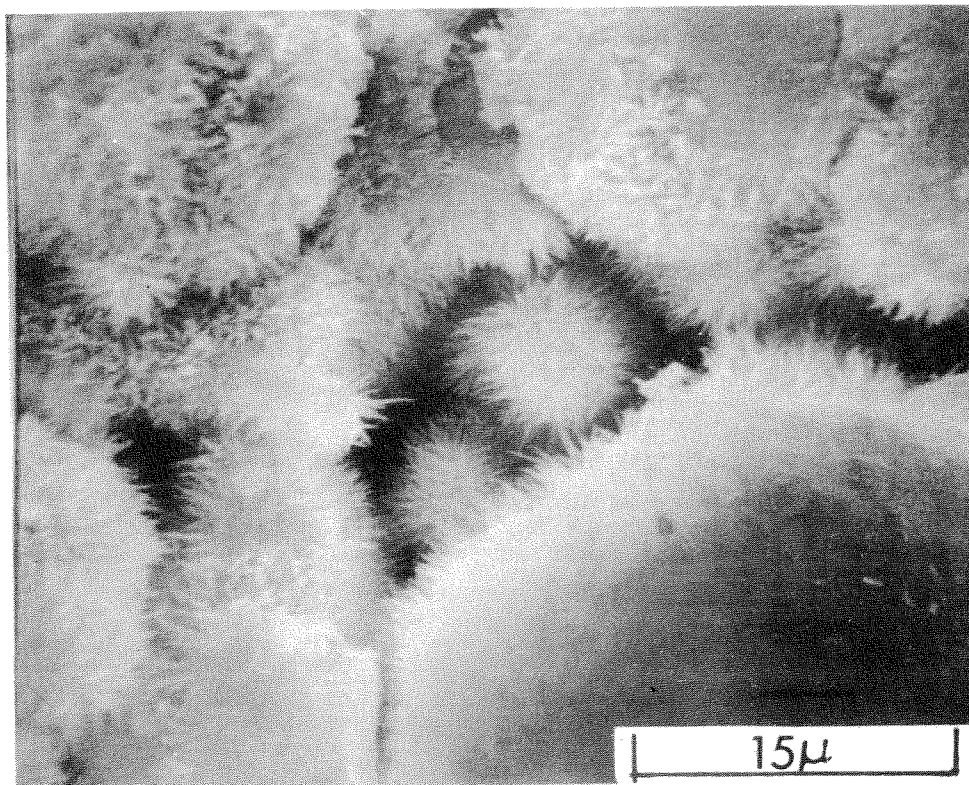


(b)

Figure 3.13 Close-ups of the fracture surface shown in the previous figure (389 day old β -dicalcium paste, vacuum dried before fracture). (a) An area marked in Figure 3.12 showing how the cement grains have been separated by the drying. (b) A close-up of an area marked in (a) which contains an air bubble.



(c)



(d)

Figure 3.13 (Continued from opposite page)....(c) A close-up of an area marked in (b). The shell of the bubble has a columnar zone growing into the originally water-filled space. (d) A close-up of the other side of the bubble, also marked in (b). Here the shell of the bubble seems thinner but still shows a columnar zone.

cracks are apparent on the fracture surface shown in Figure 3.12. The central portion of Figure 3.12 is shown at higher magnification in Figures 3.13(a,b,c,d). The two small spherical pores visible in this area are probably due to entrapped air and are similar to the pores visible in Figures 3.7(a), (b) and 3.8(a), (b). The general drying shrinkage of these specimens has highlighted the columnar zone around the pores, but the structure observed in Figures 3.13(b,c,d) is similar to that observed in specimens fractured in the wet condition such as that in the lower right hand corner of Figure 3.7(d). The outer hydration products both on the grains and on the pore walls in Figures 3.13(c) and (d) are similar to those on the grains in Figure 3.11(d). The morphology of these products will be discussed below.

3.3 Microstructure of Tricalcium Silicate Pastes

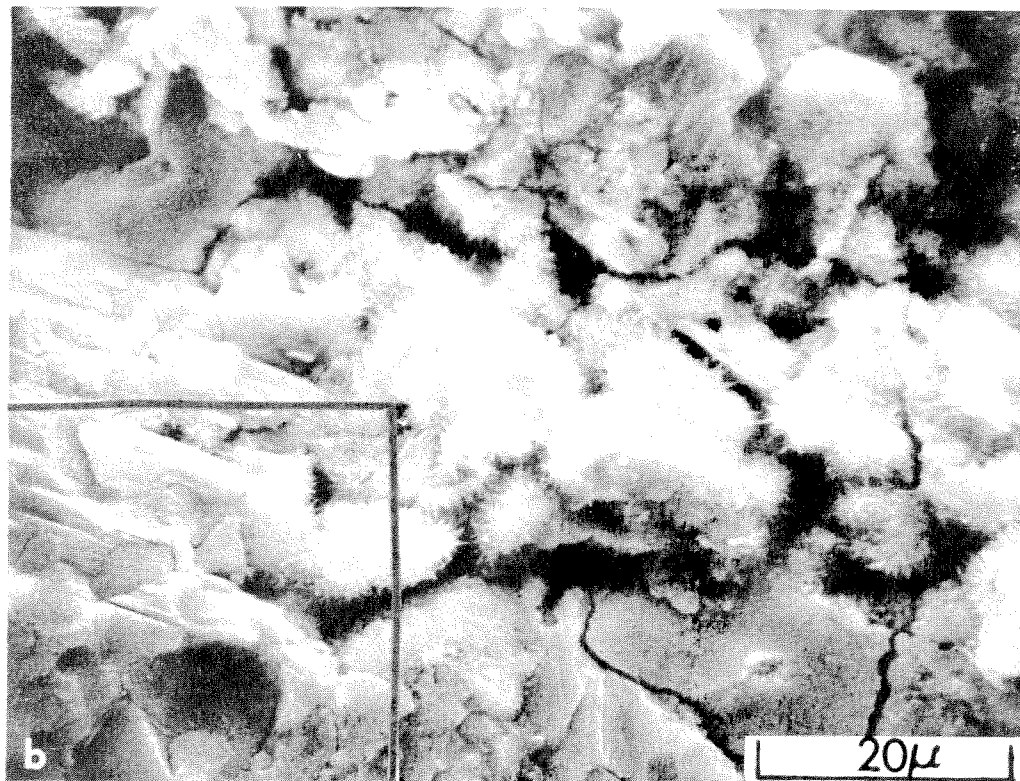
The hydration of tricalcium silicate produces three times as much portlandite as the same amount of β -dicalcium silicate, see Table 2.2 above, and the increased amount of portlandite in tricalcium silicate pastes is evident on most fracture surfaces of well cured specimens. The fracture surface shown in Figure 3.14(a) was made on a well cured specimen* of tricalcium silicate cast with a 0.5 water-to-solids ratio, and a number of features can be identified on this fracture surface. Fractured portlandite can be seen at the left of that figure and along the bottom. More detail is visible in Figures 3.14(b) and (c) where the fracture surface of the portlandite is shown at different angles

* Please see Appendix for experimental details and analysis of materials.

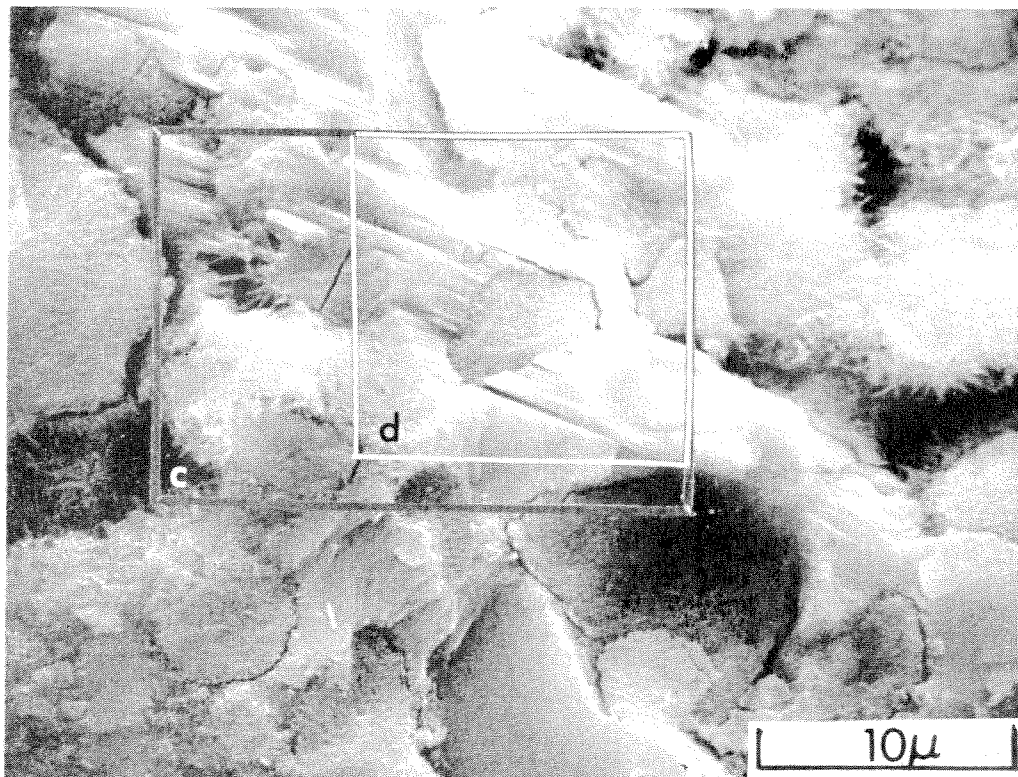
to illustrate the complexity of this surface. The two engulfed pseudomorphs of the original silicate grains appear to have affected the fracture process within the surrounding portlandite crystal. The engulfed grains are presumed to be hydrated because of the rough texture of their fracture surfaces, and it appears that their presence has had a weakening influence. This will be discussed further after more evidence has been presented.

The range of morphology of the portlandite in these pastes is illustrated in Figure 3.15(a,b,c,d). Large, space filling portlandite is shown in Figure 3.15(a) and in more detail in Figure 3.15(b). The boundary between the portlandite and the surrounding pseudomorphs has been highlighted by a shrinkage crack which is probably due to a drying shrinkage of the pseudomorphs. A small pillar of portlandite is visible in the center of the very complex fracture surface shown in Figure 3.15(c). The small pillar, shown at higher magnification in Figure 3.15(d), has been fractured and displaced slightly, but it originally grew as a bridge between two pseudomorphs. In that respect it shares the tendency of the larger portlandite crystals to grow to fill the space available between cement grains. It should be recognized that the small crystal of portlandite shown in Figure 3.15(c) and (d) may well be a fragment of a much larger crystal that existed in the other half of the fractured specimen. In that case it cannot represent a possible growth morphology.

A specimen fractured after hydrating 200 hours is shown in Figure 3.16(a) with a large portlandite crystal occupying most of the field of view. It is apparent that many silicate grains have been

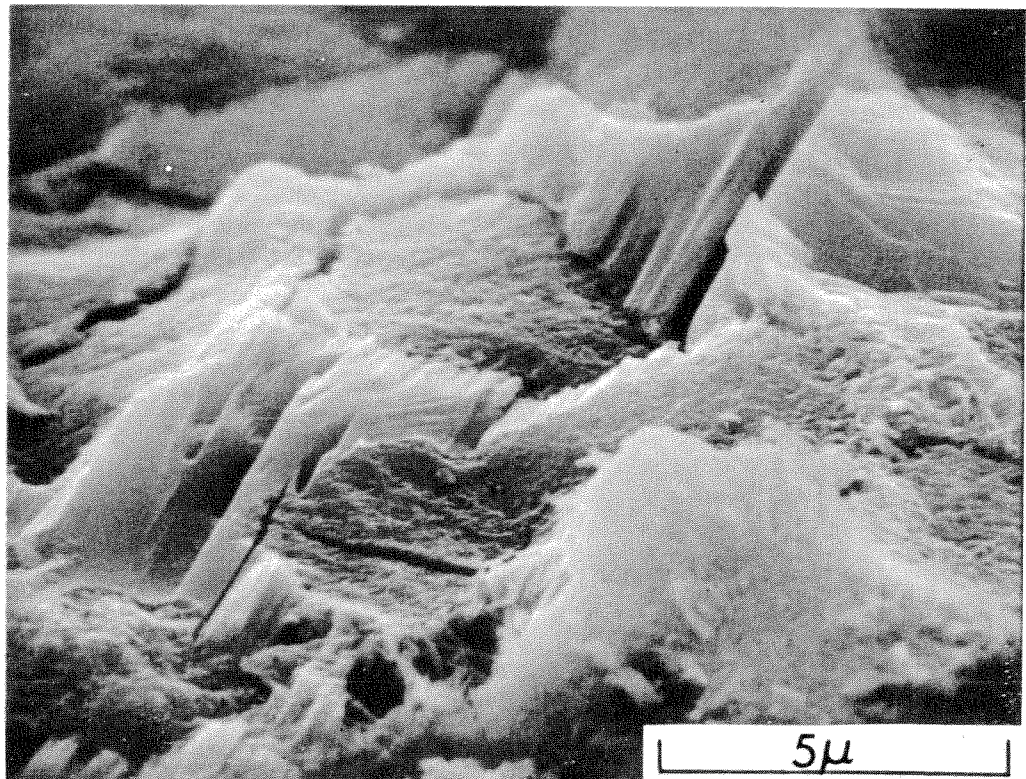


(a)

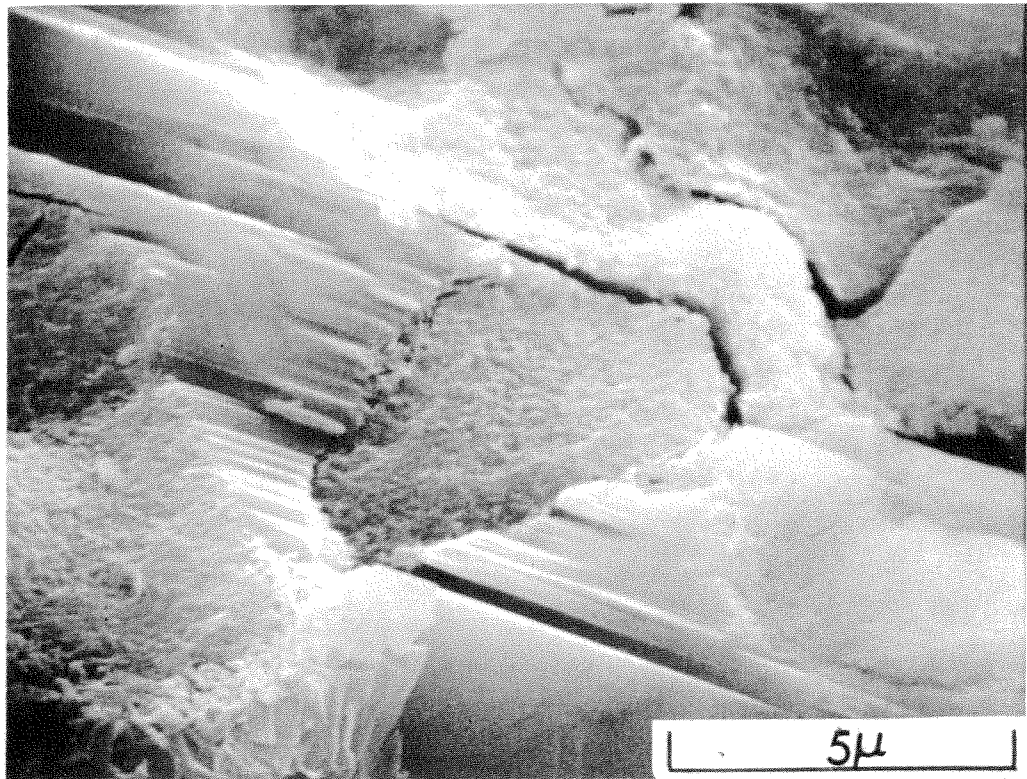


(b)

Figure 3.14 Fracture surface of tricalcium silicate paste hydrated over two years (details of specimen preparation given in Appendix). (a) Low magnification scanning electron micrograph showing that the fracture path has passed through portlandite, pseudomorphs of the original grains and pores. (b) Close-up of an area marked in (a) shows a fractured portlandite crystal with engulfed grains of cement.

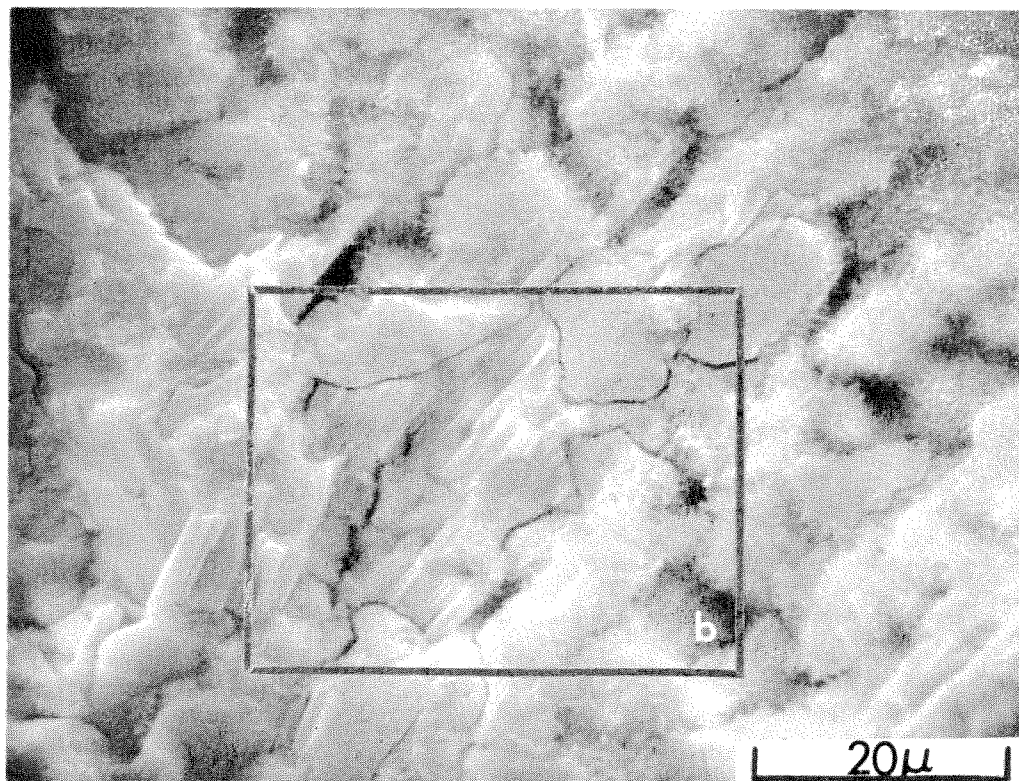


(c)

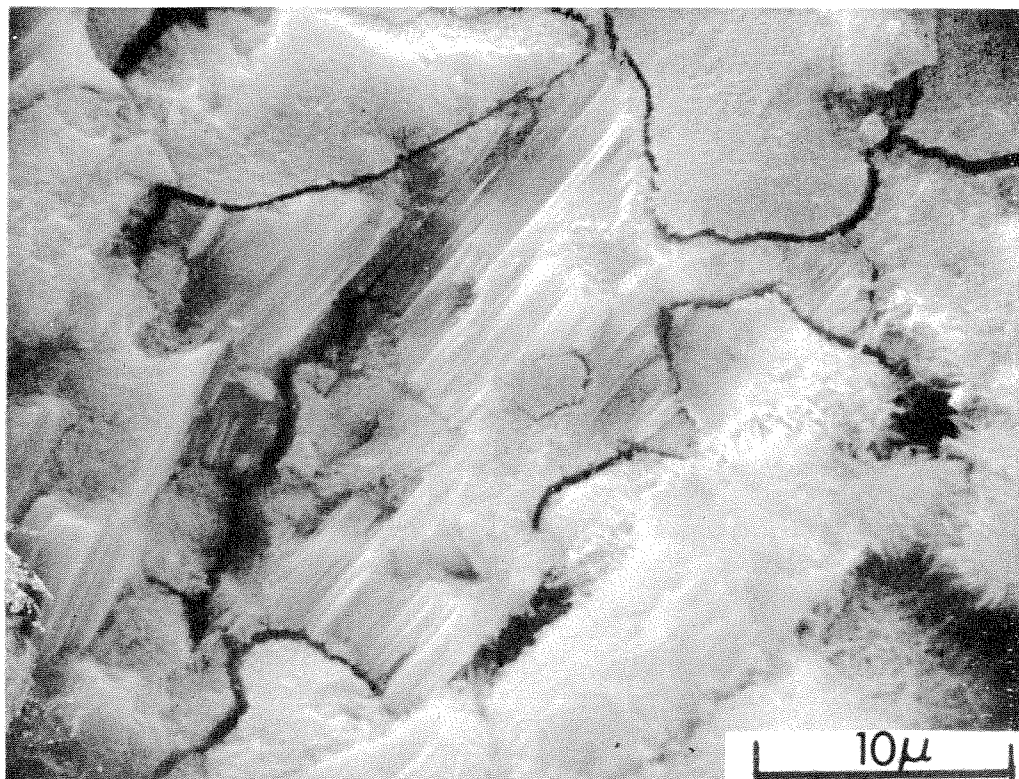


(d)

Figure 3.14 (Continued from opposite page)...(c) Close-up of an area marked in (b) from a different angle which gives a better feeling of the rough texture of the fracture surface of portlandite. (d) Close-up of an area marked in (b) (from the same angle as (b)) showing the engulfed grains where the inner hydration products have created a pseudomorph.

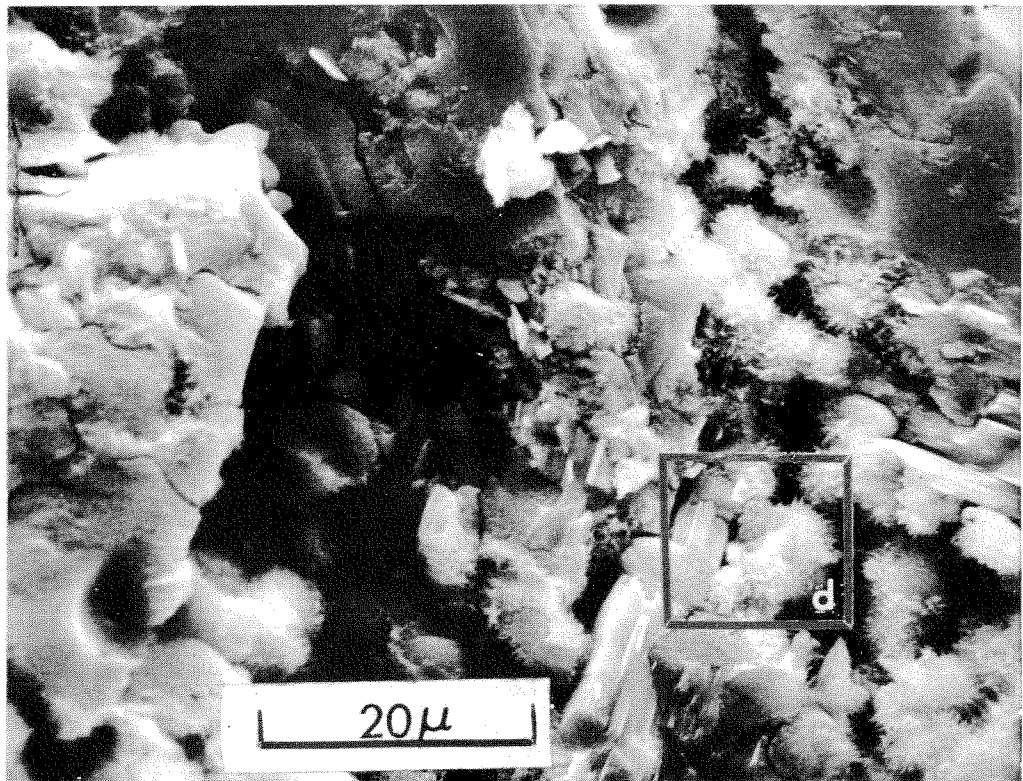


(a)

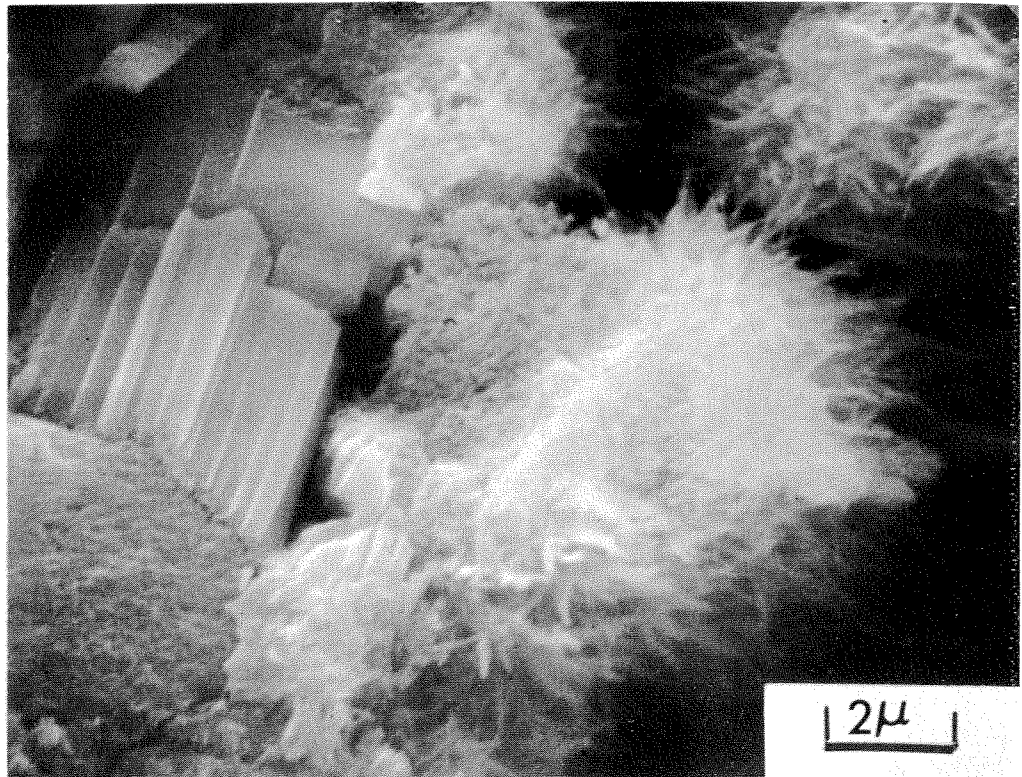


(b)

Figure 3.15 Fracture surfaces of mature tricalcium silicate pastes (age greater than two years) showing a range of morphology of portlandite. (a) A large space-filling portlandite crystal stretches diagonally across this scanning electron micrograph. (b) Close-up of an area marked in (a) shows how the portlandite crystal has filled a large region between grains of cement.

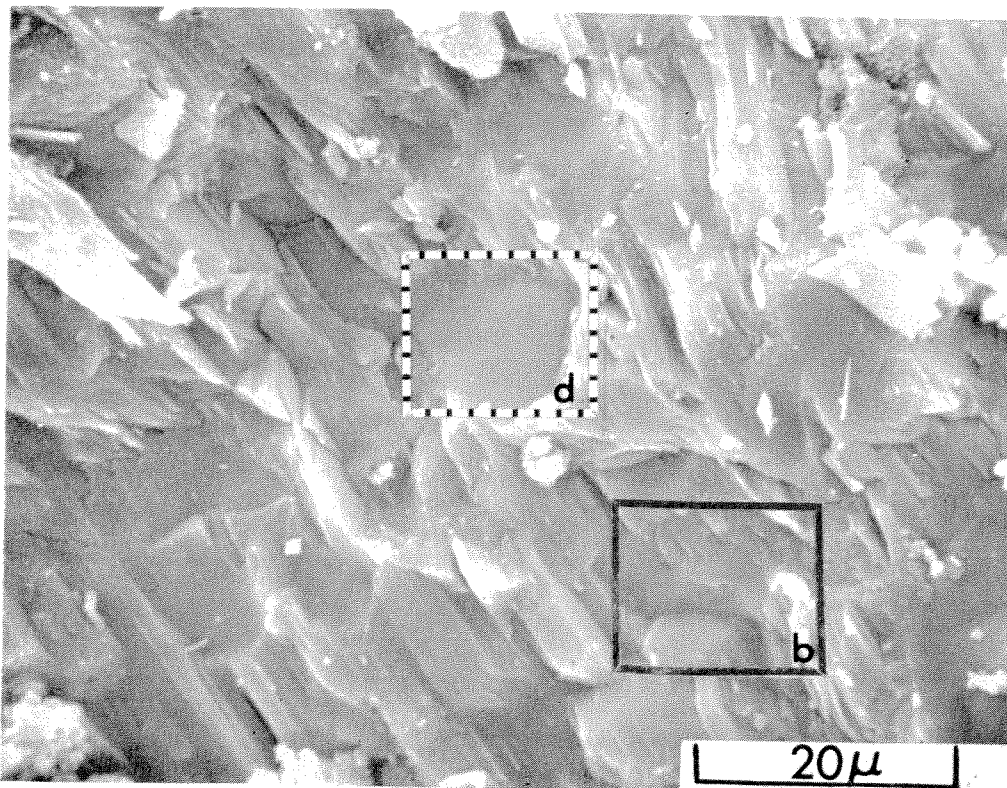


(c)

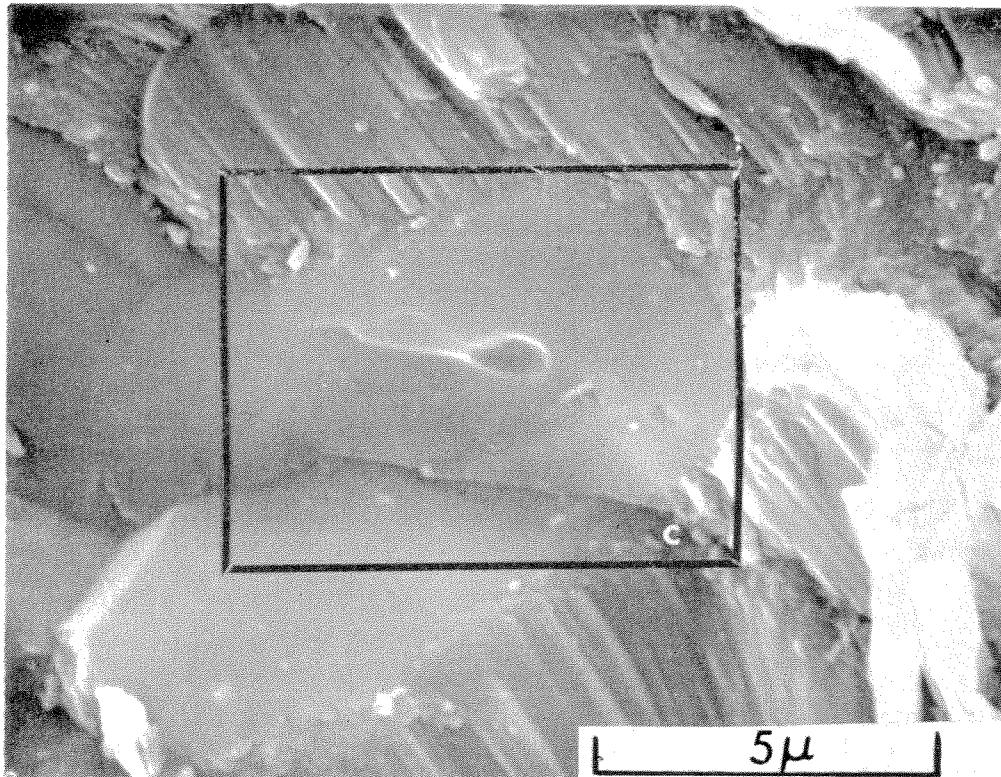


(d)

Figure 3.15 (Continued from opposite page)...(c) Another region on the same fracture surface showing several small portlandite crystals. (d) Close-up from (c) of a portlandite crystal that originally bridged the gap between two grains of cement although it is fractured and displaced slightly as shown.

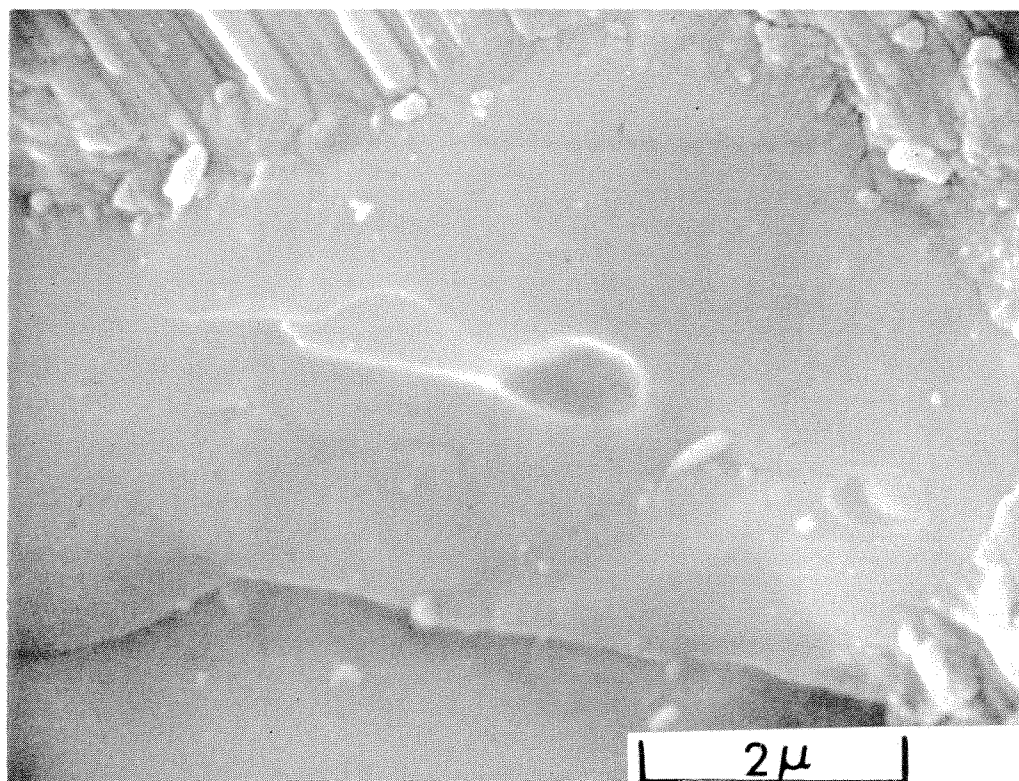


(a)

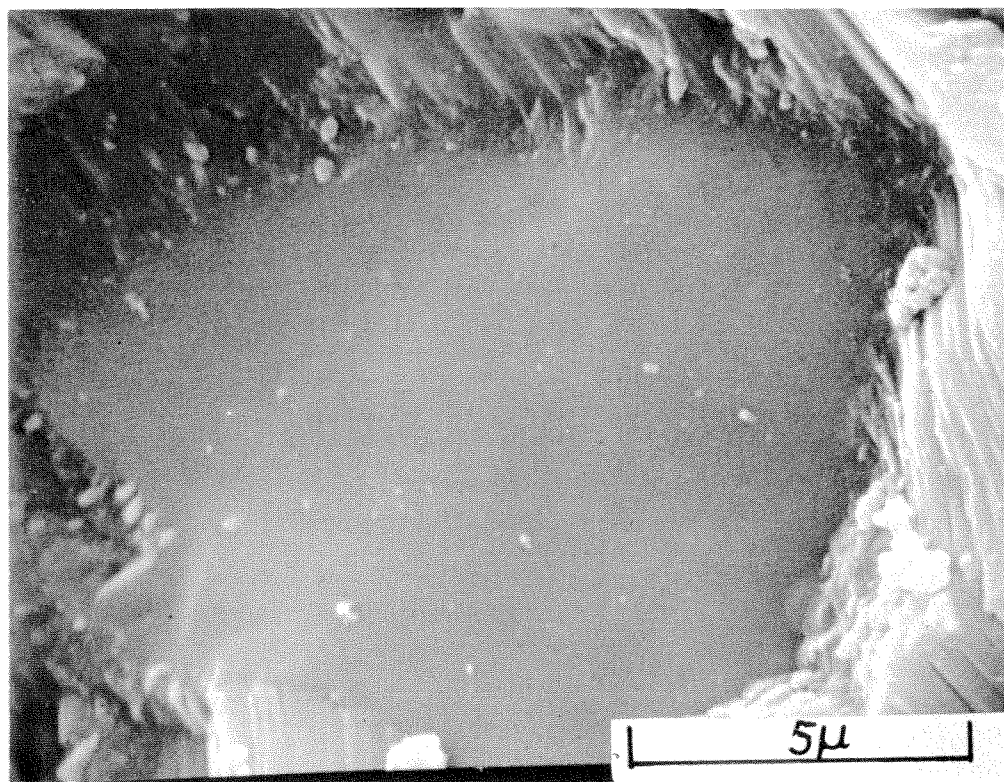


(b)

Figure 3.16 Fracture surface of a tricalcium silicate paste cured 200 hours showing apparently unhydrated cement grains engulfed by portlandite. (a) A low magnification scanning electron micrograph showing a large portlandite crystal. (b) A close up of an area marked in (a).

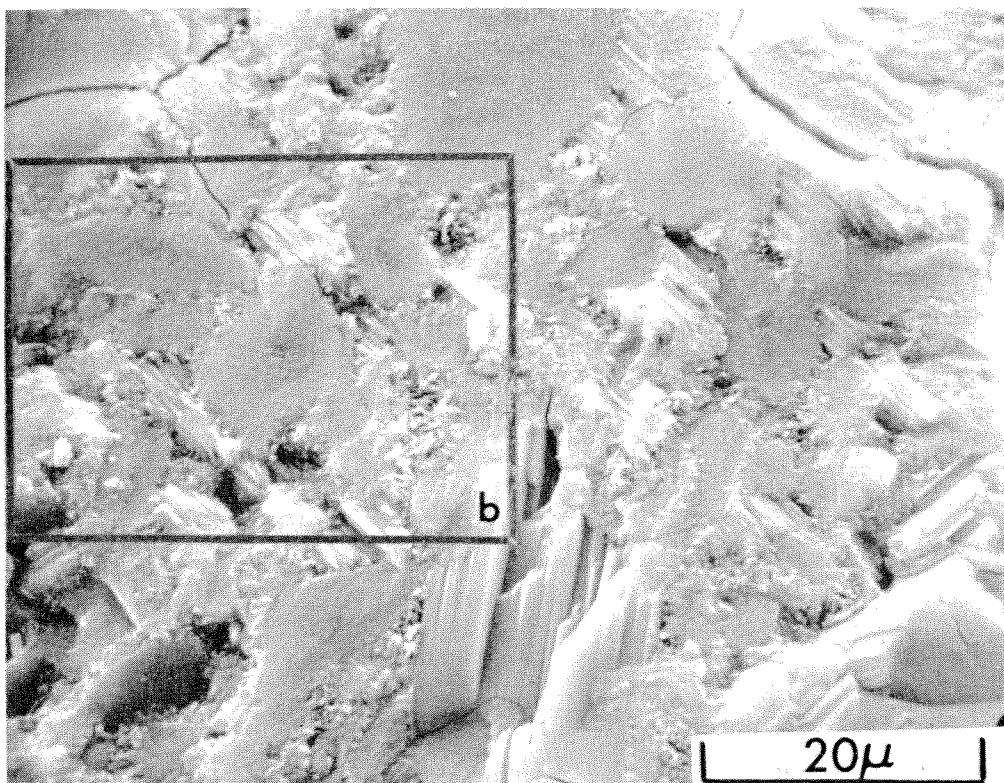


(c)

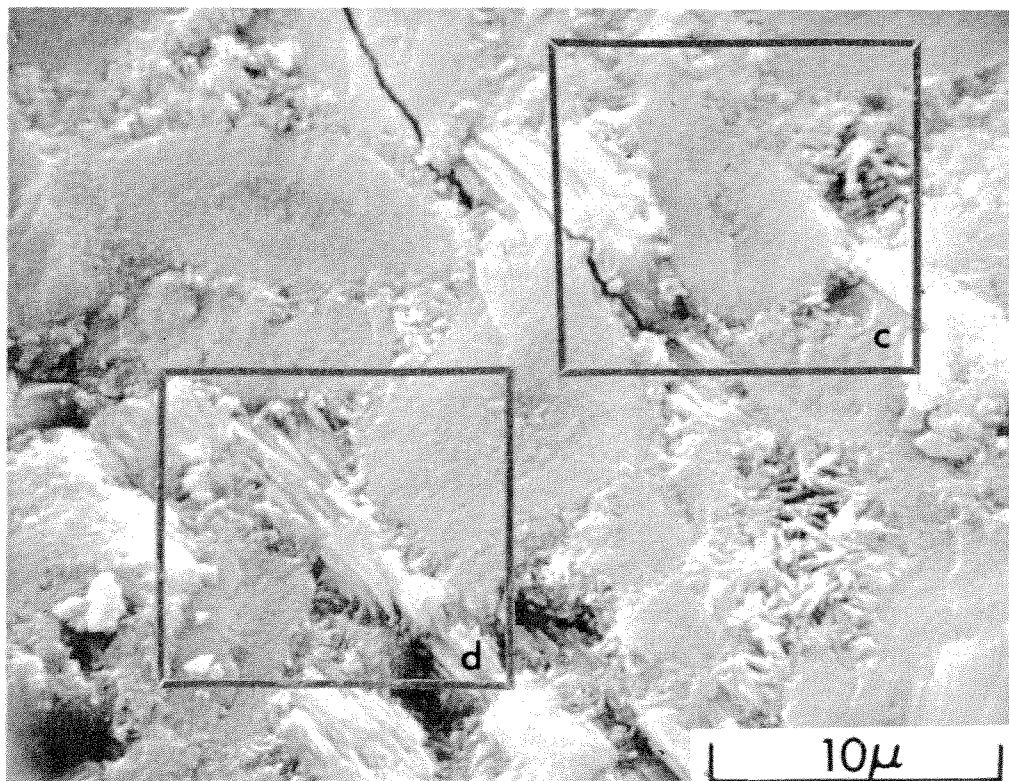


(d)

Figure 3.16 (Continued from opposite page)...(c) A close-up of an engulfed grain marked in (b) showing its smooth fracture surface. (d) A close-up of another engulfed grain marked in (a).



(a)

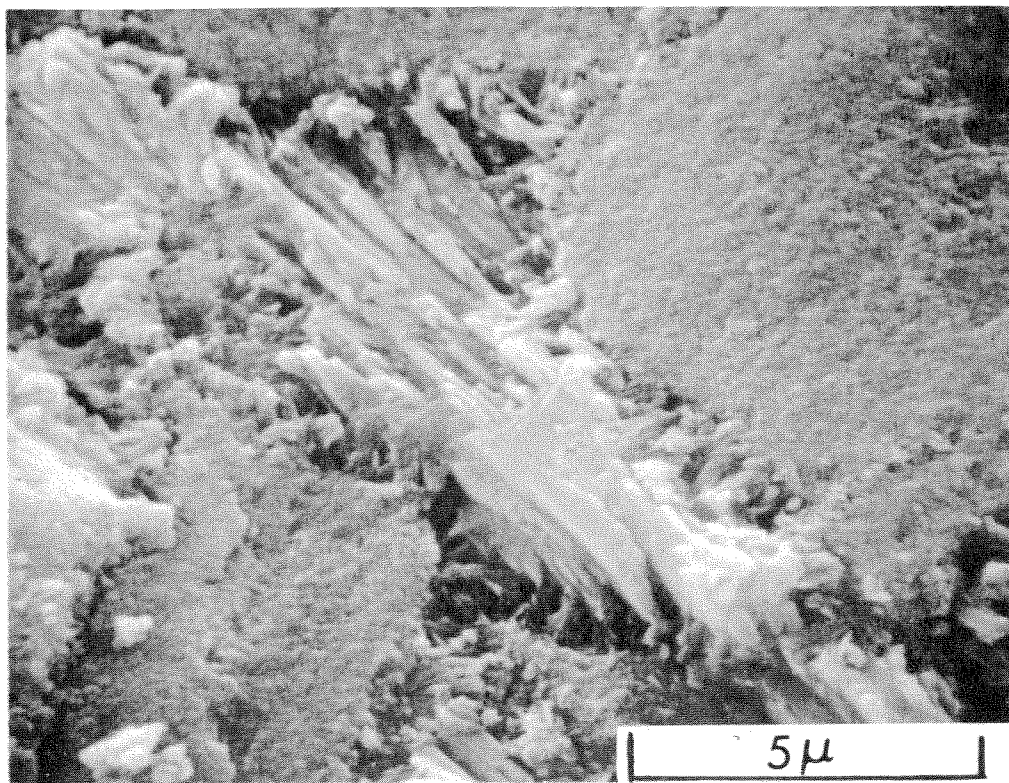


(b)

Figure 3.17 Fracture surface of a tricalcium silicate paste cured under water for four years. (a) Both well crystallized and poorly crystallized portlandite visible in this area. (b) A close-up of a region marked in (a) where a single portlandite crystal appears to have engulfed a number of hydrated cement grains.

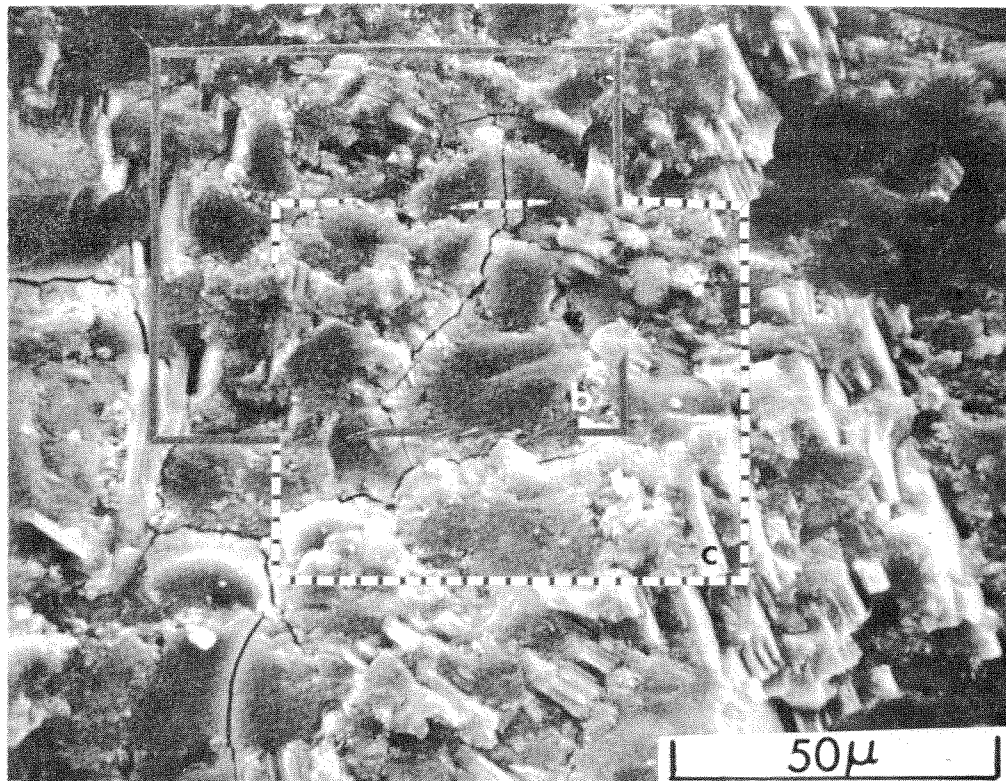


(c)

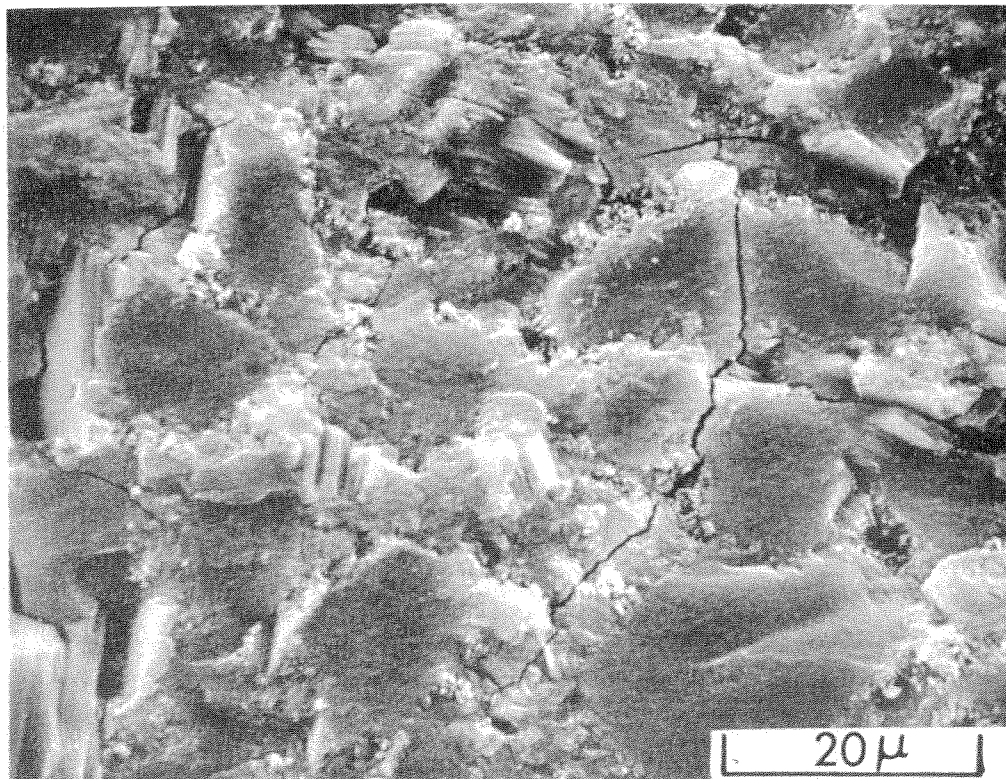


(d)

Figure 3.17 (Continued from opposite page)...(c) A close-up of an area marked in (b). (d) Another close-up of an area marked in (b) showing poorly crystallized portlandite with a columnar structure around each grain. This probably means this was some of the last portlandite to solidify in this region.

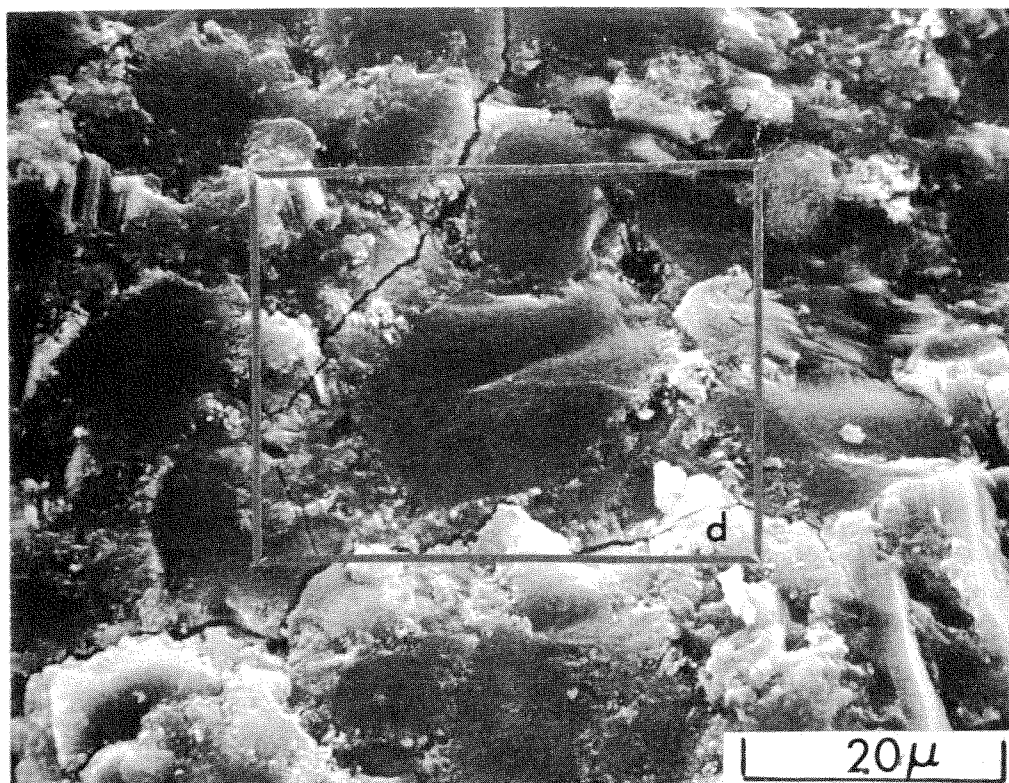


(a)

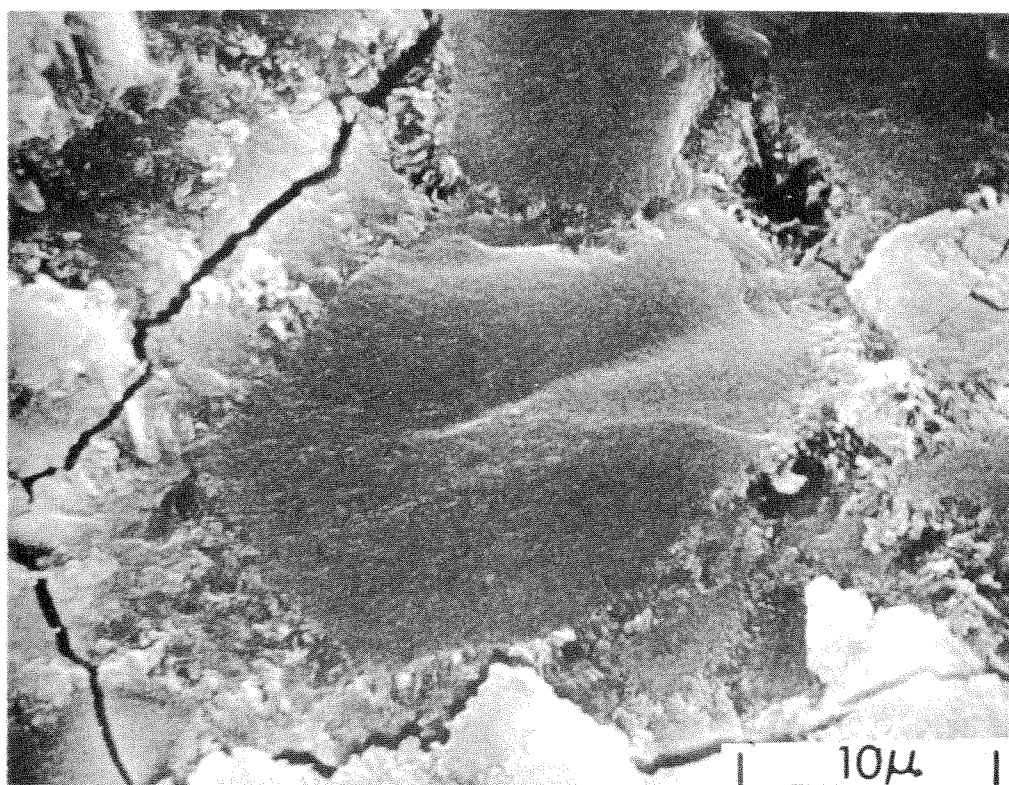


(b)

Figure 3.18 Another area on the fracture surface of the tricalcium silicate paste shown in the previous figure. (a) Low magnification scanning electron micrograph showing portlandite crystals surrounding an area of special interest. (b) A close-up of an area marked in (a) with portlandite between the cement grain pseudomorphs on the left and a more amorphous hydration product between them on the right.

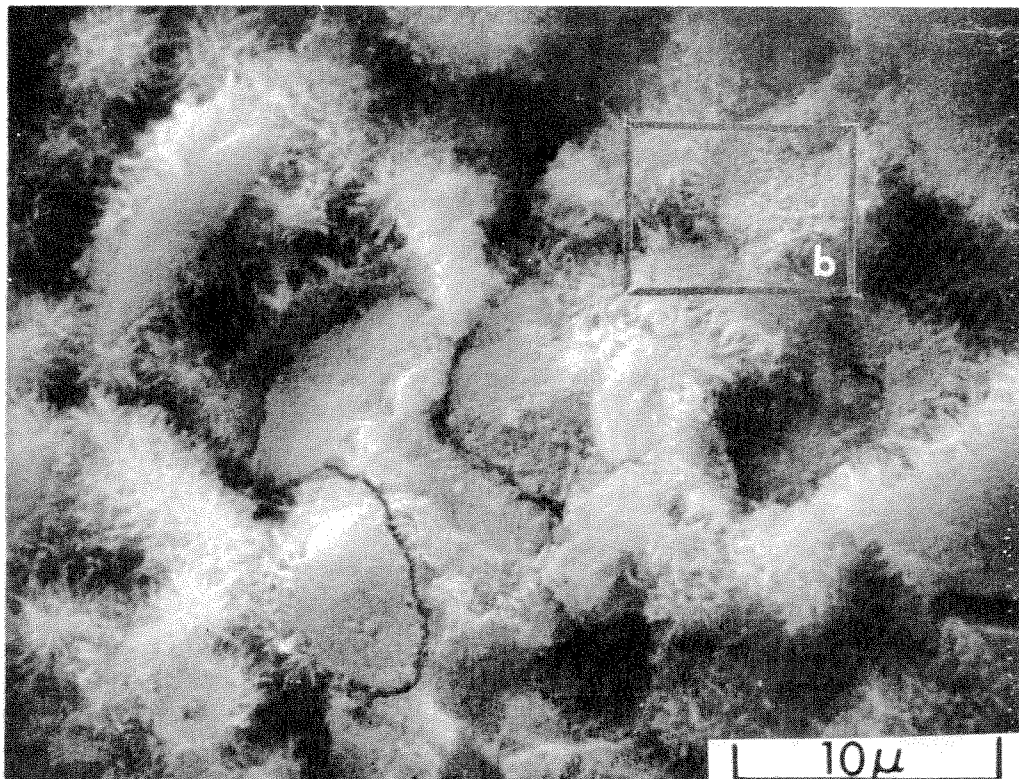


(c)

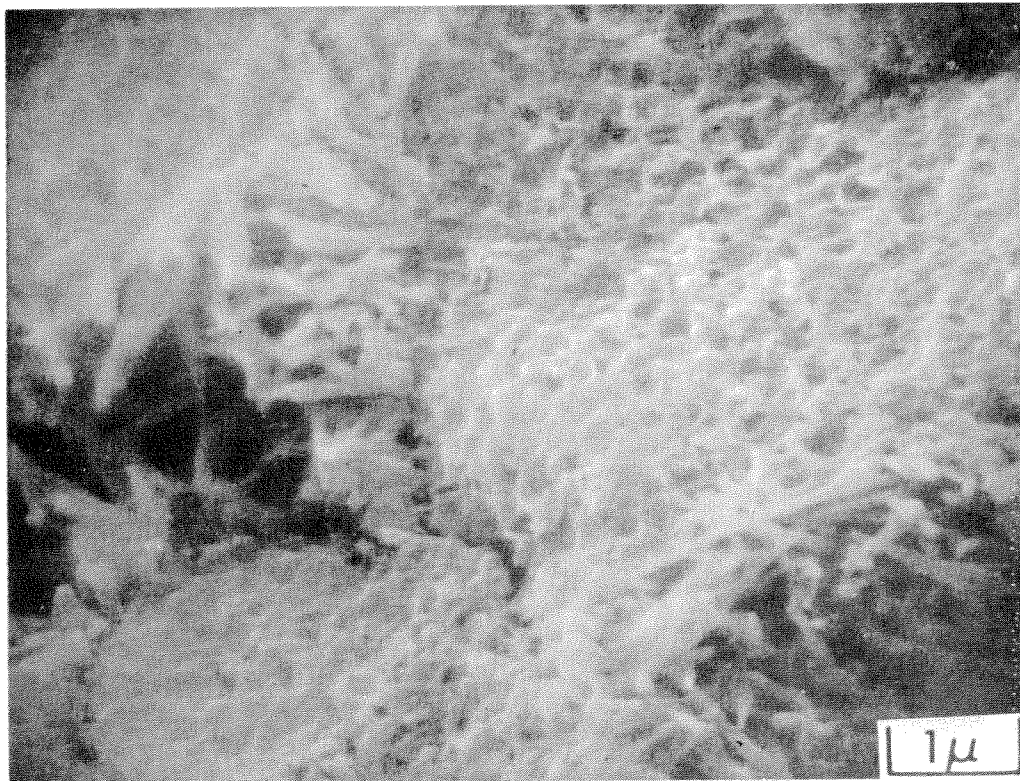


(d)

Figure 3.18 (Continued from opposite page)...(c) Another area marked in (a) showing more of the amorphous material. (d) A close-up of a pseudomorph surrounded by amorphous material marked in (c).

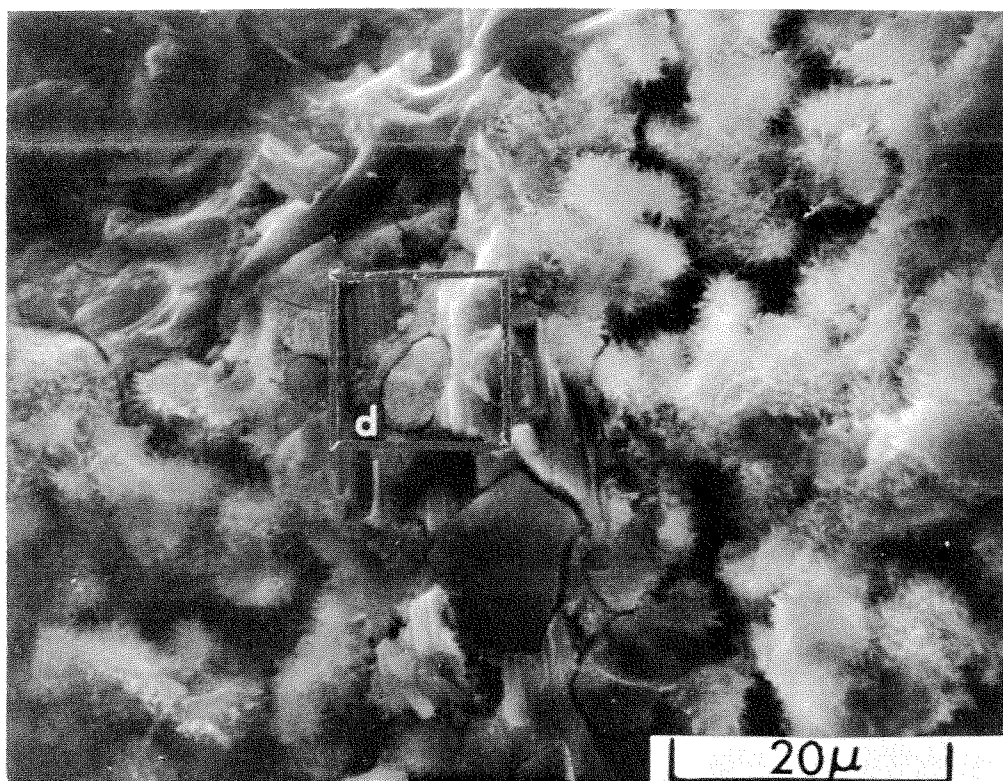


(a)

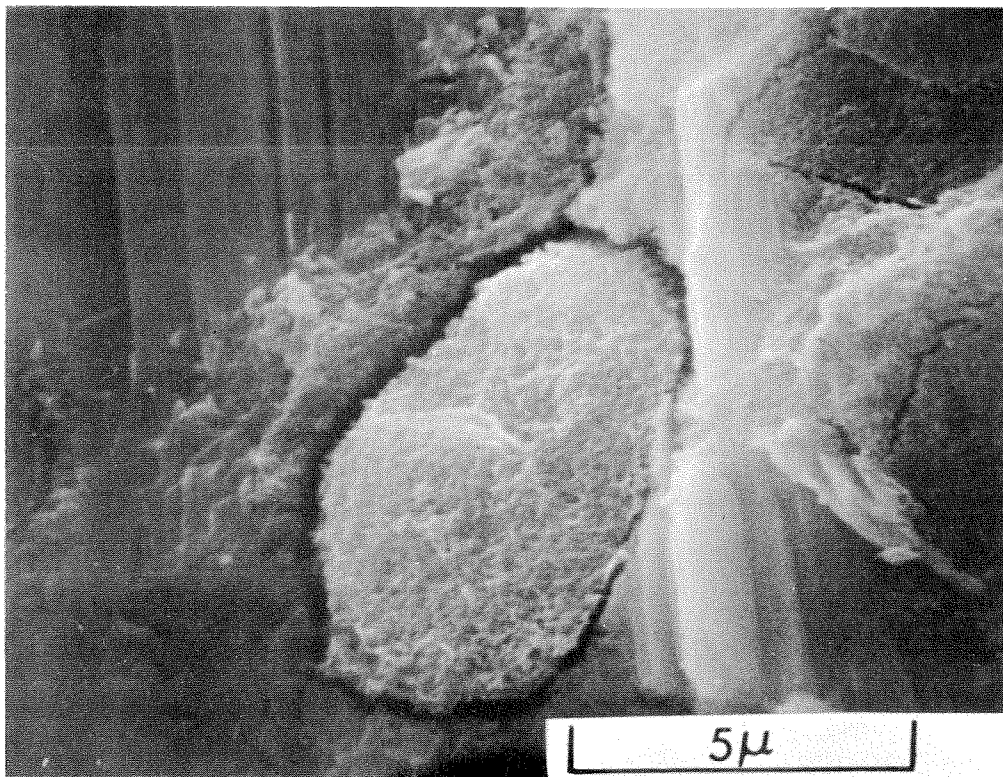


(b)

Figure 3.19 Other areas on the same fracture surface shown in Figures 3.14 and 3.15 which illustrate the differences in porosity that can be observed in the hydration products. (a) An area which contains cement grain pseudomorphs and outer hydration products, but no well defined portlandite crystals. (b) A close-up of a fine pore structure marked in (a). This is similar to the cellular structure observed in metals and other materials.



(c)



(d)

Figure 3.19 (Continued from opposite page)...(c) Another area showing both portlandite and large capillary pores. (d) A close-up from (c) of a cement grain pseudomorph which shows a fine structure within.

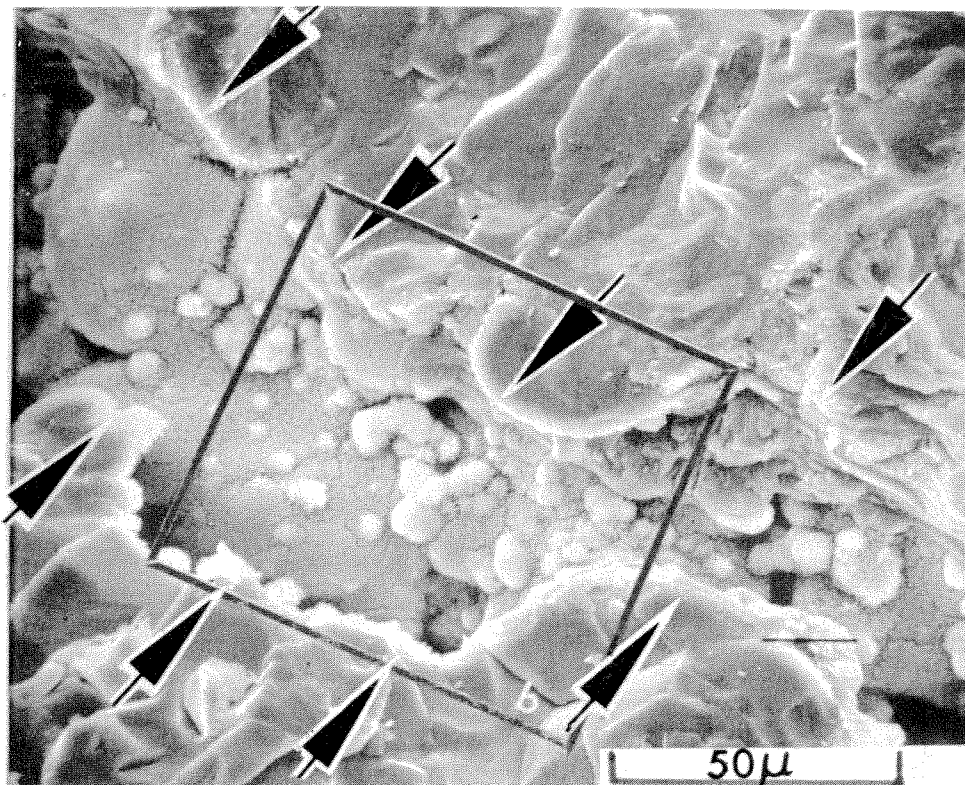
engulfed, yet in the higher magnification micrographs shown in Figures 3.16(b,c,d) there is no indication that these grains have hydrated. Even though there is no indication of hydration, these grains have fractured as readily as those shown in 3.14. This point will be discussed below.

In many cases the morphology of the portlandite varies considerably from one place to another within one specimen. In Figure 3.17(a) several regions of portlandite are visible and it appears that it grew at different times with different morphologies in this well cured paste. In Figure 3.17(a) a large portlandite crystal is visible in lower center of the field, and it is probable that this crystal has grown around several grains at an early age since there are no hydration products around the pseudomorphs of these grains as they appear on the fracture surface. A smaller region of poorly crystallized portlandite is shown in Figure 3.17(d) to have grown between several grains. This portlandite appears to have crystallized later since there is a region of hydration products around each pseudomorph. Another area on the same fracture surface is shown in Figures 3.18 (a,b,c,d) where although the pseudomorphs are distinct they appear to be held together by an amorphous glue. As noted in the Appendix, that specimen was cured under water for over four years, and part of the microstructure in the last two sets of figures may be the result of a continuous aging process.

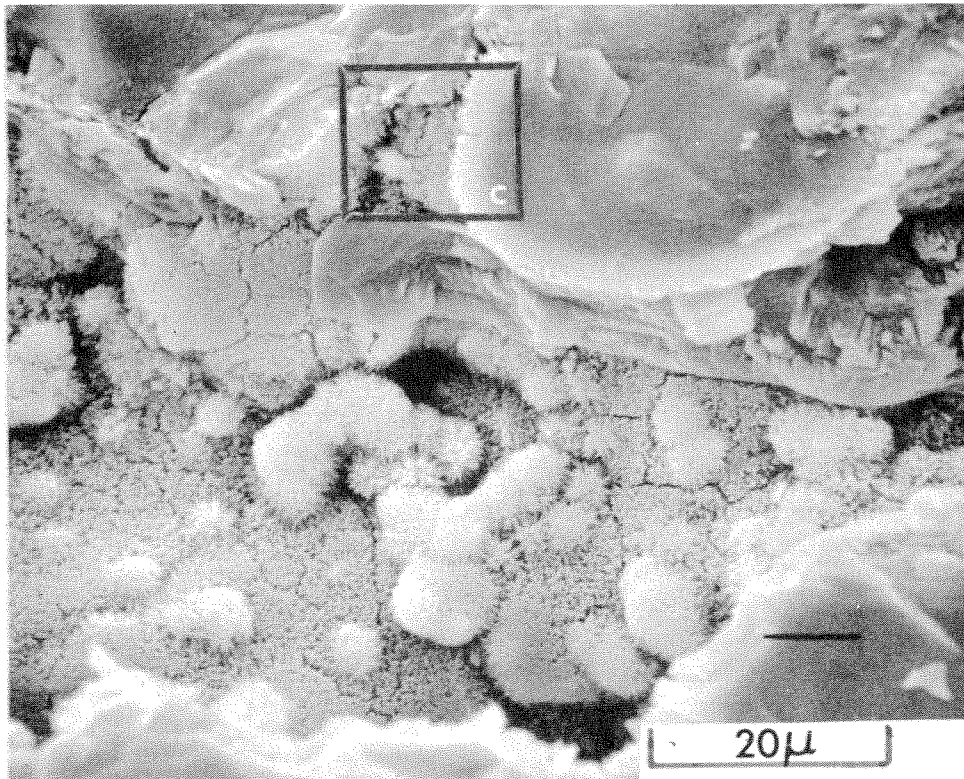
Finally, several micrographs are shown in Figures 3.19(a,b,c,d) which illustrate the differences in porosity that can be observed in the hydration products on or in the cement grains. These will be discussed below.

3.4 Microstructure of Hydrated Portland Cement

The hydration products of normal portland cement have begun to be investigated by means of the scanning electron microscope (34,35,36) and there is beginning to be a general body of knowledge about the morphology of these hydration products viewed with this instrument. For the most part the information gained from normal portland cement samples has been consistent with the morphology shown above for the pure phases. The initial hydration products are illustrated in Figures 3.20(a,b,c,d) where a limited amount of hydration was permitted to occur within a pore of an unground clinker. In this specimen a number of clinker particles between about 0.01 and 0.1 cm were used as an aggregate in a cement paste prepared from the same clinker ground to cement fineness. The fracture process has revealed an internal passage within the clinker particle which was exposed to water for at least some part of the seven day curing period. The bottom of the passage shows the growth of hydration products and the depth of the hydration reaction can be seen where the fracture passed through the clinker phases surrounding the passage. The ball-like forms visible in Figure 3.20(b) on the bottom of the passage may be hydration products which were freely suspended in water and settled out on the bottom of the passage. The paste was cured for seven days before fracture, but it is not certain that the reaction shown in Figure 3.20 represents that age or less since the water supply to the passage could have been cut off. The same passage is shown from another angle in Figure 3.21(a,b,c,d), and that angle highlights the differences in texture between the reaction products and the smooth ceramic fracture

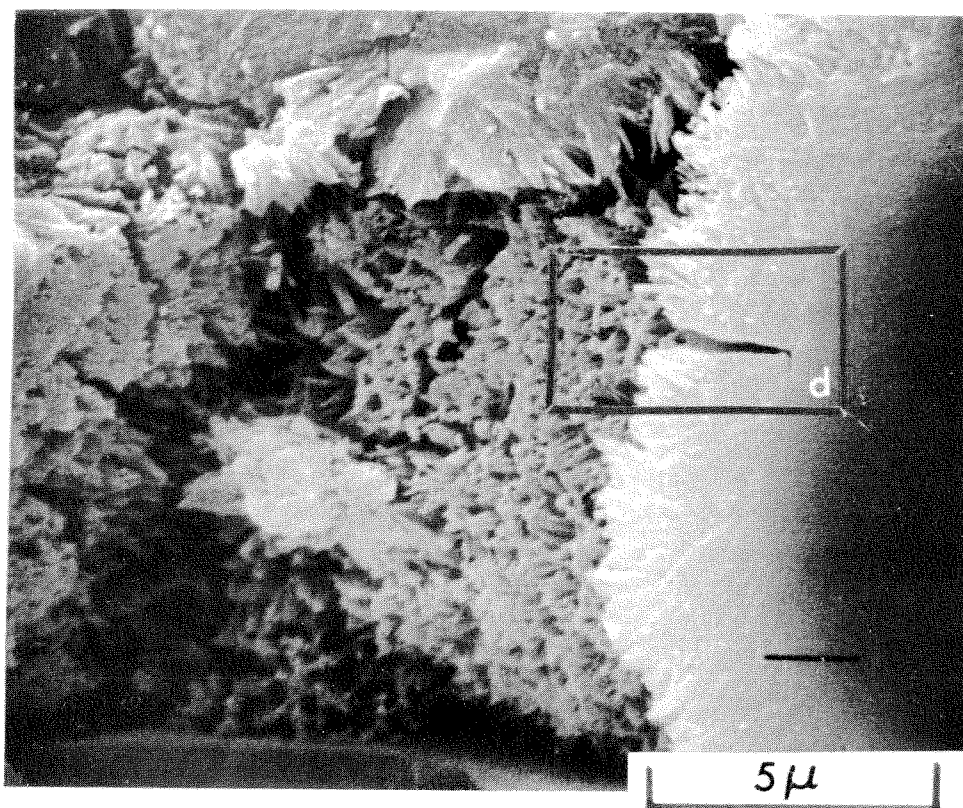


(a)

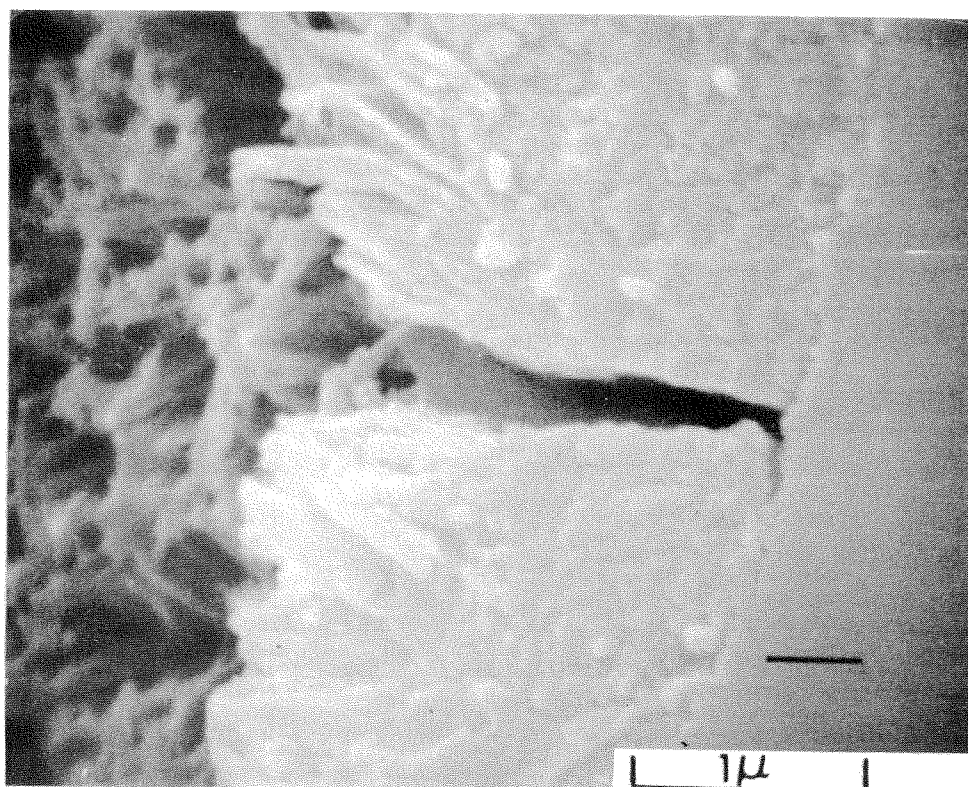


(b)

Figure 3.20 The initial hydration products are visible in a pore of an unground particle of clinker which had been embedded in a fresh cement paste, cured for seven days, and then fractured. (a) The boundaries of the pore are indicated by arrows. (b) A close-up of an area marked in (a) shows the hydration products on the bottom of the pore and on the walls.

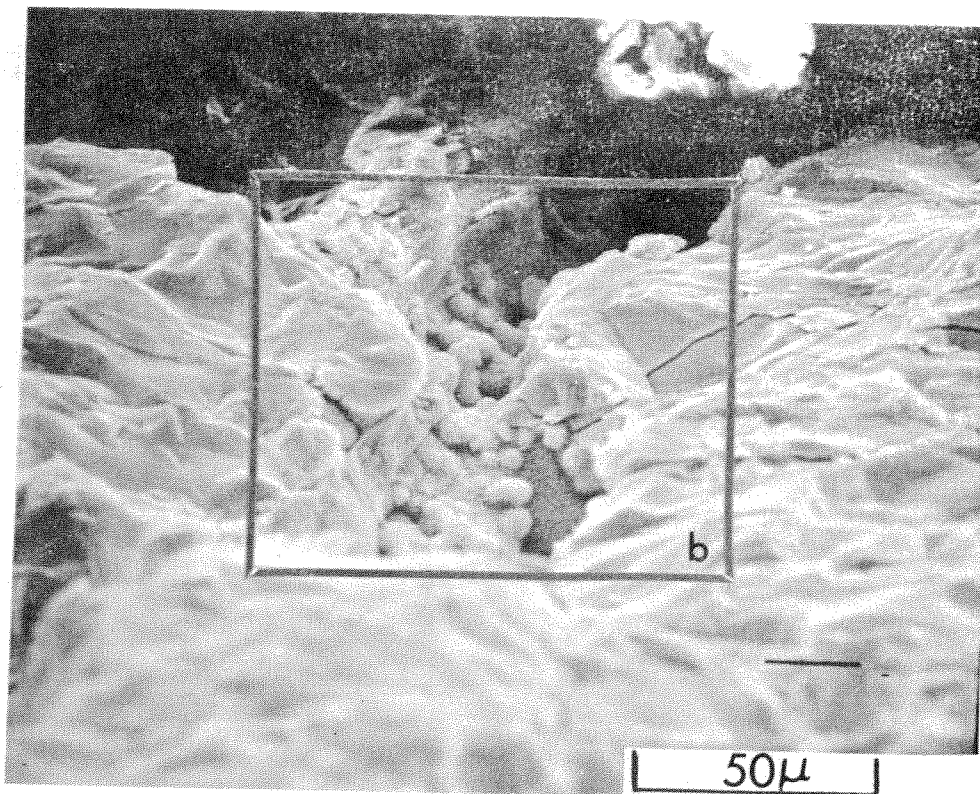


(c)

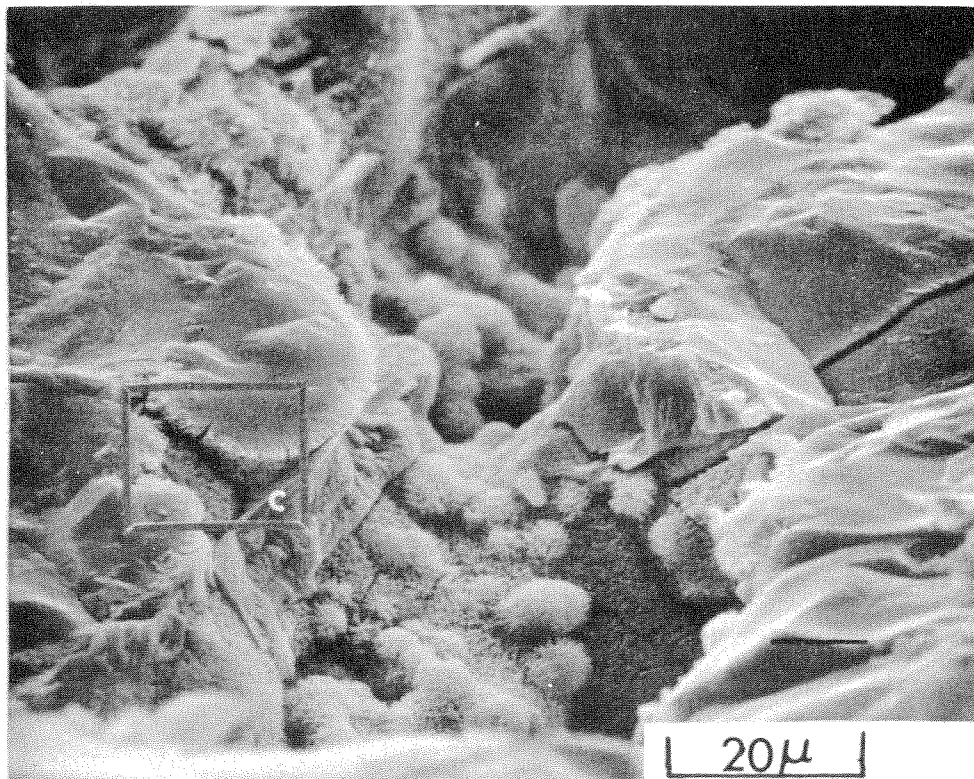


(d)

Figure 3.20 (Continued from opposite page)... (c) A close-up of an area marked in (b) showing a cross-section through the columnar zone and inner product at the fracture plane as well as the end-on view of the columnar zone at the left. (d) A close-up of an area marked in (c) showing the cross-section through the hydration products and the unhydrated clinker.

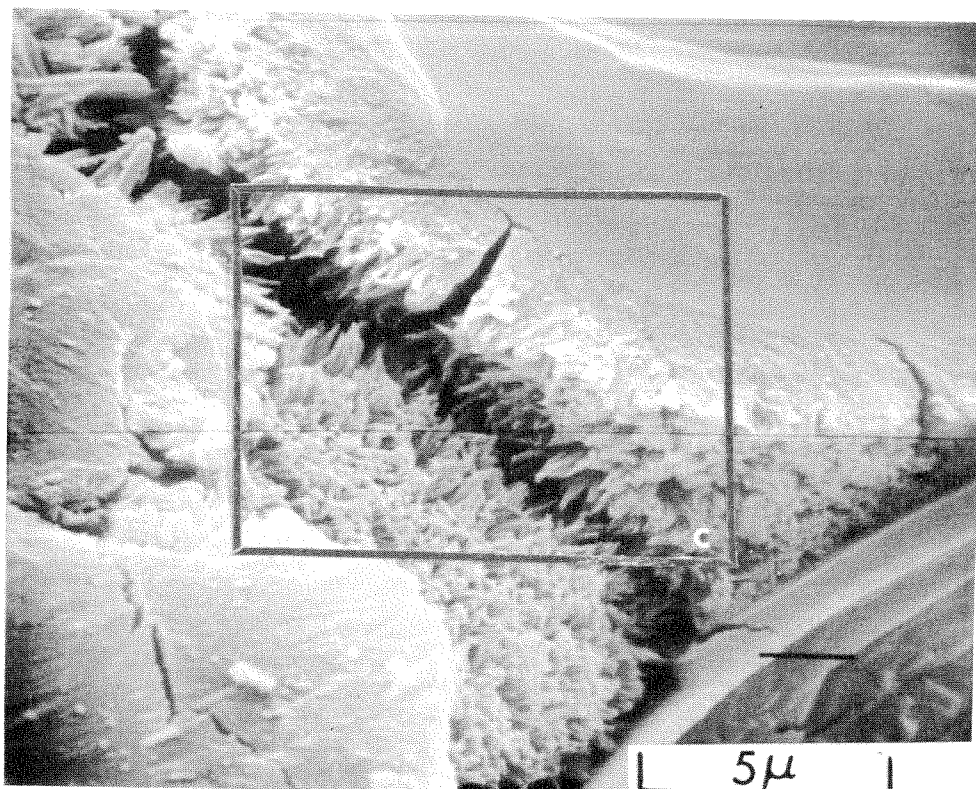


(a)

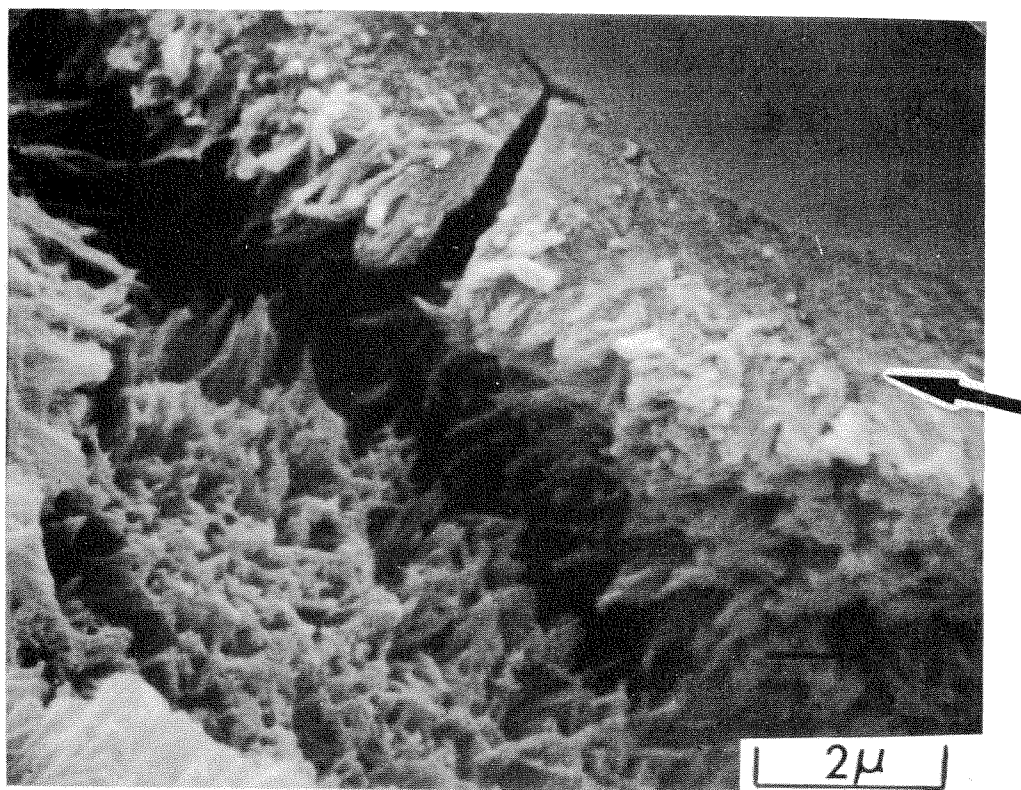


(b)

Figure 3.21 The initial hydration products in the pore of the clinker shown in the previous figure are shown here at a different angle. (a) The pore is in the center of this micrograph and it has been rotated approximately 90° counter clockwise and the angle changed approximately 45° . (b) A close-up of an area marked in (a) which is almost the same area shown in Figure 3.20 (b).

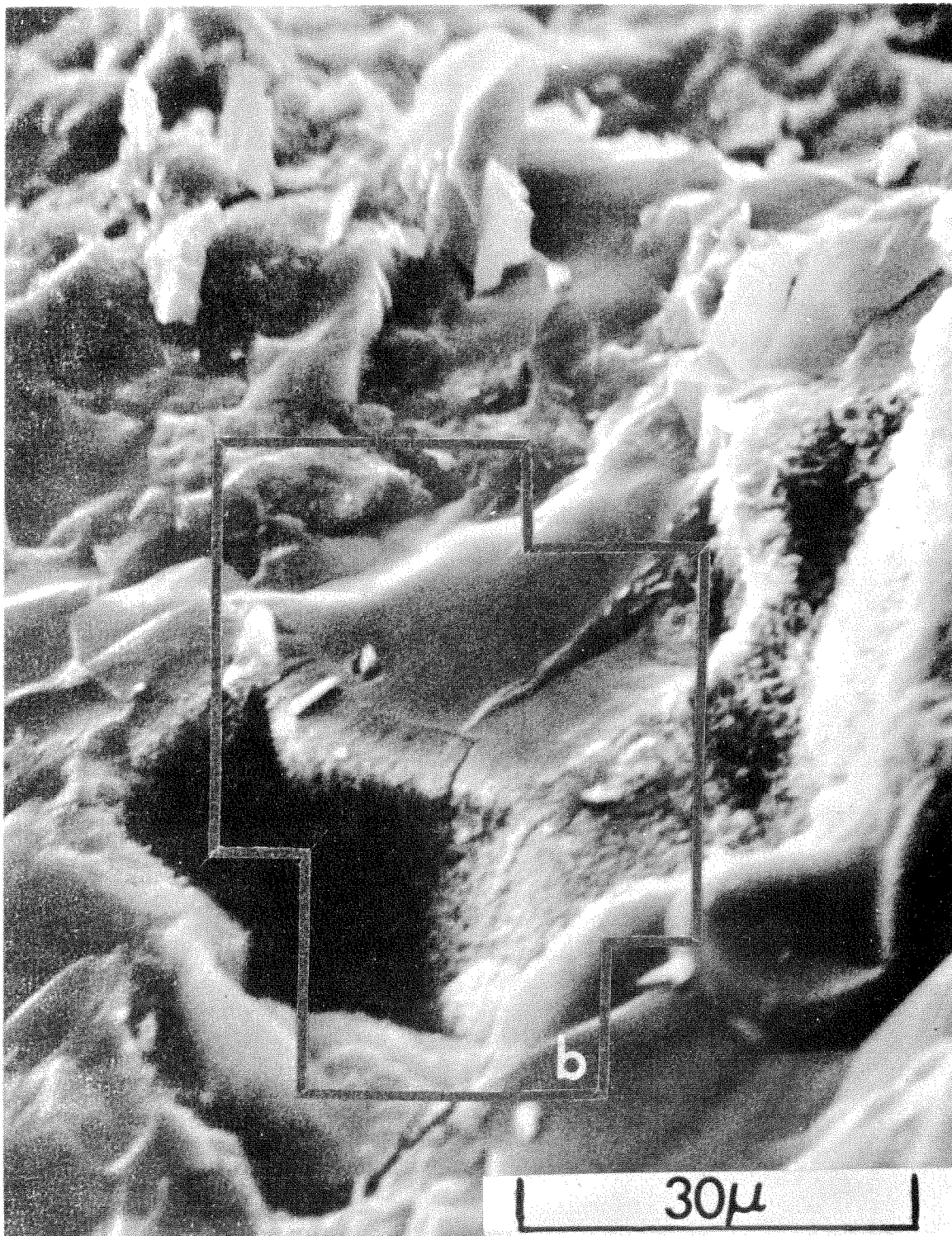


(c)



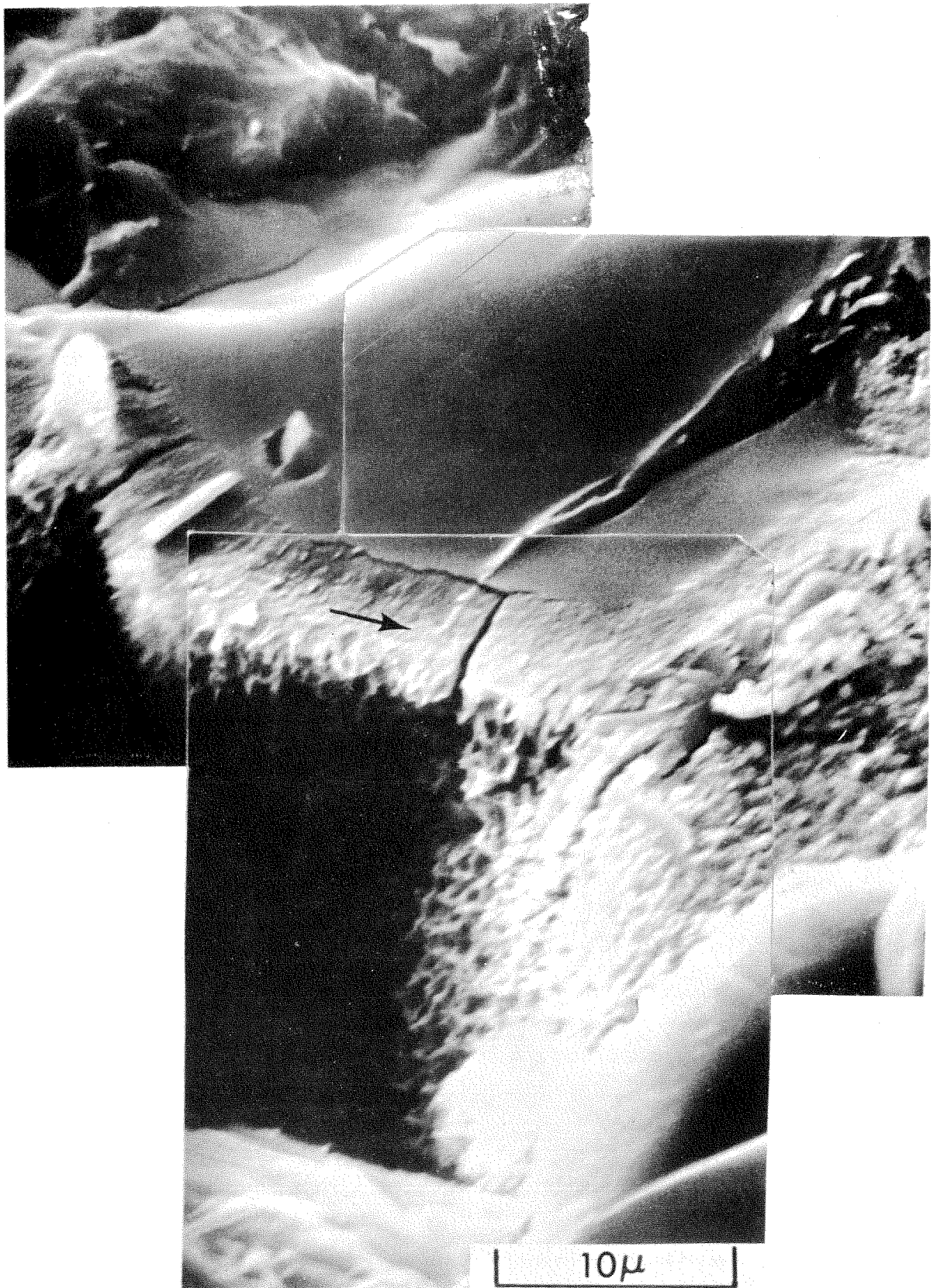
(d)

Figure 3.21 (Continued from opposite page)...(c) A close-up of an area marked in (b) showing a cross-section similar to that shown in Figure 3.20(c), but the angle is more appropriate to show some of the differences between the hydration products. (d) A close-up of an area marked in (c) showing cross-section through the hydration products and unhydrated clinker. The possible location of the original clinker surface is indicated by an arrow.



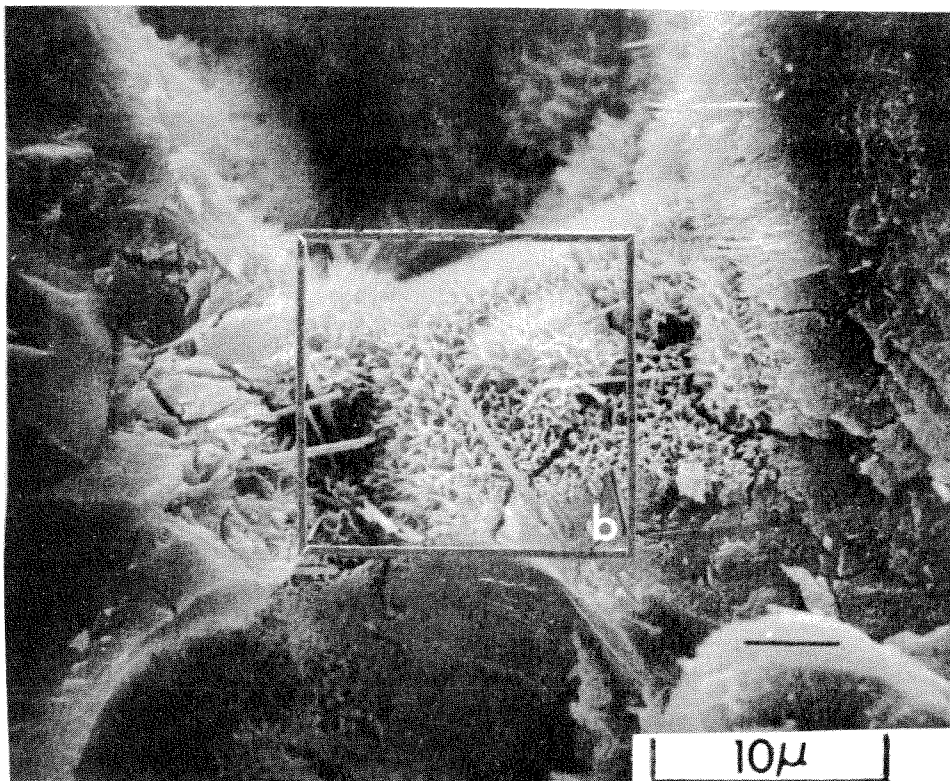
(a)

Figure 3.22 Another area of the clinker shown in Figures 3.20 and 3.21 shows a cross-section of another hydrated pore. (a) The pore is visible on the fracture surface with a narrow rim of rough hydration products making a contrast to the rather smooth ceramic fracture of the unhydrated material.

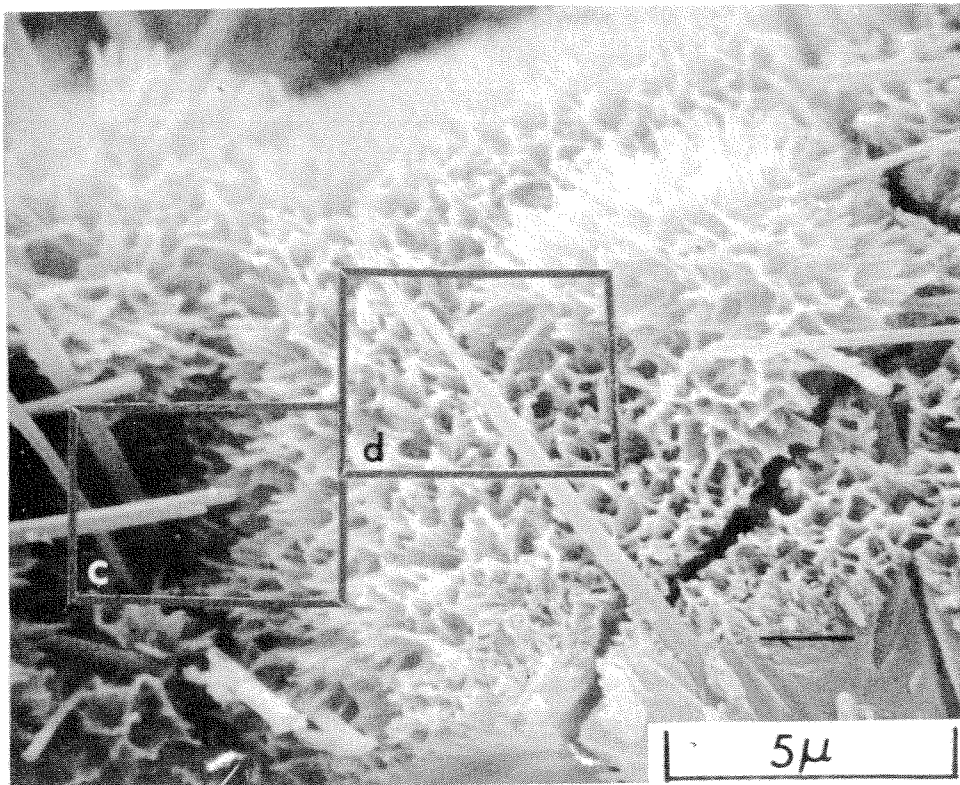


(b)

Figure 3.22 (Continued from opposite page)... (b) A composite of several close-up micrographs showing an area marked in (a). The arrow indicates the possible location of the original clinker boundary.

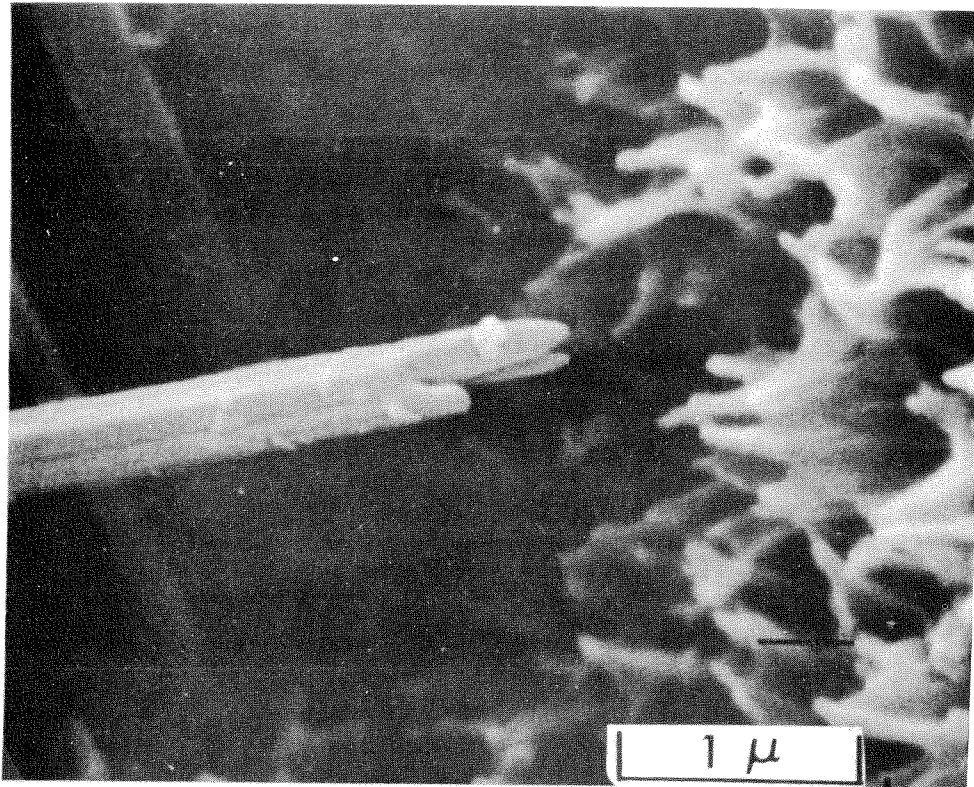


(a)

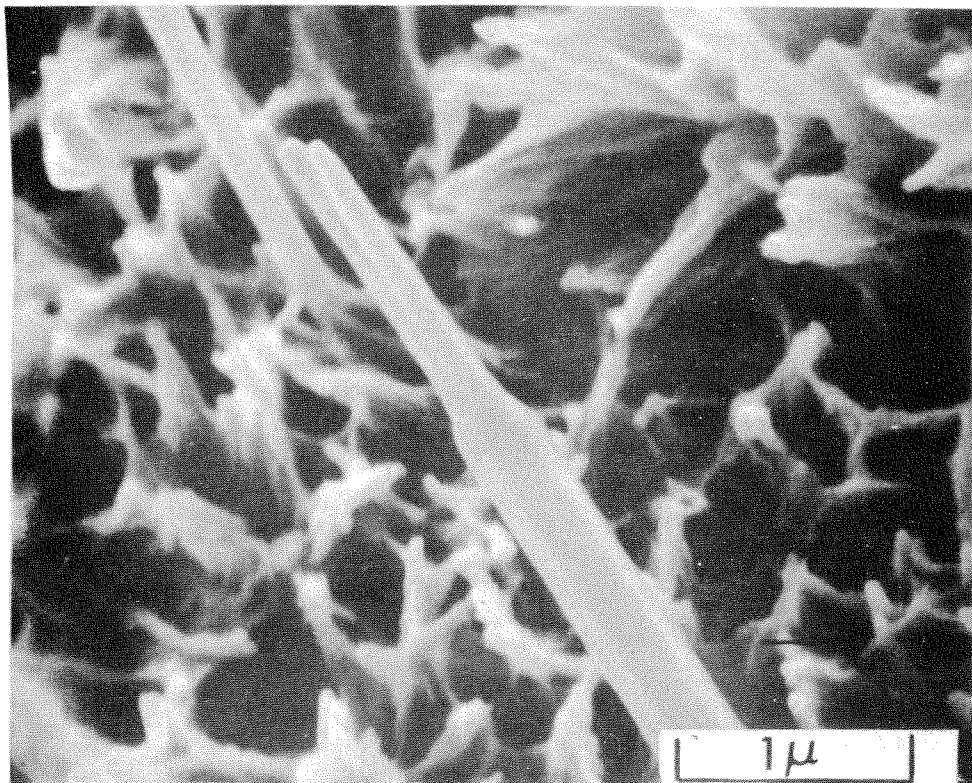


(b)

Figure 3.23 Another clinker fracture surface similar to that shown in the previous three figures which shows the morphology of the outer hydration products. (a) An area on a water-filled passage showing a plateau covered with hydration products in the center. (b) A close-up of an area marked in (a) showing the morphology of the outer hydration products.

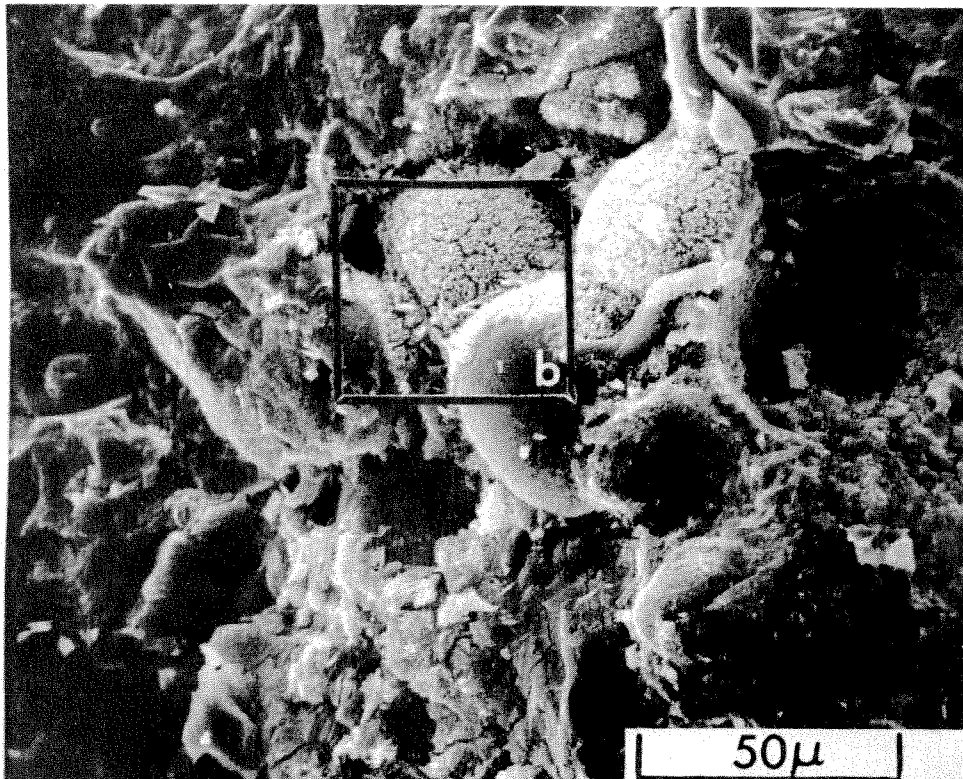


(c)

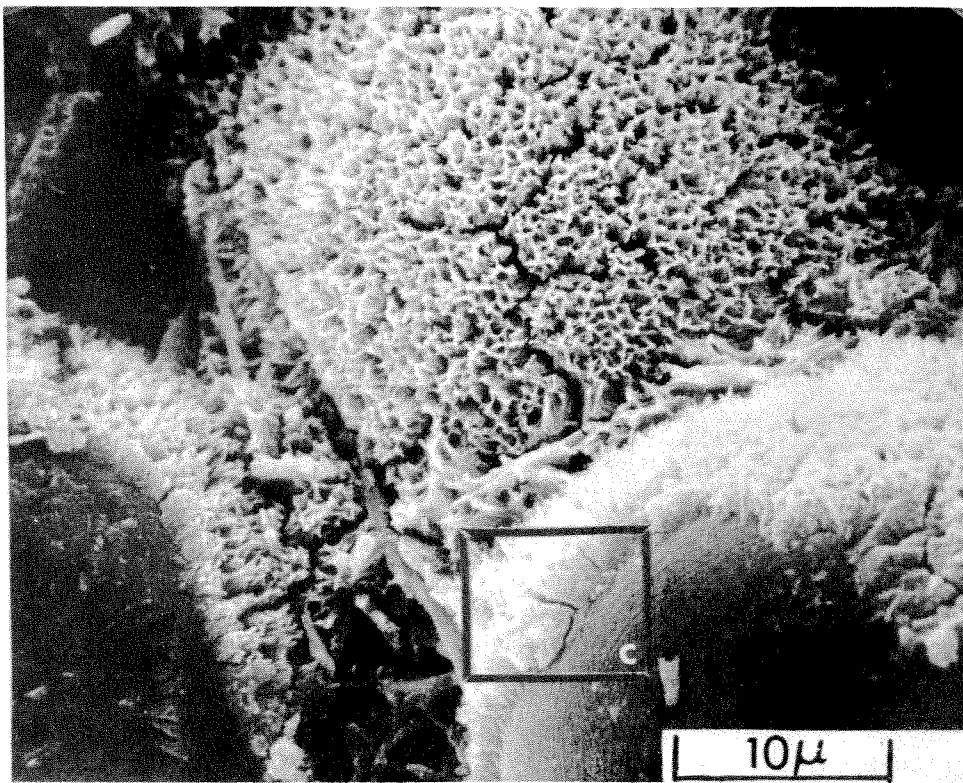


(d)

Figure 3.23 (Continued from opposite page)....(c) A close-up of the tip of a needle-like crystal marked in (b). (d) Another needle-like crystal as marked in (b) shows a decrease in thickness at mid-height. Both of these needles have morphologies similar to dendrites of other materials.

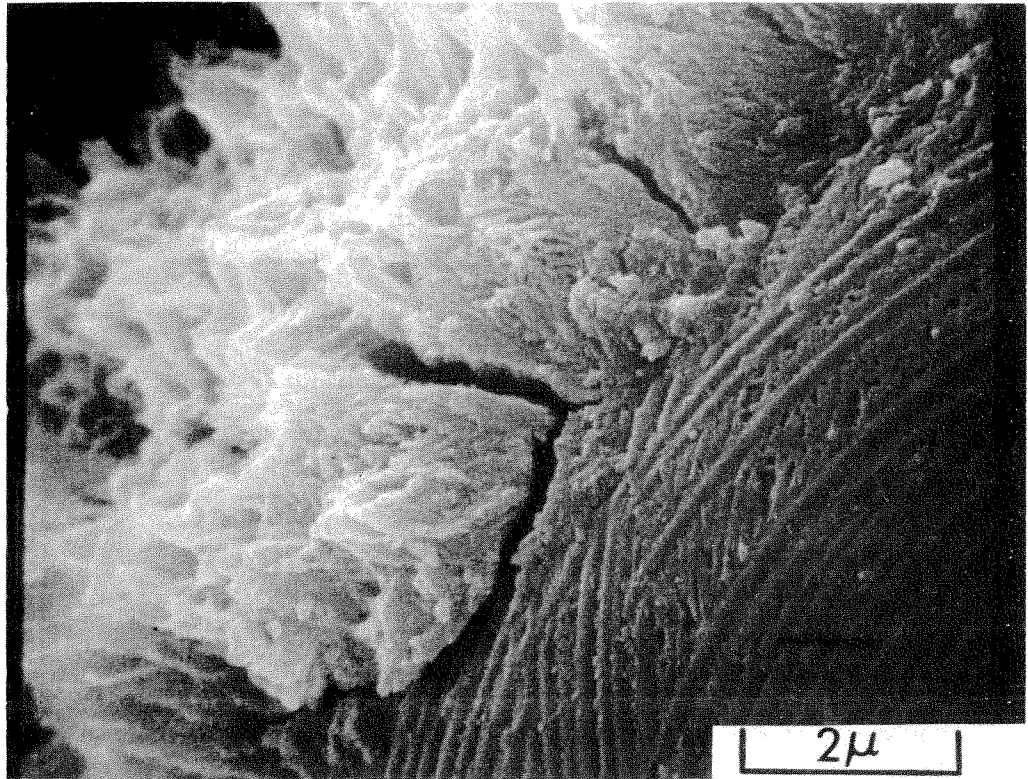


(a)



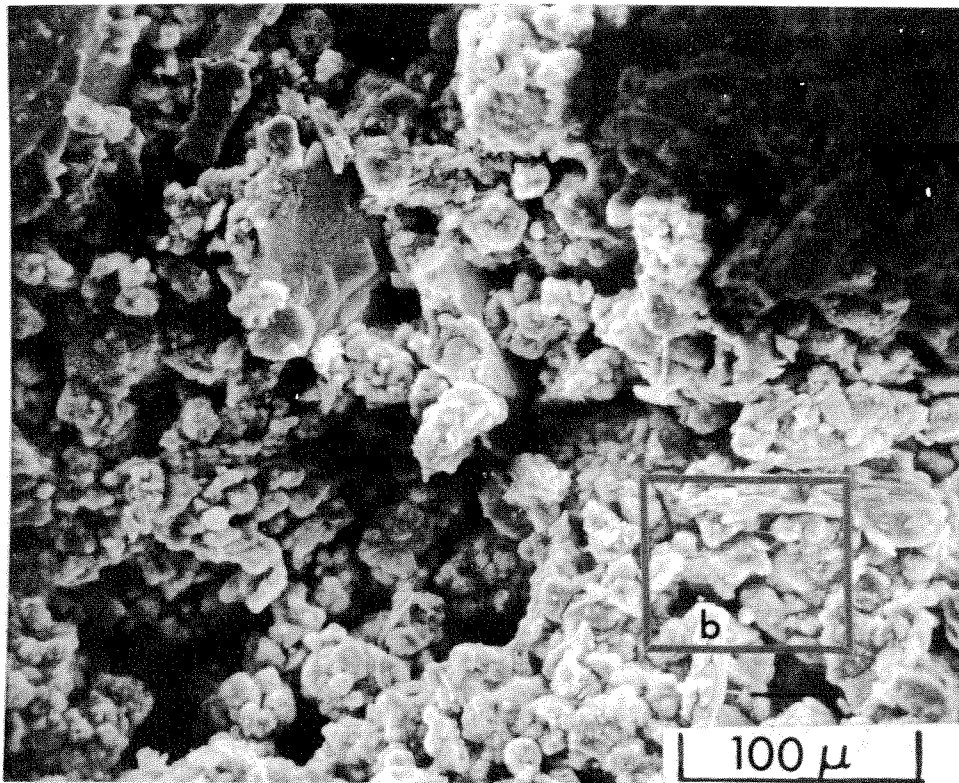
(b)

Figure 3.24 Another area of the clinker shown in the previous figure illustrates new morphology of the outer hydration products. (a) The only hydrated area appears to be in the center where three rounded grains in the clinker structure have hydrated. (b) A close-up of the area in the center of (a) as marked.

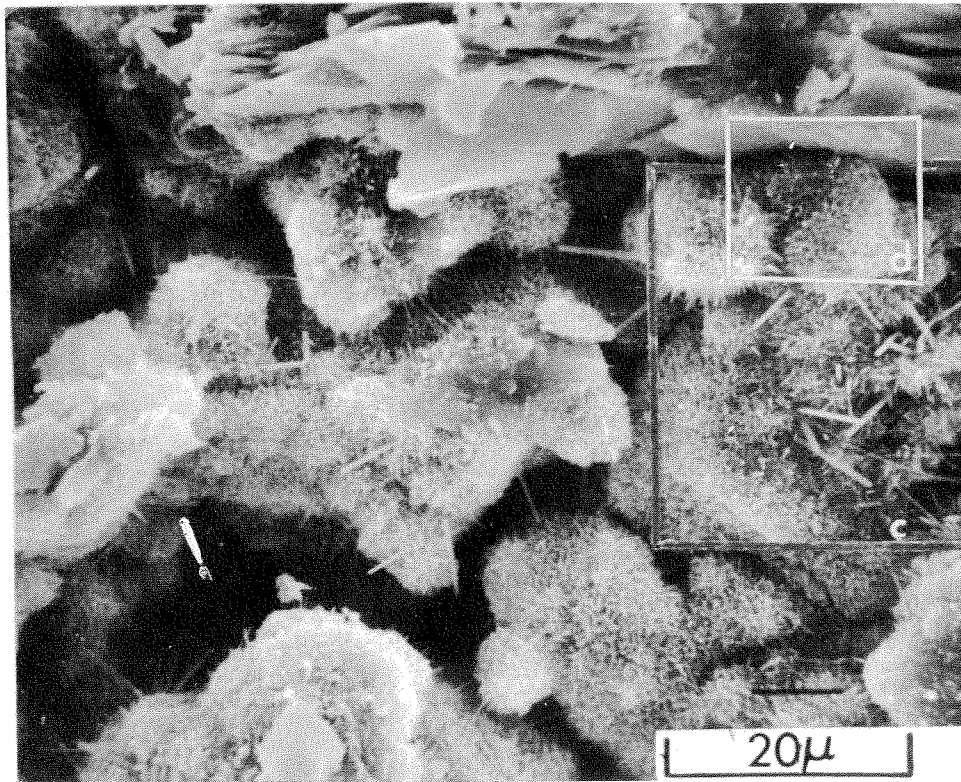


(c)

Figure 3.24 (Continued from opposite page)...(c) A close-up of the boundary between the outer hydration products and some inner product. The curved lines seen on the right may be the first product to grow on the surface of the cement.

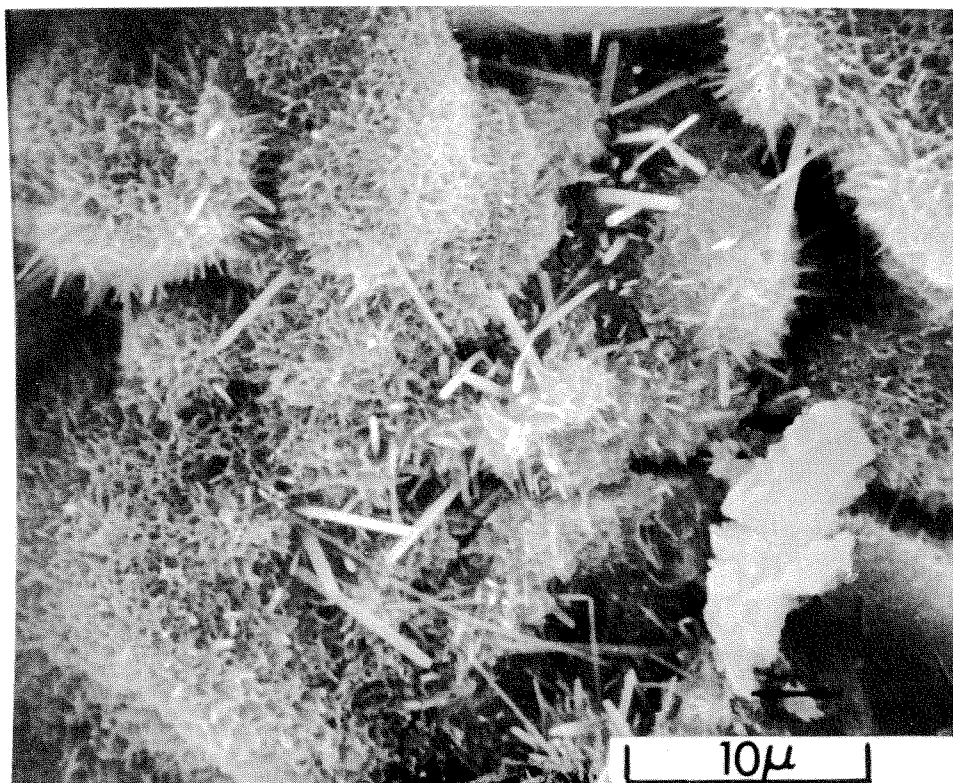


(a)

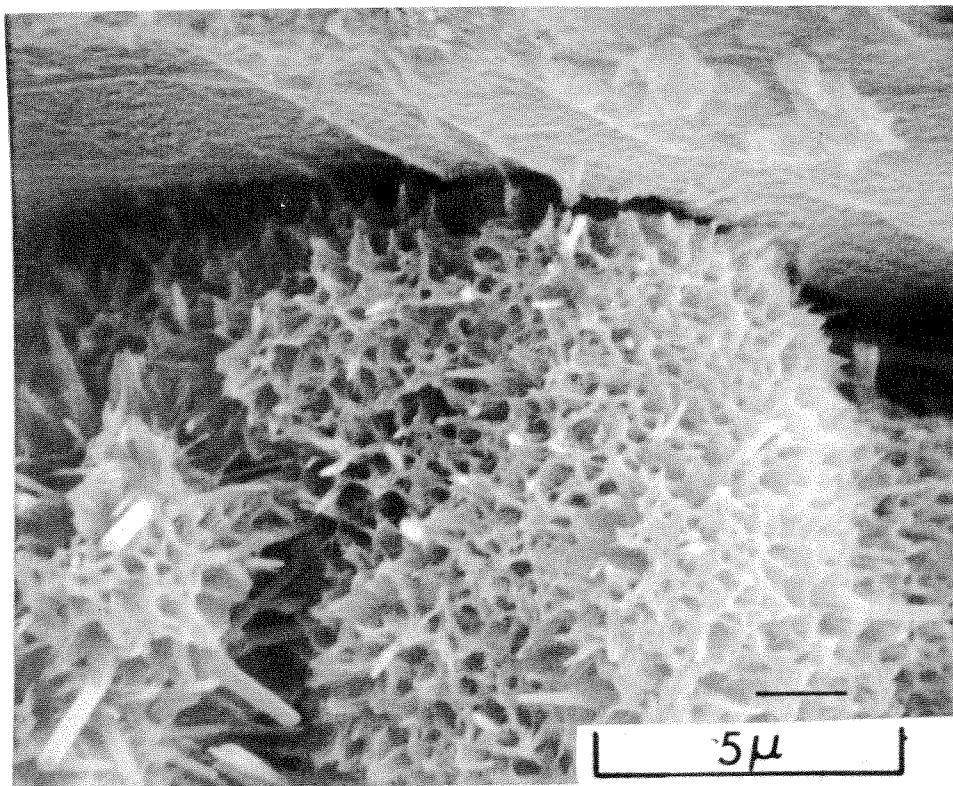


(b)

Figure 3.25 Fracture surface of a poorly hydrated portland cement paste. (a) The individual cement grains are visible in this low magnification scanning electron micrograph. (b) A close-up of an area marked in (a) shows the individual grains are covered with a columnar zone which has not grown together.



(c)



(d)

Figure 3.25 (Continued from opposite page)....(c) A close-up of an area in (b) shows the texture of the columnar zones of these cement grains is similar to that shown in the previous two figures. (d) A close-up of several of the grains as marked in (b) shows how the portlandite crystal along the upper edge of the micrograph appears to have been bonded to the columnar zone. The needle crystals are also visible here.

surface of the interior of the clinker. The original grain boundary of the anhydrous material would be the boundary between the inner and outer hydration products (see Figure 3.1), but there is not a clear indication exactly where this is in Figures 3.20(c) or 3.21(b) or (c). Another passage in the same piece of clinker is shown in Figures 3.22(a, b), and a possible clue to the location of the original boundary is present in these micrographs. A fracture surface mark appears to end at the original clinker boundary, and there is a difference in contrast at approximately the same place.

The morphology of the outer product columnar zone can be observed to take on many different forms on clinker surfaces exposed to water. An interesting pattern is shown in Figure 3.23(a) and (b) which Diamond (35) has called a "reticular" network. This pattern is somewhat like the cellular interface observed on the solid-liquid interface in impure metals (3,37). The morphology of the long needles shown in Figures 3.23(c) and (d) is also similar to dendrites in metals and other materials such as ice (38). The reticular network morphology is again shown in Figure 3.24(a) and (b), but perhaps the underlying layer is shown in Figure 3.24(c). The reticular network morphology is shown on many cement grains in the poorly hydrated portland cement paste pictured in Figure 3.25(a,b,c,d). It is evident that the hydration has not proceeded very far, but the cement grains have begun to bind together by having their columnar zones intergrow. This may well be one of the important binding mechanisms of cementitious materials.

3.5 The Hardening of Cement Paste-- A Solidification Process

The fracture surfaces of hydrated cement pastes presented above illustrate the microstructure that resulted from the growth of solids within the originally water-filled space, and they will now be discussed in terms of a solidification process. As noted previously, optical microscopy has also shown many of the features of this solidification process, and these observations will be included in the discussion.

The columnar zone, by the definition given earlier, contains outer hydration products that have formed on a surface and have growth features generally aligned perpendicularly to that surface. This is in contrast to the large crystals of portlandite which have been shown by optical microscopy to grow freely in the originally water-filled space. These portlandite crystals frequently engulf the cement grains, but there does not appear to be much effect of this process on the growth of the portlandite. In other words, the portlandite crystals viewed on the fracture surface appear to be homogeneous and there are no easily recognizable impurity zones around the engulfed cement grains. The fracture process has been affected by the presence of the engulfed grains, but this is a separate issue. Terrier and Moreau (30) have called these large space-filling crystals "primary portlandite," (or portlandite 1), and they are analogous to the "primary" or "proeutectic" solid which forms in a metallic eutectic alloy when the composition is not initially at the eutectic composition.

The analogy between the primary portlandite and the proeutectic crystals in the metallic system deserves to be defined in some detail.

ATOMIC PERCENT COPPER

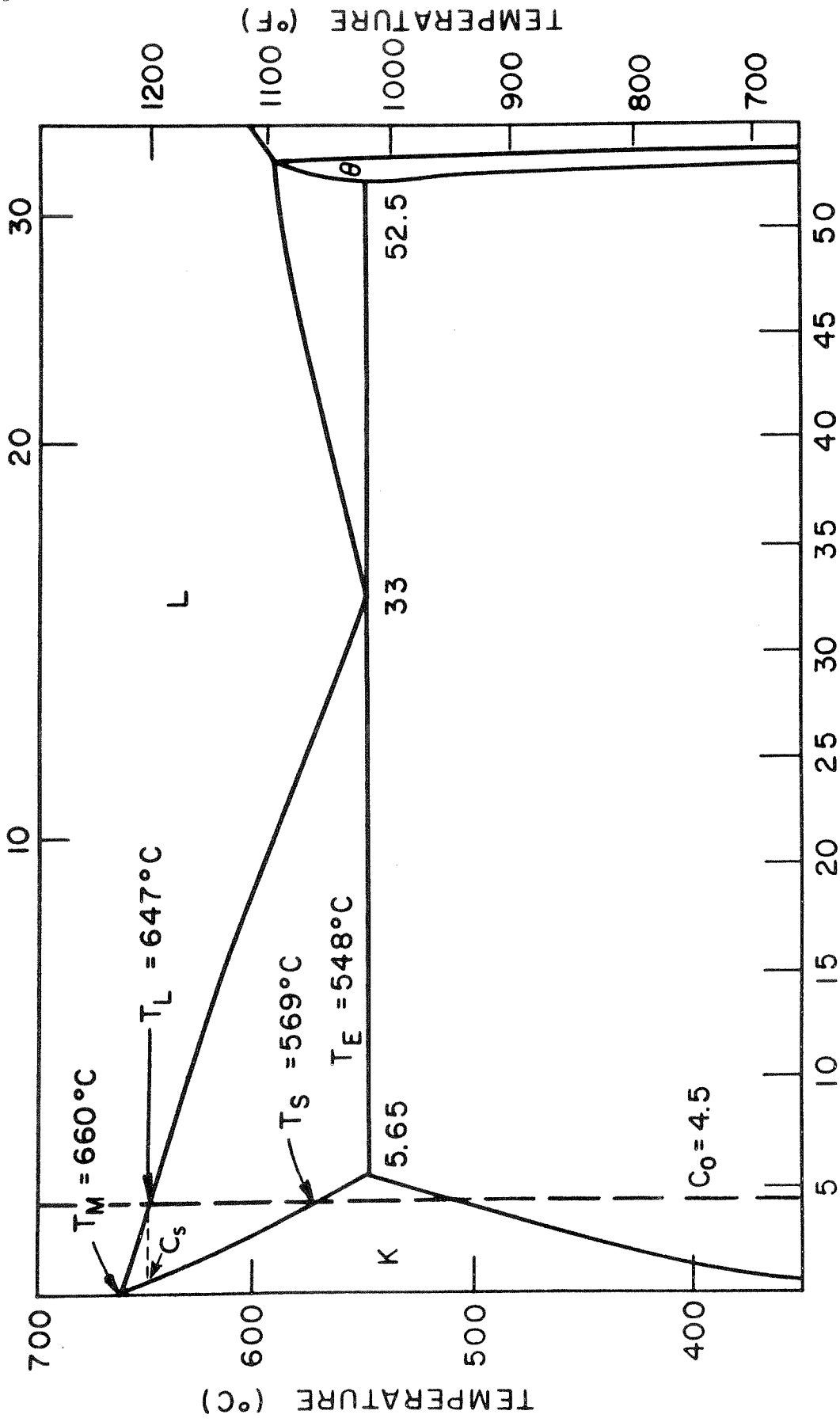


Fig. 3.26 Equilibrium phase diagram for aluminum-copper alloys (A.S.M., Metals Handbook, 1948).

The solidification process of a eutectic casting alloy can be illustrated by a specific example. Let the initial composition be C_0 as schematically shown for the aluminum-4.5% copper alloy in Figure 3.26. Solidification begins (neglecting undercooling) at 647°C with the formation of solid of composition C_s (approximately 1% copper); as solidification proceeds, the concentration of the solute (i.e., copper) increases in the liquid close to the solid-liquid by diffusion and mixing. The sequence of events beyond this point depends on many parameters such as rate of solidification, temperature gradient, and mixing. If mixing were complete, the whole of the liquid would change composition until it reached the eutectic composition (33% copper). Under those conditions and neglecting diffusion in the solid, the crystals of the aluminum-copper solid solution (K) would have a "cored" composition with the center at C_s and the outside at 5.65% copper. The remaining liquid would then solidify as a eutectic where crystals of the solid solution K and crystals of the intermetallic compound $\text{Al}_2\text{Cu}(\theta)$ form in close proximity. In this case the phases form in a lamellar morphology with parallel sheet-like crystals of each phase growing at right angle to the solid-liquid interface. The solidification of eutectic alloys has been reviewed by Chadwick (39), and their morphologies are extremely varied.

The single phase solid solution that formed before the liquid reached the eutectic composition is described as the "primary" or "proeutectic" solid. If mixing is less complete, the primary solidification can take place dendritically, but in any case, the primary solid continues to grow until the remaining liquid has reached the

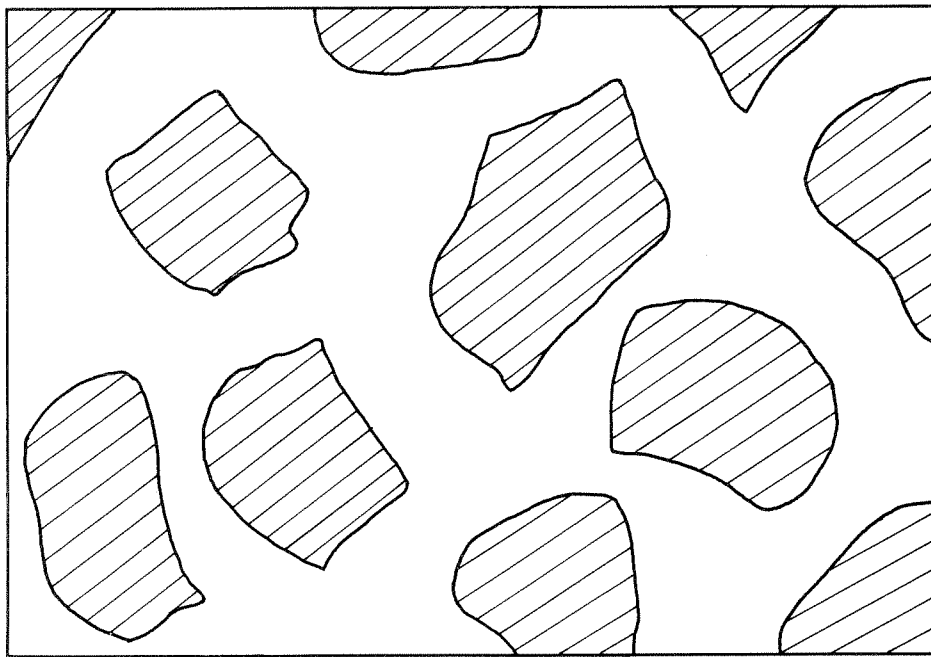
eutectic composition. The solidification of the eutectic liquid in the interdendritic regions allows observation of the morphology of the primary solid since the sample can be cut, polished, and differentially etched to show the outline of the boundary at the onset of eutectic growth.

It is important to note that the true equilibrium condition represented by the phase diagram would not allow any eutectic material to form from the melt. This rarely happens, since it would require the solid to follow the solidus curve (i.e., including "complete mixing" in the solid). The eutectic material has been observed in aluminum castings containing only hundredths of a percent of copper. The rejection of solute ahead of a growing crystal surface coupled with the relatively slow diffusion in the solid are the principles underlying the process of Zone Melting or Zone Refining invented by W. G. Phann (40).

The solidification of the hydrating cement paste has enough similarity to the metallic alloy to make the analogy useful; although the system also has many differences. The initial state of a fresh cement paste is schematically represented in Figure 3.27(a) for a 0.5 water-to-cement ratio; isolated cement grains are surrounded by water-filled space. The hydration starts by primary portlandite crystallizing at numerous centers within the water-filled space and by other products forming in and on the cement grains. This is schematically represented in Figure 3.27(b) at 33% hydration. The primary portlandite is crystallizing from the calcium hydroxide released into the water surrounding the cement grains. As the primary portlandite

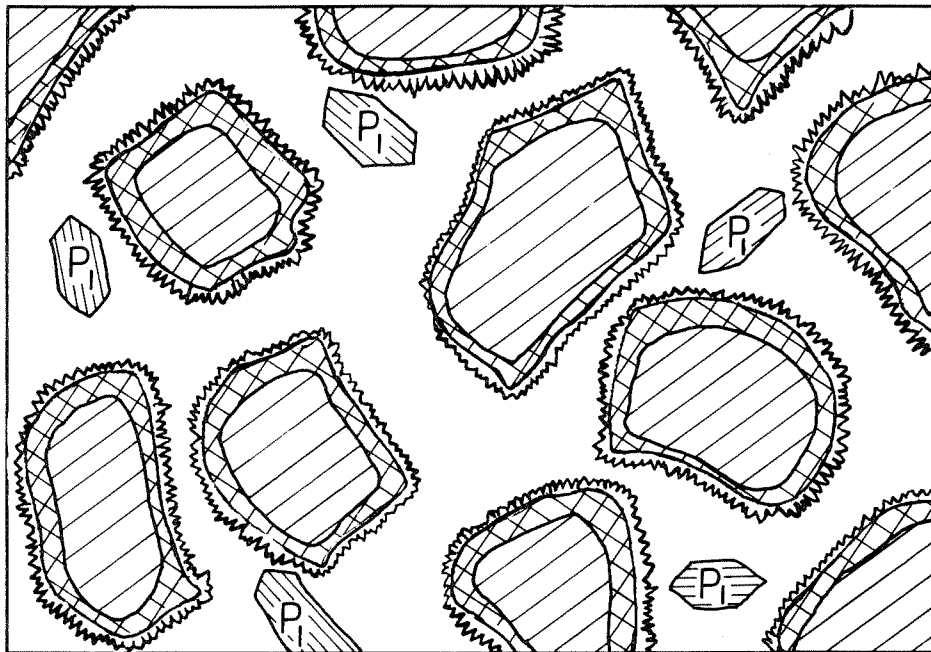
grows it rejects those solutes that cannot be accommodated in its crystal structure, the most important probably being silica, and this process enriches the remaining aqueous solution. Berger and McGregor (26) have reported that the later growth of portlandite is highly dendritic, and this is possibly due to the lateral rejection of solute from the protuberances characteristic of the dendritic morphology. Metallic dendrites formed by the rejection of solute are the common growth morphology for the primary solids found in alloys cast in most industrial processes. The analogy is probably very close in this respect. The dendritic morphology of the primary portlandite schematically shown in Figure 3.27(c) is patterned after Berger and McGregor's observation that growth in the c-axis terminated after a few hours and the later dendritic growth was perpendicular to the c-axis.

The dendritic growth of portlandite probably leads to considerable amounts of silica being trapped in the interdendritic regions. The poorly crystallized plates shown in the scanning micrograph in Figure 3.17(d) are due to the dendritic growth of primary portlandite. It should be noted that the dendritic morphology is not represented in the final schematic diagram in Figure 3.27(d) since its only trace would be in the distribution of silica in the interdendritic spaces which by that time would be filled with solids. A possible way to look at this is that since calcium hydroxide has a high surface energy and silica gel has a low surface energy one would expect a low specific surface for pure calcium hydroxide and a high specific surface for the silica gel. The interdendritic spaces of portlandite would be filled with a calcium silicate gel which would reduce the total surface energy of the crystal and stabilize the platey dendritic morphology.






FRESH PASTE

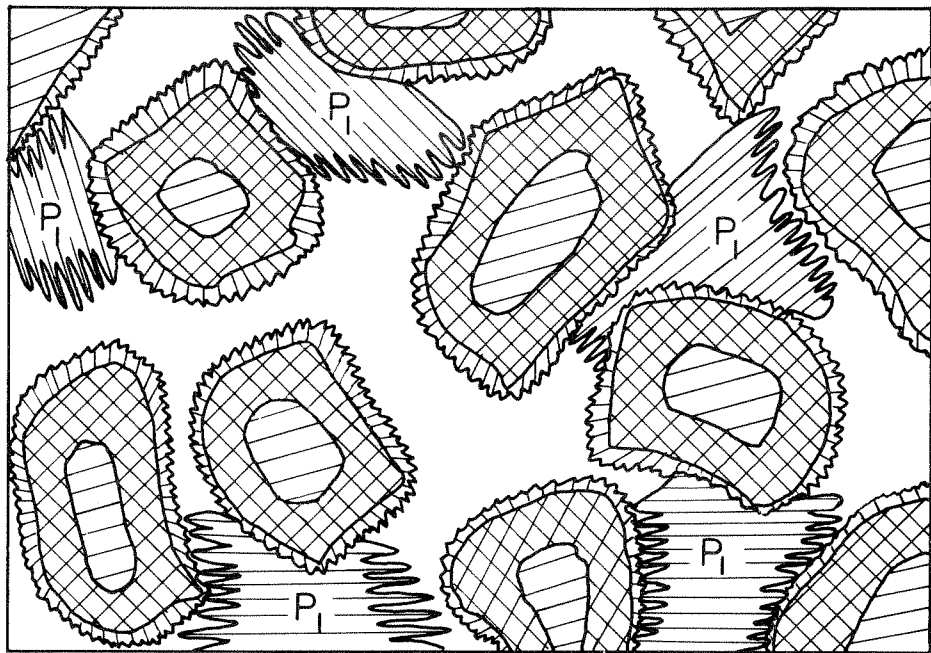
(a)



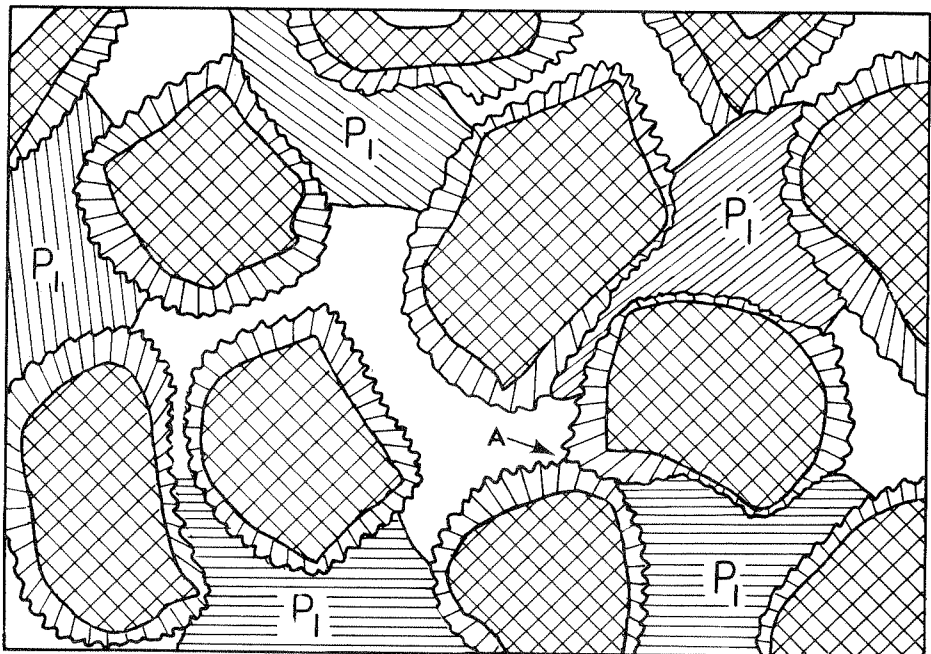
33% HYDRATED

(b)

Figure 3.27 A schematic representation of the hydration of cement based on the relative volumes shown in Figure 3.1. The multiphase nature of the cement grains has been neglected so this is like the hydration of tricalcium silicate alone. (a) Fresh paste of water-to-cement ratio of 0.5 is shown with unhydrated cement represented by  and the originally water-filled space clear. (b) After 33% hydration the inner hydration products are represented by  and the outer products by . The primary portlandite is labeled P_1 and the columnar zone is shown around each grain.



67 % HYDRATED (c)



100 % HYDRATED (d)

Figure 3.27 (Continued from opposite page)...(c) After 67% hydration the unhydrated cores are clearly surrounded by thick "rims" of inner hydration products and the columnar zone of outer products is growing on the outer surface of each grain. The primary portlandite, P_1 , is shown with the dendritic morphology reported in the optical study of Berger and McGregor (26). (d) At 100% hydration the unhydrated cement has been consumed but the shape of the original cement grains can be distinguished if the inner product differs from the columnar zone of outer products. The intergrowth of the columnar zones from two different grains is only shown at one place, marked A, but this would be more common at lower water-to-cement ratios.

Williamson (41) has suggested that the dendritic growth of hydration products of portland cement could be due to a constitutional supersaturation similar to the constitutional undercooling that is responsible for the dendritic morphology of metallic alloys. A two-phase model of the calcium silicate hydrate has been proposed to be made up of Ca(OH)_2 -like lamellar regions with silicate material on the surfaces which constrains them to growth in a plane (41). This can lead to thin lamellar crystals that are analogous to the chain-folded polymer crystals which show a wide range of growth morphologies. The columnar zones growing on the solid surfaces of cement grains and even on the surfaces of entrapped air voids (see p. 56) are probably examples of this kind of growth. These zones may change considerably during the complete hydration process, but their initial growth is by fine Ca(OH)_2 needles or plates growing in eutectic-like bunches. This is similar to the growth of eutectic structures which follows the growth of the primary or proeutectic phase in a metallic system just as the primary portlandite grows first in the cement system. Further discussion of this analogy will be presented in subsequent reports.

4. RELATIONSHIP OF MECHANICAL PROPERTIES TO MICROSTRUCTURE

4.1 Stress Concentration in Multiphase Brittle Microstructure

The fracture of brittle materials occurs at applied stress levels far below those expected from a theoretical consideration of the bonding forces in the material. The classic explanation of this phenomenon is due to Griffith (42), who postulated that fracture occurred at sub-microscopic structural defects, now called Griffith flaws. The existence of these flaws has been substantiated for relatively simple materials (43), and the more complex materials, such as cement paste or concrete, are assumed to possess many flaws whose character has not yet been identified. The scanning electron microscope has allowed direct observations on the fracture surfaces of both complex and simple materials, and these observations can be used to characterize the relative effects of microstructural features of cement paste on the fracture process. For instance, the portlandite crystals have been suspected of weakening the paste since they cleave easily, but this has not been shown explicitly. In fact, in some circumstances portlandite may give cement paste some of its strength, particularly at early ages. These points will be discussed below.

In more complex materials it is not sufficient to just identify the Griffith flaws; it is also necessary to understand how each of the microstructural components affects the fracture process. Hasselman and Fulrath (44) have investigated the relative effects of microstructural features, such as pores, on the origin of fracture from Griffith flaws. Williamson and Hester (45) have applied this approach to the fracture of neat cement pastes.

In any complex material there are some structural features which can be looked upon as flaws or defects and other structural features which act as micromechanical stress concentrators to change the distribution of stress near the flaws. The central objective of Hasselman and Fulrath's work (44) was to interrelate the effects of these two types of microstructural elements. They hypothesize that the relative size of the stress concentrator (they chose pores specifically) with respect to the Griffith flaw size can be a framework for understanding the observed fracture behavior of the material. To develop the hypothesis three cases can be chosen:

Case I. The microstructural feature and the resultant micromechanical stress fields are large relative to the size of the Griffith flaw,

Case II. the microstructural feature is of the order of magnitude of the size of the Griffith flaw, and

Case III. the microstructural feature is small relative to the size of the Griffith flaw.

In case I the flaw lies entirely in the zone affected by the large stress concentrating feature. As an example, an engineering structure with drilled holes or grooves comes under this case since the flaws are of microscopic dimensions and the areas of stress concentration are large in comparison. At least one flaw will always "feel" the presence of the stress concentrator, and thus the introduction of only one such feature will substantially decrease the observed strength of the material or structural system. The decrease in strength will correspond to the

maximum stress concentration factor which will usually be two or more.

In case III the stress concentration covers a very small area compared to the dimensions of the Griffith flaws so that there will be little influence on the fracture process. The strength should show a monotonic decrease in strength as the volume fraction of the stress concentrators increases, and this is in direct contrast to the precipitous decrease in strength characteristic of case I. Hasselman and Fulrath note that the effects of porosity on high strength polycrystalline ceramics fall under this case. In that kind of system the pores represent stress concentrators, but in alumina Passmore, et al. (46) found them to be an order of magnitude smaller than the flaw size which was of the order of the grain size. In case III situations the "cross-sectional area" approach of Knudsen (47) and Brown, et al. (48) for the effects of porosity on strength appear to be more applicable than the stress concentration approach.

In the intermediate case II the flaw size is the order of magnitude of the stress concentration zone so that on the average only a segment of a flaw is subjected to the stress concentration. The introduction of the first stress concentrating microstructural feature in this size range will cause a precipitous decrease in strength but only half or less of case I where the maximum stress concentration was applied to the flaw. As will be discussed below, this is probably the most important case for portland cement pastes.

The effects of the three cases on the relative strength of a brittle material are summarized in Figure 4.1. The discontinuous drop associated with the introduction of one flaw of either case I or case II is shown in Figure 4.1 for spherical stress concentrators for

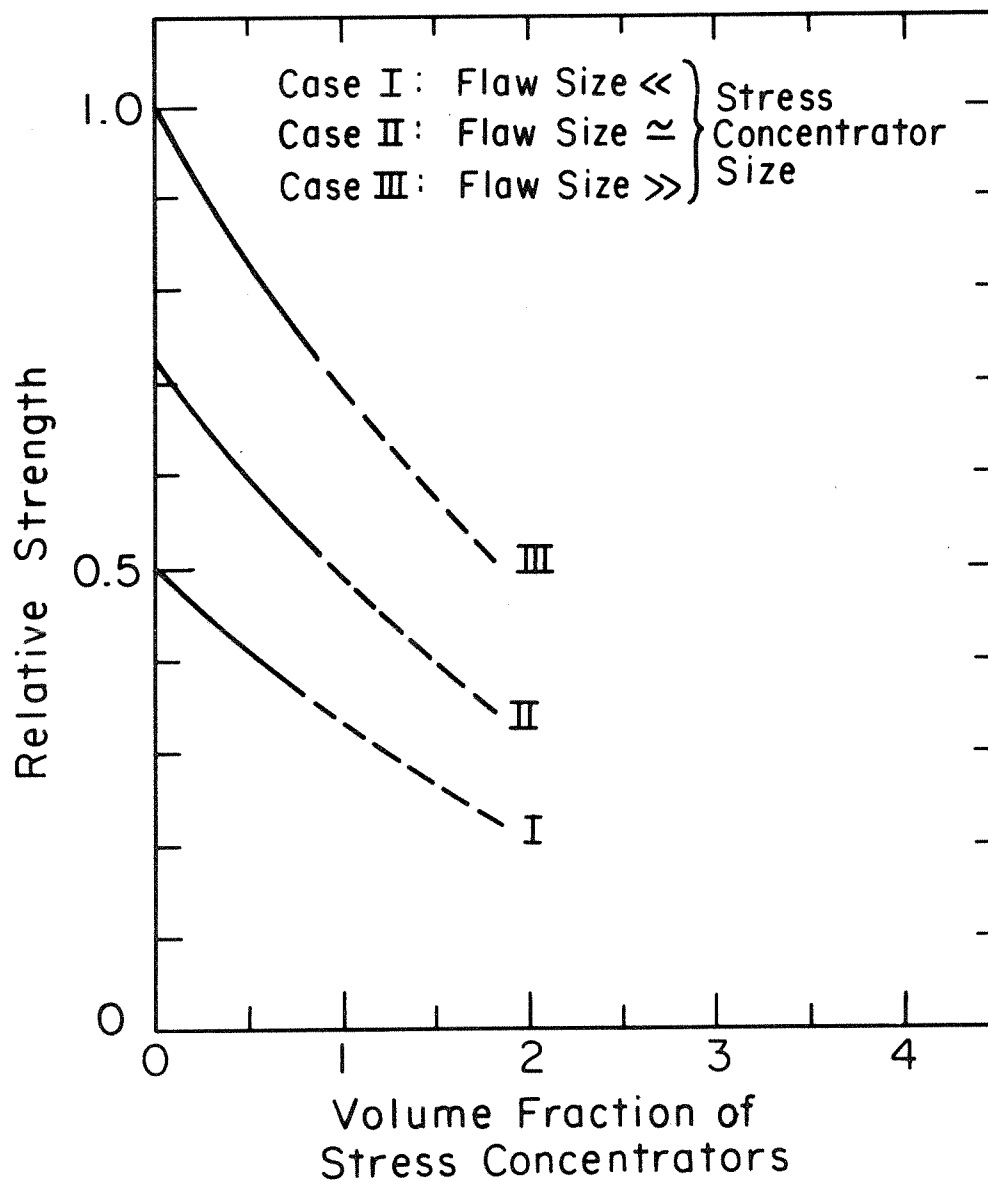


Figure 4.1 The effect of stress concentrators on strength of brittle solids is schematically shown for three possible cases of stress concentrator size with respect to flaw size [after Hasselman and Fulrath (44)].

which the maximum stress concentration factor under biaxial conditions is two. If the stress concentrator has another shape or the stress is uniaxial the loss of strength would be even greater. The most important feature of Hasselman and Fulrath's analysis is that there can be discontinuous loss of strength with the addition of a single microstructural feature.

4.2 Flaws and Stress Concentrators in Cement Paste

Since the strength of cement paste continues to increase over long periods of time, the relative effects of flaws and stress concentrators are continually changing over the same periods of time. The development of strength of the pure phases of portland cement are shown in Fig. 2.4 over a period of two years, and the parallel development of microstructure is shown in the scanning electron micrographs of Chapter 3. The solidification process is schematically represented in Fig. 3.27 from fresh paste to complete hydration, and this can be used to start the discussion of how the strength of the paste is related to the microstructure.

A portion of Fig. 3.27 is redrawn in Fig. 4.2 with externally applied loads represented to be acting on surfaces normal to the plane of the paper. The fresh paste shown in Fig. 4.2(a) has no strength, but it is shown here to make the point that a cement paste starts its hydration with a substantial volume of liquid. It is the solidification of material within that liquid which gives cement paste its strength. This is just as surely a solidification process as the casting of metals and, as discussed above, there are many similarities to metal solidification. After the specimen has hydrated 33% the outer products have begun to intergrow on some closely spaced grains as represented by grains

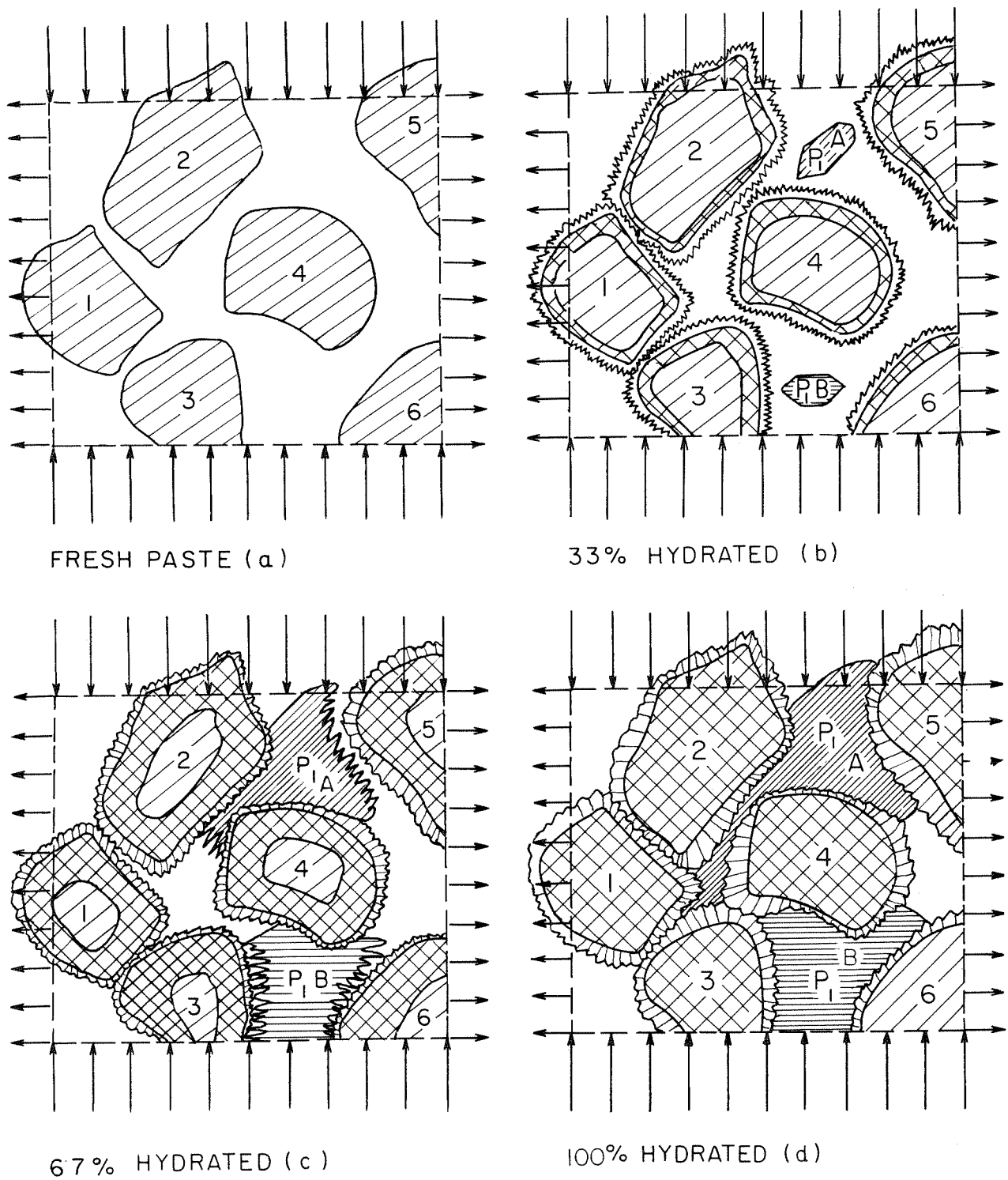


Figure 4.2 A schematic representation of the hydration of cement chosen to show the development of strength. The originally water-filled space is clear and the other products are represented as in Figs. 3.1 and 3.27.

numbered one, two, and three in Fig. 4.2(b), but there is still little strength although the paste has "set." The origin of the weakness lies in the many water-filled spaces which have not yet been filled by hydration products such as those shown between grains numbered four, five, and six. This is the stage of hydration we know least about since it is almost impossible to "decant" the water from a fresh fracture surface without the dissolved materials precipitating and obscuring the actual morphology of the paste at 33% hydration. This is similar to the effects Chadwick (49) found for decanted eutectic samples.

After the paste has hydrated 67% the primary portlandite crystals have reached essentially their final size and have occupied some of the originally water-filled space between the cement grains. This is schematically shown in Fig. 4.2(c) where the portlandite crystals labelled A and B have filled much of the space above and below grain number four. At the same time those cement grains close to each other, such as grains numbered one, two, and three in Fig. 4.2(c), have been fused together by their columnar zones coming in contact and probably intergrowing. The compressive component of the applied load shown in Fig. 4.2(c) can be carried by both the portlandite crystals on the right and the fused grains on the left. The tensile component of the applied load, however, will probably cause the paste to fail at the boundaries between the two portlandite crystals and cement grains numbered five and six. One weakening influence in the microstructure shown in Fig. 4.2(c) is the large water-filled space, or pore, between grains four, five, and six which acts as a stress concentrator to cause failure to occur along the above-mentioned boundaries. Those boundaries do not appear very

sound at this age because of the dendritic structure of the portlandite. The boundary between one microstructural feature and another can be considered a flaw in the sense discussed in the previous section.

It would appear that at 100% hydration both the compressive and tensile component of the applied load can be resisted by the rather sound microstructure shown in Fig. 4.2(d). This is probably more true of the compressive component since the pores will concentrate the tensile stress at various potential weak points, i.e., flaws, within the paste.

In considering the strength of the paste microstructure schematically represented in Fig. 4.2(c) and (d), a number of potential flaws and stress concentrators can be identified. Several of these potential flaws and stress concentrators change during the later stages of curing and several can be controlled by such factors as water-to-cement ratio, cement grain size, placement conditions, and type of cement used. One set of flaws can be characterized as the boundaries between the various microstructural features while others are more unique. A list of potential flaws:

A. The boundary between:

- (1) unhydrated core and inner hydration product of each cement grain;
- (2) inner hydration product and outer product columnar zone in each grain;
- (3) outer product columnar zones of two different grains;
- (4) portlandite and outer product columnar zone of cement grains;
- (5) portlandite crystals (i.e., a grain boundary);
- (6) the hydration products of the minor compounds and other features;

- B. The cleavage planes of portlandite crystals;
- C. Cracks caused by shrinkage or other effects.

The possible stress concentrators are:

- A. Portions of the originally water-filled space which remain as pores in the final microstructure (generally the result of high water-to-cement ratios);
- B. The entrapped and/or intentionally entrained air voids visible in most cement pastes;
- C. The pseudomorphs of original cement grains, particularly when entrapped in portlandite crystals.

Most of these potential flaws and stress concentrators are visible in some or all of the scanning electron micrographs shown in Chapter 3. They are also represented in the schematic drawing in Figures 3.27 and 4.2, and the discussion of latter figure interprets how some of these flaws will affect the strength of the cement paste. The relative importance of the potential flaws listed above is now being investigated and will be discussed in a future report. The relationship between the stress concentrators and the flaws is also being studied and it is hoped that this information can be applied to make cement paste a better material. The identification of the possible flaws and stress concentrators will now end this report, and a future report will start from this point to develop the subject further.

REFERENCES

1. F. Gille, I. Dreizler, K. Grade, H. Krämer and E. Woermann, Mikroskopie des Zementklinkers, Bilderatlas, Betou-Verlag BmbH, Düsseldorf, 1965.
2. A. Grudemo, "The Microstructure of Hardened Cement Paste," Proc., 4th Intern. Symp. Chem. of Cement, Washington, D.C. (1960), U.S. Bur. Stand. Monogr. No. 43, 615-47..
3. B. Chalmers, Principles of Solidification, J. Wiley, N. Y., 1964.
4. B. Chalmers, Physical Metallurgy, J. Wiley, N. Y., 1959.
5. S. Brunauer and L. E. Copeland, "The Chemistry of Concrete," Scientific American, 210, No. 4 (1964), 80-91.
6. R. W. Nurse, "Phase Equilibria and Constitution of Portland Cement Clinker," 4th Intern. Symp. Chem. of Cement, Washington, D.C. (1960) U.S. Bur. Stand. Monogr. No. 43, 9-21.
7. H. G. Midgley, "The Formation and Phase Composition of Portland Cement Clinker," Chapter 3, The Chemistry of Cements, H.F.W. Taylor, ed., Academic Press, N. Y. and London, 1964.
8. H.F.W. Taylor, "The Chemistry of Cements," Royal Inst. of Chemistry, Lecture Series, 1966, No. 2, London.
9. H.F.W. Taylor, "The Calcium Silicate Hydrates," Proc., 5th Intern. Symp. Chem. of Cement, Tokyo, 1968.
10. W. C. Hansen and J. S. Offutt, Gypsum and Anhydrite in Portland Cement, 2nd edition, published by United Gypsum Corp. Chicago, Ill., 1969.
11. T. C. Powers, "Structure and Physical Properties of Hardened Portland Cement Paste," J. Am. Ceram. Soc., 41, (1958) 1-6.
12. J. H. Taplin, "A Method for Following the Hydration of Portland Cement Paste," Australian J. Appl. Sci., 10, (1959) 329-45.
13. T. C. Powers, "Some Physical Aspects of the Hydration of Portland Cement," J. PCA Res. and Dev. Lab, 3, (1961), 47-56.
14. S. Brunauer and S. A. Greenberg, "The Hydration of C_3S and $\beta-C_2S$ at Room Temperature," Proc., 4th Intern. Symp. Chem. of Cement, Washington, D.C., (1960), 135-165.
15. R. F. Feldman, private communication.

16. T. C. Powers, "Physical Properties of Cement Paste," Proc., 4th Intern. Symp. Chem. of Cement, Washington, D.C., (1960), U.S. Bur. Stand. Monogr. No. 43, 577-613.
17. W. C. Hansen, "Solid-Liquid Reactions in Portland Cement Pastes," Mat. Res. and Stand., 2, (1962), 490-93.
18. R. H. Bogue and W. Lerch, "Hydration of Portland Cement Compounds," Ind. Eng. Chem., 26, (1934).
19. H. LeChatelier, Thesis 1887: "Récherches Experimentales sur la Constitution des Moitiers Hydrauliques," (1904), 2nd Ed. Dunod, Paris (English translation), McGraw Pub. Co. (1905), 132 pp.
20. E. Stern, "New Experiments on Cement," Chem.-Ztg., 32, (1908), 1029-31.
21. E. Stern, "Discussions on the Microstructure of Portland Cement," Ztschr. Amorg. Chem., 63, (1909), 160-67.
22. A. Ambronn, "Crystallization and Gel Formation in the Hardening of Cement," Chem.-Ztg., 33, (1909), 270-72.
23. A. A. Klein and A. J. Phillips, "Hydration of Portland Cement," U.S. Bureau of Standards Tech. Paper No. 43, (1914), 71 pp.
24. B. Erlin and N. R. Greening, "Hydration Studies by Time-Lapse Photomicrography," J. PCA Res. Develop. Lab., 10 [2], (1968), 58-61.
25. R. Kondo and S. Ueda, "Kinetics and Mechanism of the Hydration of Cements," Proc. 5th Intern. Symp. Chem. Cement, 2, (1969), 203-48.
26. R. L. Berger and J. D. McGregor, "Influence of Temperature and Water-Solide Ratio on Growth and Morphology of Calcium Hydroxide Formed During the Hydration of C_3S ," presented at West Coast Meeting, Am. Ceram. Soc., Pasadena, Calif., 1968.
27. R. J. Colony, "Petrographic Study of Portland Cement," Columbia School of Mines Quart., 36 [1], (1914), 1-21.
28. K. Kumagai and H. Takata, "Hydration Phenomena of Cement," J. Soc. Chem. Ind. Japan, 34, (1931), 87-8.
29. L. S. Brown and R. W. Carlson, "Petrographic Studies of Hydrated Cements," Proc. of ASTM, 36, (1936), 332-50.
30. P. Terrier and M. Moreau, "Research on the Pozzolanic Action of Fly Ash in Cement," Cent. Etud. Rech. Ind. Liants Hydr. Tech. Pub. 176, (1966), 32 pp.

31. L. S. Brown, "Discussion to A. Grudemo's paper," Ref. (2), Proc., 4th Intern. Symp. Chem. of Cement, Washington, D.C., (1960), U.S. Bur. Stand. Monogr. No. 43, 655-6.
32. R. B. Williamson, "Portland Cement: Pseudomorphs of Original Cement Grains Observed in Hardened Pastes," Science, 164, (1969), 549-51.
33. L. E. Copeland and D. L. Kantro, "Chemistry of Hydration of Portland Cement at Ordinary Temperature," Chapter 8, Chemistry of Cements, H.F.W. Taylor, ed., Academic Press, N. Y. and London, (1964), 313-70.
34. S. Chatterji and J. W. Jeffery, "Three-Dimensional Arrangement of Hydration Product in Set Cement Paste," Nature, 209, (1967), 1233-1234.
35. S. Diamond, "Application of Scanning Electron Microscopy to the Study of Hydrated Cement," Proc., 3rd Scanning Electron Microscope Symp., IIT Res. Inst., Chicago, Ill., (1970), 385-92.
36. R. H. Mills, "Collapse of Structure and Creep in Concrete," Intl. Conf. Struc., Solid Mech., and Eng. Design of Civil Eng. Matls., Southampton, England, April, 1969.
37. R. B. Williamson, "Constitutional Super-Saturation in Portland Cement Solidified by Hydration," J. Crystal Growth, 3, (1968), 787-94.
38. R. B. Williamson and B. Chalmers, "Morphology of Ice Solidified in Undercooled Water," Crystal Growth (supplement to The J. Phys. Chem. Solids), H. S. Peiser, Pergamon Press, Oxford, (1967), 739-43.
39. G. A. Chadwick, "Eutectic Alloy Solidification," Progress in Materials Science, ed., Pergamon Press, Macmillan Co., N. Y., 1963.
40. W. G. Phann, Zone Melting, J. Wiley and Sons, N. Y., 1958.
41. R. B. Williamson, "Constitutional Supersaturation in Portland Cement Solidified by Hydration," J. Crystal Growth 3,4 (1968), 787-794.
42. A. A. Griffith, in Proceedings First International Congress of Applied Mechanics, J. Waltman, Jr., ed., Delft, Holland, (1924), 55-63.
43. C. J. Phillips, "Strength and Weakness of Brittle Materials," Am. Scientist, 53, (1965), 20-51.

44. D.P.H. Hasselman and R. M. Fulrath, "Mechanical Stress Concentrations in Two-Phase Brittle-Matrix Ceramic Composites," J. Am. Cer. Soc., 50, (1967), 399-404.
45. R. B. Williamson and W. Hestor, "Relationship between Microstructure and Fracture Strength of Hydrated Portland Cement Pastes," presented at Annual Meeting of Am. Ceramic Society (1970), (to be submitted for publication).
46. E. M. Passmore, R. M. Spriggs, and T. Vasilos, "Strength-Grain Size-Porosity Relations in Alumina," J. Am. Ceram. Soc., 48, (1965), 1-7.
47. F. P. Knudsen, "Dependence of Mechanical Strength of Brittle Polycrystalline Specimens on Porosity and Grain Size," J. Am. Ceram. Soc., 42, (1959), 376-87.
48. S. D. Brown, R. B. Biddulph, and P. D. Wilcox, "A Strength-Porosity Relation Involving Different Pore Geometry and Orientation," J. Am. Ceram. Soc., 47, (1964), 320-22.
49. G. A. Chadwick, "Decanted Interfaces and Growth Forms," Acta Metallurgica, 10, (1962), 1-12.

APPENDIX

The preparation of specimens for optical microscopy have been described by most of the investigators listed in Section 3.0 above. In a similar fashion the preparation of transmission electron microscope samples have been presented by those who have used this technique, and several references are given in Section 3.0. There are many variations in the preparation of scanning electron microscope (SEM) samples and several methods of preparing cement samples for viewing in the SEM will be presented in this appendix. The specific treatment of the samples shown in this report will be given after the general techniques are shown.

The SEM allows the direct observation of large samples (up to centimeters in linear dimensions) at magnifications from 20X to almost 100,000X. The resolving power of the current instruments is approximately 250 \AA , and the means of obtaining contrast are much more varied than the optical microscope or the transmission electron microscope. The instrument holds great potential for investigating cementitious materials, but it should be emphasized that it will require considerable development to yield its full potential.

In the SEM a finely focused electron beam is scanned over a small region of the sample. Simultaneously the secondary electrons produced by the primary beam are detected and displayed on a cathode ray tube. The scan of the cathode ray tube is synchronized with the scanning of the electron beam on the sample so that there is a one-to-one correspondence between a point on the sample emitting secondary electrons and the point on the cathode ray tube. The secondary electron production

is represented on the screen of the cathode ray tube by varying the intensity of light and an image of the specimen surface is thereby created. The magnification is achieved by sweeping the electron beam over a small area on the sample and producing the larger image of the surface on the cathode ray tube approximately ten centimeters square. Thus if a 0.01 cm square is scanned on the sample, then the magnification is approximately 1000 \times . If the area of scan is reduced to 0.001 cm, then there is a 10,000 \times magnification. The increase in magnification does not have the decrease in depth of field characteristic of the optical microscope. This allows the observation of the rough fracture surfaces of cement paste. It should be pointed out in passing that signals other than secondary electrons can be used to form an image of the sample, and these give different information and lead to different kinds of contrast. More information about these techniques is now being gathered and will be discussed in a future report.

The basic technique of preparing the cement paste specimens has been to fracture a sample, place it as soon as possible in a vacuum evaporator, and evaporate a gold or platinum-palladium film on the fresh fracture surface. The film thickness was judged to be between 100 and 200 \AA thick, and the specimen has been rotated about an axis perpendicular to the fracture surface in order to obtain a uniform metal coat. This conductive layer is necessary to drain the electron beam current of the SEM away from the non-conductive cement surfaces. Considerable care was taken to prevent CO₂ contamination of the surface between the time of fracture and of placement in the vacuum evaporator. After being coated the specimens were stored at 65 $^{\circ}$ -70 $^{\circ}$ F with 50% relative humidity and viewed in the SEM within a few days. Some samples

were observed in the SEM within minutes after being coated, and some of these have been re-examined after varying lengths of time up to one year and found to be unchanged over large portions of their surface.

Many of the specimens were prepared in a special metal mold which could be opened to reveal a fresh fracture surface on a paste or mortar specimen. A sketch of this mold is shown in Figure A.1. This mold can

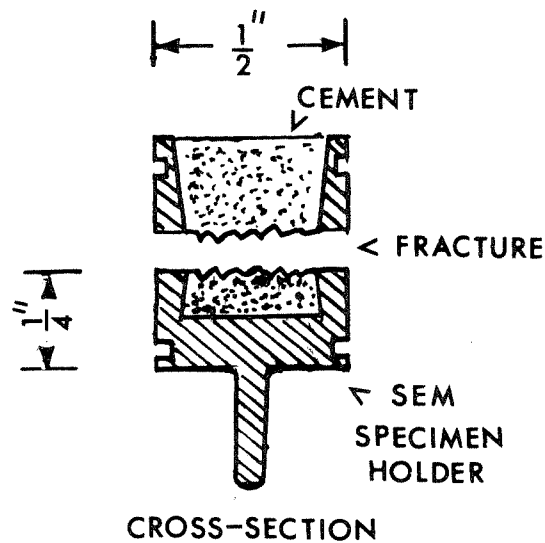


Figure A.1 Sketch of special metal mold used to simplify the SEM specimen preparation. The samples of cement paste are cast in the mold with the top and bottom pieces held together by tape or more recently with an outer jacket. The paste specimen is fractured by separating the top and bottom pieces of the mold and the bottom half of the mold becomes the SEM specimen holder and the specimen is already mounted and ready for coating.

be placed directly into the two SEM models used in this study (Cambridge Instrument Company's Stereocan and Japan Electron Optics Corp's JSM-1). This special mold has a 0.5 inch diameter and the cavity is approximately 0.1 inch deep with approximately 10° of taper away from the plane of the fracture so that the paste specimen is restrained by the walls of the mold during the fracture process. The primary advantage of this special

mold is that the specimen can be placed in the vacuum evaporator within seconds after the fracture.

The following list gives the specific details of how the specimen was prepared for each figure.

Figures 3.3 through 3.11: Neat paste specimens were cast on 25 July 1969 using β -dicalcium silicate, Blaine 3670, stabilized with B_2O_3 (obtained from the PCA laboratories) at a water-solids ratio of 0.5. The special molds of the type shown in Figure A.1 were used and the specimens were stored under water until fractured.

Figures 3.12 and 3.13: Same preparation as the samples shown in Figures 3.3 through 3.11 except that the specimen was placed in the vacuum for two days before fracture.

Figures 3.14, 3.15 and 3.19: The neat paste specimens were prepared by L. Trescony and A. Kline using tricalcium silicate prepared in the U. C. Engineering Materials Laboratory. The neat paste specimens were cast on 2 June 1964, sealed in butyrate tubes until age 3 days, then mold was stripped and specimens were immersed in distilled water in covered polystyrene bottles. On 27 June 1964, age 25 days, specimens were scraped of $Ca(OH)_2$ on exterior and were coated with epoxy resin. The specimens were put under triaxial compression until 19 May 1966, age two years, and stored in desiccator until use in SEM in 1968.

Figures 3.16: The neat paste specimens of tricalcium silicate had a water-to-solids ratio of 0.5 and were prepared in a manner similar to those above.

Figures 3.17 and 3.18: This specimen is the same as that in Figure 3.14 except the hydration was carried out for four years under water.

Figures 3.20 through 3.24: A Type I clinker was ground to fine aggregate size according to ASTM C227-67. The specimens of clinker were used as fine aggregate with an Ideal White Type I.

The microscopes used in this study were in the Donner Laboratory and the Electronics Research Laboratory, both of the University of California; the latter microscope was purchased under grant GB-6428 from NSF, and is operated under grant GM-15536 from NIH.